École polytechnique de Louvain

Effective Stiffness of Non-Rectangular Reinforced Concrete Structural Walls and Engineering Beam-truss Models in Seismic Design and Analysis

Author: **Mathis Keirle**
Supervisors: **João Saraiva Esteves Pacheco de Almeida, António Araújo Correia**
Readers: **Ryan Hoult, Catherine Doneux, Carlos Andrés Blandón Uribe**
Academic year 2021–2022
Master [120] in Civil Engineering

Abstract

When reinforced concrete walls are subjected to severe earthquakes, damage and cracking will appear throughout the structure. As a consequence, this will result in a reduction of the walls stiffness. Most of design codes propose to apply a reduction factor between 0.35 and 0.5 on the uncracked wall stiffness for evaluating the effective stiffness. These reduction factors were based on studies made on rectangular cross-section walls. However, design codes still allow using these factors for assessing the effective stiffness of non-rectangular cross-section walls. The present work aims at verifying if the reduction factors proposed by design codes are overestimated or underestimated when dealing with non-rectangular cross-section walls. For this purpose, 14 different cross-section shapes of walls will be numerically modeled by means of beam-truss model. The reduction factors of each wall will then be derived from the numerical results by applying different procedures. Finally, the numerically obtained factors can be compared to the ones proposed by design codes.

Aknowledgements

This master's thesis is the result of a year of work which would not have been possible without the help of several key people.

First of all, I would like to express my deep gratitude to my thesis supervisor, Professor J. Saraiva Esteves Pacheco de Almeida, for having proposed this fascinating master's thesis topic. I would like to thank him for his great availability and for the many constructive exchanges that we had on a daily basis.

I would also like to extend my thanks to both my thesis co-supervisors, Dr. A. Araújo Correia and Dr. R. Hoult, for taking the time to guide me throughout the year.

Finally, I wish to thank my family for their support and encouragement throughout my study.

Table of contents

List of Figures

List of Tables

Chapter 1

Introduction

1.1 Motivation

The present work will focus on analyses of structural walls made of reinforced concrete (RC). RC walls are widely used in the world as they provide a good way for buildings to resist lateral forces coming from the wind or earthquakes. Indeed, such structures are capable of developing sufficient ductility to dissipate energy in case of seismic activity through the formation of plastic hinges [10].

The stiffness of such structural reinforced concrete walls will influence the nonlinear dynamic responses of buildings. When a RC structure made of walls is hit by an earthquake, it will be subjected to severe reversible lateral forces that yield to cracking in its walls. This will result in a reduction of the walls stiffness, then called effective stiffness, to a value less than the initial uncracked stiffness and as a consequence will affect the distribution of forces throughout the walls as well as their deformations. For these latter reasons, the present work will focus on the evaluation of the effective stiffness as it is one of the main concerns for the design of RC structures [8].

The evaluation of the effective stiffness will yield to the use of numerical softwares. Reinforced concrete walls can be modeled in different ways. The more accurate way is the use of a finite element program. However, this is generally not used in practice by designers as it requires good knowledge on nonlinear structural analysis in order to understand the results coming from the software. Moreover, the running time to get the results from such models can be huge. For these reasons, this work will intend to focus on easier and less time-consuming models such as the stick, wide-column and beam-truss models.

1.2 Goals

Various empirical expressions exist in order to evaluate the effective stiffness for reinforced concrete structural walls. Besides that, many design codes estimate the effective stiffness by the uncracked moment inertia of the wall with a reduction factor [28]. For example, the European code EN 1998-1 [23] tells us to take one half of the uncracked stiffness of the wall as value for the effective stiffness.

However, the reduction factor values proposed in design codes are based on investigations on rectangular cross-section RC walls. For this reason, the main goal of this work is to provide a comparison between the reduction factors provided by codes and the reduction factors obtained by numerically modelling non-rectangular cross-section RC walls such as I-shaped, T-shaped and U-shaped walls.

1.3 Document organisation

The following chapter of this document is intended to present a summary of all theoretical aspects that can be found for the evaluation of the effective stiffness. Moreover, this chapter will present different ways of numerically modelling non-rectangular RC structural walls.

The next chapter, Chapter 3, will show a comparison between the numerical results and the experimental data of the two walls WSH4 and TUB when the latter are modeled using different types of model. A small conclusion will be done to sum up which type of model will be chosen to model the various walls presented in Chapter 4.

The fourth chapter aims at presenting the numerically obtained force-displacement curves for different rectangular and non-rectangular cross-section walls. The numerical curves of those walls are then compared with their corresponding experimental data curves.

Chapter 5 will present the reduction factor results obtained by applying different procedures on the force-displacement curves of Chapter 4. These numerically obtained reduction factors will be then compared to those from experimental data as well as to reduction factor values proposed in design codes.

The last chapter is a conclusion of all the work done in this master's thesis and discussing concerning possible future developments.

Chapter 2

Literature review

2.1 Effective stiffness: Definition and importance for seismic design and assessment

2.1.1 Basic principles

The lateral stiffness K, also called the lateral rigidity, of a reinforced concrete structural wall can be defined as the ratio between the horizontal force that is applied on top of the wall and the horizontal displacement that results from this application, as illustrated in Figure 2.1.

$$K = \frac{F}{\delta} \ [N/m]$$

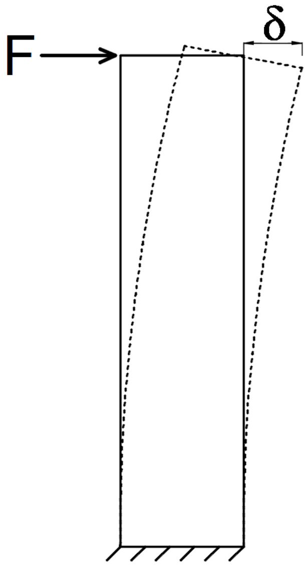

Figure 2.1: Illustration of a wall subject to a force F.

Making a linear analysis of such a wall is only possible if there is a linear relationship between the force exerted at the top of the wall and the resulting displacement. In that case, as shown on the left graph in Figure 2.2, the value of the lateral stiffness K, represented by the slope of the linear curve, will remain constant throughout the analysis.

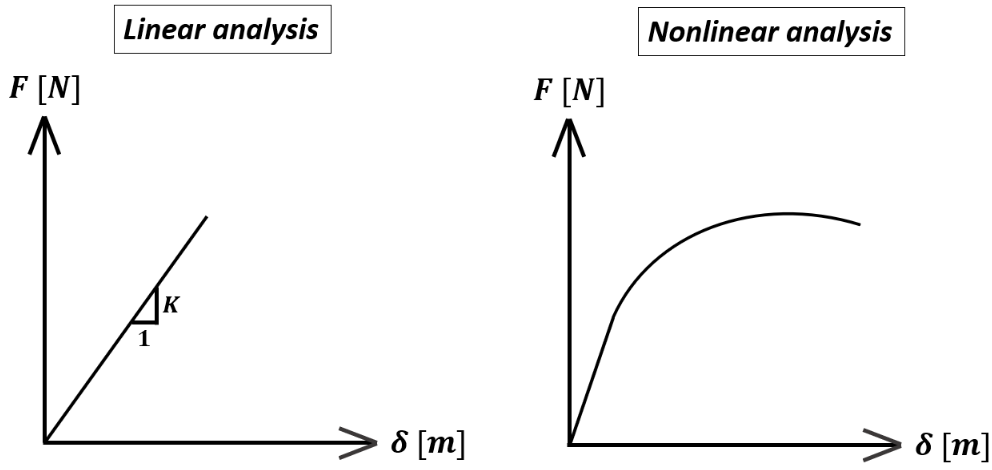

Figure 2.2: Force-displacement relationship for linear and non-linear analyses.

However, making the design of walls that are in seismic zones in such a way that their force-displacement relationship remains linear is not economically viable. Indeed, the lateral top displacement caused by an earthquake will be so large that a certain portion of the wall needs to enter in plastification, i.e., undergo permanent deformations, in order to dissipate the earthquake energy. As presented on the right graph in Figure 2.2, the lateral stiffness during such a nonlinear analysis will not remain constant.

Nonlinear analyses take both material and geometric nonlinearities into account. Material nonlinearities are due to the nonlinear stress-strain relationship of the materials that constitute walls. The geometric nonlinearities are due to changes in the geometry of the cross-section of the elements during the analysis. These changes in geometry will cause additional stresses in walls.

2.1.2 Definitions for effective stiffness

There are different definitions of effective stiffness. Two of those were described in document [15] written by B. Li & al. (2011).

One first definition of the effective stiffness corresponds to the slope of the secant of the lateral force, also called shear force, versus lateral displacement relationship passing through the point at which the applied force reaches 75 % of the maximum lateral force that the structure can withstand. This definition is illustrated in Figure 2.3 in which the effective stiffness corresponds to the slope of the line passing through point A.

A second definition for the effective stiffness consists in taking the stiffness of the wall at first yield. The first yield of a wall is reached when either the first longitudinal reinforcing bar yields or when the maximum concrete compressive strain at the critical section of the wall reaches 0.002. This second definition is illustrated in Figure 2.3 in which the effective stiffness corresponds to the slope of the line passing through point B.

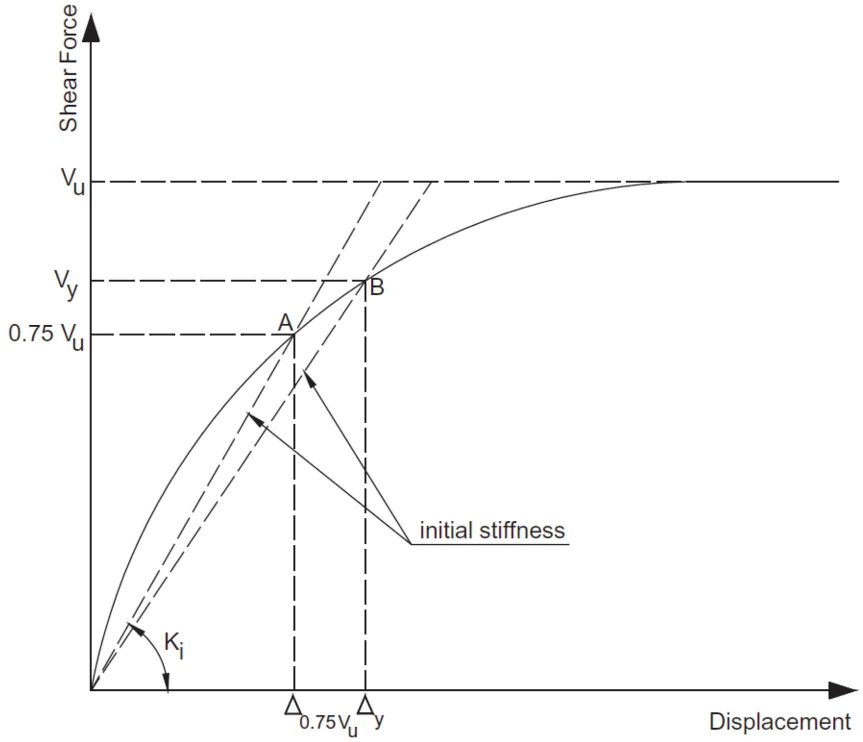

Figure 2.3: Definitions of the effective stiffness from [28].

2.1.3 Importance for seismic design and assessement

As explained in document [8] written by S. Das & al. (2019), the results of a nonlinear analysis of a reinforced concrete wall are greatly influenced by its stiffness. When such a wall is subjected to an earthquake, the structure experiences damage and cracking which will reduce the stiffness to a value less than its initial uncracked stiffness. This new stiffness is called the effective stiffness and has been defined in Section 2.1.2. The value of the effective stiffness will affect the top displacement of the wall, its fundamental period as well as the distribution of forces throughout the structure. This is why the estimation of the effective stiffness of a reinforced concrete structure is one of the main concerns in seismic design.

2.2 Code and research expressions for effective stiffness

This section is intended to present a summary of all the existing expressions for the estimation of the effective stiffness of rectangular and non-rectangular reinforced concrete structures. Some of them are provided from researchers and others from design codes.

All the expressions that will be presented aim at giving what we call an effective stiffness ratio which is defined as the ratio between the effective moment of inertia (I_{eff}) and the gross moment of inertia (I_g) of the wall cross-section: $\frac{I_{eff}}{I_g}$. From this ratio and the gross moment of inertia (I_g), which can be easily calculated, the effective moment of inertia (I_{eff}) can be computed.

2.2.1 Effective stiffness: Rectangular RC walls

Before going into the presentation of the different expressions that exist to calculate the effective stiffness of rectangular reinforced concrete walls, let us have a look at what the codes recommend to take as a value for the effective stiffness ratio.

As it is stated in the European code EN 1998-1 [23], "Unless a more accurate analysis of the cracked elements is performed, the elastic flexural and shear stiffness properties of concrete and masonry elements may be taken to be equal to one-half of the corresponding stiffness of the uncracked elements." In other words, the European code tells us to take an effective stiffness ratio equal to one-half:

$$\frac{I_{eff}}{I_g} = 0.5$$

Besides that, the ACI 318-11 code [5] from the American Concrete Institute and the CSA A23.3-14 code [7] from the Canadian Standards Association propose to take a value for the effective stiffness ratio equal to 0.35:

$$\frac{I_{eff}}{I_g} = 0.35$$

A summary of all values of effective stiffness ratio that are recommended by various codes can be found in document [27] written by J. M. Wong & al. (2017).

The different expressions for calculating the effective stiffness ratio of rectangular reinforced concrete cross-section walls are presented herebelow:

- The first expression to calculate the effective stiffness ratio of a rectangular cross-section is the one proposed by Paulay and Priestley (1992) [20]:

$$\frac{I_{eff}}{I_g} = \frac{100}{f_y} + \frac{P}{f_c A_g}$$

  The parameters affecting this effective stiffness ratio are the yield strength in $[MPa]$ of the longitudinal reinforcement f_y and the axial load ratio $\frac{P}{f_c A_g}$ in which P is the total vertical load that is applied on top of the wall in $[N]$, f_c is the compressive concrete strength in $[MPa]$ and A_g is the gross cross-section area in $[mm^2]$. Moreover, as we are in the case of a rectangular cross-section, the gross moment of inertia I_g is equal to $\frac{bh^3}{12}$ where h is the length of the wall and b is its thickness.

- A second expression that can be used is the one proposed by Fenwick and Bull (2000) [12] in which the effective stiffness ratio depends on the axial load ratio $\frac{P}{f_c A_g}$, the yield strength of the longitudinal reinforcement f_y in $[MPa]$ and the compressive concrete strength f_c:

$$\frac{I_{eff}}{I_g} = 0.267\left(1 + 4.4\frac{P}{f_c A_g}\right)\left(0.62 + \frac{190}{f_y}\right)(0.76 + 0.005 f_c)$$

- Another expression that is intended to evaluate the effective stiffness ratio of squat rectangular reinforced concrete walls, i.e., walls that have a ratio between their height and their length lower than 2 was proposed by Li and Xiang (2011) [15]:

$$\frac{I_{eff}}{I_g} = 0.19\left(\frac{100}{f_y} + \frac{P}{f_c A_g}\right)\left(0.53 + 0.37\frac{H}{l_w} + 0.31\frac{H^2}{l_w^2}\right)$$

The parameters affecting the effective stiffness ratio are the axial load ratio $\frac{P}{f_c A_g}$, the yield strength of the longitudinal reinforcement f_y in $[MPa]$, the height of the wall H and its length l_w.

- Then, instead of just taking a value of 0.35 for the effective stiffness ratio, ACI 318-11 code [5] proposes a more accurate alternative expression:

$$\frac{I_{eff}}{I_g} = (0.10 + 02\rho)(1.2 - 0.2\frac{b_w}{d}) \leq 0.5$$

The expression hereabove depends on the reinforcement steel ratio ρ, i.e., the ratio between the total area of longitudinal steel bars and the area of concrete that is intercepted by them, the wall thickness b_w and the distance d between the extreme compression fiber in the wall and the center of the first longitudinal steel bar that will be in tension.

- Finally, the European code EN 1998-2 [24] proposes to compute the effective moment of inertia I_{eff} by using the following formula:

$$I_{eff} = \nu \frac{M_{Rd}}{E_c \phi_y}$$

In this expression hereabove, ν is a "correction coefficient reflecting the stiffening effect of the uncracked part of the pier" [24] and is equal to 1.2, E_c is the Young's modulus of concrete, M_{Rd} is the design ultimate moment and ϕ_y is the yield curvature of the plastic hinge section.

The design ultimate moment M_{Rd} is the multiplication of the height of the corresponding wall by the maximum lateral force that can be taken directly from its force-displacement curve once the wall has been numerically modeled. Concerning the yield curvature ϕ_y, it can be determined thanks to the following expression in which "d_s is the depth of the section to the center of the tension reinforcement, ϵ_{sy} is the yield strain of the reinforcement and ϵ_{cy} is the compressive strain of concrete at yielding of the tension reinforcement" [24]:

$$\phi_y = \frac{(\epsilon_{sy} - \epsilon_{cy})}{d_s}$$

Once the effective moment of inertia I_{eff} has been calculated, it is enough to divide it by the gross moment of inertia I_g to get the effective stiffness ratio.

2.2.2 Effective stiffness: Non-Rectangular RC walls

Most of the expressions for the effective stiffness that we have presented in Section 2.2.1 cannot be used when dealing with non-rectangular reinforced concrete structures as their respective effective stiffness is significantly different.

However, some empirical expressions for T-shaped and U-shaped walls has been proposed by Z. Zhang & al. (2018) [28] in order to compute the effective stiffness ratio:

- The following expression can be used when a T-shaped wall is loaded in such a way that its flange is in tension:

$$\frac{I_{eff}}{I_g} = 2.35\frac{P}{f_c A_g} + \frac{185}{f_y}$$

- When a T-shaped wall is loaded in such a way that its flange is in compression, the following expression can be used:

$$\frac{I_{eff}}{I_g} = 1.75\frac{P}{f_c A_g} + \frac{125}{f_y}$$

- The following expression can be used when a U-shaped wall is loaded in its strong axis direction:

$$\frac{I_{eff}}{I_g} = 1.82\frac{P}{f_c A_g} + \frac{60}{f_y}$$

- If a U-shaped wall is loaded in such a way that its flanges are in compression, then the following expression can be used:

$$\frac{I_{eff}}{I_g} = 1.85\frac{P}{f_c A_g} + \frac{180}{f_y}$$

- Finally, when a U-shaped wall is loaded in such a way that its flanges are in tension, then the following expression can be used:

$$\frac{I_{eff}}{I_g} = 3.02\frac{P}{f_c A_g} + \frac{183}{f_y}$$

All the expressions hereabove expressions depend on the axial load ratio $\frac{P}{f_c A_g}$ and on the yield strength of the longitudinal reinforcement f_y in $[MPa]$.

The expression proposed by the European code EN 1998-2 [24] that was presented in Section 2.2.1 can also be used for assessing the effective stiffness ratio of non-rectangular cross-section walls. As a reminder, the expression is as follows:

$$I_{eff} = \nu\frac{M_{Rd}}{E_c \phi_y}$$

Another expression that can be used to assess the effective stiffness ratio is the one proposed by M. N. Fardis & al. (2015) [11] and does not require numerical results as opposed to the previous expression:

$$\frac{I_{eff}}{I_g} = a\left(0.8 + ln\left(max\left(\frac{L_s}{H}; 0.6\right)\right)\right)\left(1 + 0.048\ min\left(50\ [MPa]; \frac{P}{A_g}\right)\right)$$

In this expression, L_s is the length of the wall, H is its height, P is the total vertical force which is exerted at the top of the wall, A_g is the gross cross-section area of the wall and the constant a is equal to either 0.11 if we are in the case of a rectangular cross-section wall or 0.09 if we are in the case of a T, I or U cross-section wall. Note that this expression does not take into account the steel reinforcement of the wall.

Finally, as we have seen in Section 2.2.1 for rectangular cross-section walls, codes advise to use values of 0.35 or 0.5 for assessing the effective stiffness ratio. In fact, codes tell us that these values can also be used when dealing with non-rectangular cross-section walls even if there were likely derived from rectangular walls studies.

2.3 Numerical models

Different ways to numerically model RC structures are presented in this section. All these model types aim at obtaining the force-displacement curve of a wall for which we will later determine the effective stiffness. In Chapter 3, a comparison between the results from all these numerical model types will be presented on two case studies (walls WSH4 and TUB).

2.3.1 Stick model

Stick models are the easiest and less time-consuming way to numerically model a wall. The stick model approach consists in representing a wall by only one vertical beam finite element located in the middle of its cross-section. This will be a one-dimensional model. Figure 2.4 represents an example of stick model for a rectangular cross-section wall.

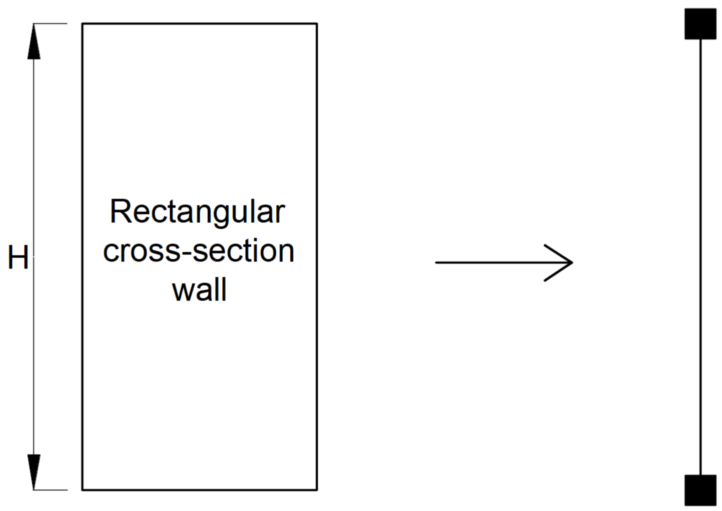

Figure 2.4: Stick model of a rectangular cross-section wall.

The main drawback of such a model is that when modelling a non-planar wall, for example a U-shaped wall, the stick model will have difficulties in simulating the distribution of internal lateral forces, also called shear forces, between the different parts of the wall. Therefore, as it is explained in document [2] by K. Beyer & al. (2008), "the lateral shear deformation will be the same whether the total shear force is actually carried by one flange alone or equally distributed between the two flanges." Note that what are called the flanges in a U-shaped wall are the two parts of the U that are parallel to each other.

2.3.2 Wide-Column model

Figure 2.5 shows an example of a wide-column model for a U-shaped wall. In that example, the wall has been subdivided into three rectangular cross-sections. The wide-column model consists in modelling each part of the wall by vertical beam elements located at the middle of their cross-section. Those vertical elements are then linked together by rigid horizontal links. Unlike the stick model, the wide-column model of a non-planar wall enables to consider the distribution of the total lateral forces between its different parts.

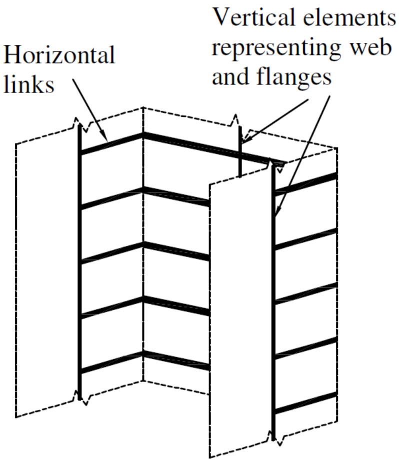

Figure 2.5: Wide-column model of a U-shaped wall from [2].

One of the main disadvantage of building a wide-column model is that the designer needs to make a lot of assumptions. For example, as it is stated in document [2], designers will need to take decisions about:

- The vertical spacing between the horizontal rigid links.
- The subdivision of the wall section into planar wall sections.
- The number of vertical elements representing the planar wall sections.
- The properties of the horizontal rigid links and vertical beam elements.

However, B. Stafford Smith & al. (1986) [22] propose to take one fifth of the total height of the wall for the vertical spacing between the horizontal rigid links. Moreover, the rigid links can be made of elastic beam elements for which great values for the flexural and shear rigidities will be assigned.

2.3.3 Beam-Truss model

Another type of model which is interesting when dealing with non-planar walls is the beam-truss model. As its name suggests, this approach consists in modelling a wall by using beam and truss elements.

On the left picture of Figure 2.6, the perspective view of a T-shaped wall is represented. On the right picture of Figure 2.6, there is its corresponding beam-truss model. We can see that the cross-section of the wall is divided into several parts. To model the concrete and steel in each parts, vertical truss elements will be used except in the parts at the extremities of the wall where it is vertical beam elements that are used. Those vertical beam elements are represented in red in Figure 2.6.

The particularity of the beam-truss model is that it enables to catch the flexure-shear interaction thanks to horizontal truss elements. Diagonal truss elements are also used for representing the compression of concrete in the diagonal directions.

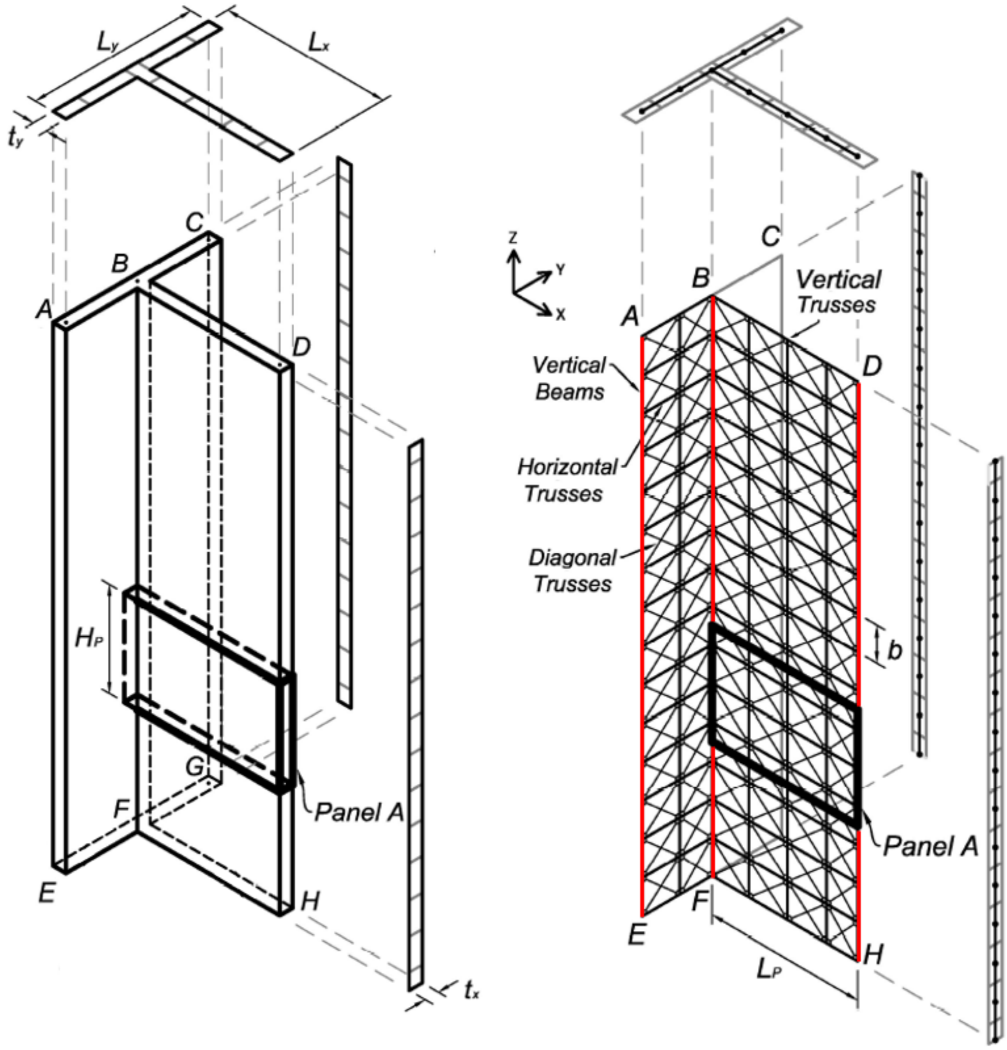

Figure 2.6: Beam-truss model of a T-shaped wall from [16].

The division of the wall cross-section is not done randomly. In fact, it depends on the angle that the diagonal elements make with respect to the horizontal. An expression for evaluating this angle is proposed by Y. Lu & al. (2014) [16]:

$$\theta_d = tan^{-1}\left(\frac{V_{max}}{f_{y,t}\rho_t t_w d}\right) \leq 65\ ^\circ$$

In this above expression, $f_{y,t}$ is the yield strength of the transverse reinforcement, ρ_t is the transverse reinforcement ratio, i.e., the ratio between the volume of horizontal steel bars used in the wall and the volume of concrete, t_w is the thickness of the wall, d is the distance between the two vertical beam elements at the extremities of the model and V_{max} is the maximum lateral force that the structure can resist. This latter value V_{max} can be easily found if the experimental data of the wall are available since it will consist in taking the maximum force in the force-displacement diagram. If the experimental data are not available, then an iteration procedure need to be done to find its value. In that case, we will assume a first value for the angle θ and then build the beam-truss model with it. Once the beam-truss model is built, we can obtain the maximum lateral force V_{max} that we can insert in the above expression to have a new value of the angle θ and redo another iteration.

Figure 2.7 shows in a closer view the "Panel A" of Figure 2.6. The hatched area in the left picture of Figure 2.7 represents the part of the wall that needs to be taken into account by the horizontal truss elements. Indeed, this part has a height that is equal to the vertical distance between two horizontal elements represented by b in Figure 2.6. On the right picture of Figure 2.7, the hatched area represents the part of the wall that needs to be taken into account by the diagonal truss elements. The height of this latter part is denoted b_{eff}. Y. Lu & al. (2014) have proposed to used the below expression for determining it in which a is the distance between two vertical elements:

$$b_{eff} = a\ sin(\theta_d)$$

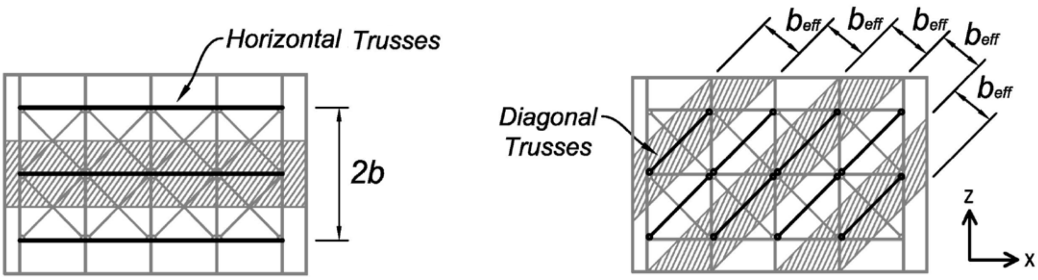

Figure 2.7: Horizontal and diagonal geometry in a beam-truss model from [16].

2.3.4 Finite elements model

Finally, reinforced concrete structural walls can be modeled by using other types of finite elements than trusses and beams. For example, shell, membrane or solid elements can be used for modelling reinforced concrete walls. Generally, these elements types allow to obtain more accurate numerical results.

However, the main drawbacks of using shell, solid or membrane elements are the difficulty to interpret the results and the running time to get these results from the numerical model. For these reasons, this report is primarily based on the three other types of models that have been explained previously:

- Stick model
- Wide-column model
- Beam-truss model

Documents [19] and [14] written respectively by JD. Palermo & al. (2007) and J. Almeida & al. (2022) are studies based on results obtained when modelling reinforced concrete structures with the VecTor2 software. This software is a nonlinear finite element program.

Chapter 3

Numerical simulation of RC walls with nonlinear beam elements

This chapter will first discuss about the SeismoStruct software that was used to model the various walls that will be presented in Chapter 4 and will then present a comparison between the numerical results and the experimental data of the two walls WSH4 and TUB modeled using a stick model, wide-column model or a beam-truss model.

3.1 The nonlinear beam element

3.1.1 Introduction to SeismoStruct

As explained in the SeismoStruct User Manual (2021) [21], SeismoStruct is a Finite Element package of the Seismosoft software for structural analysis that is capable of predicting the large displacement behaviour of structures under static or dynamic loadings, taking into account both geometric nonlinearities and material inelasticity. Beside that, the choice of using this software was also based on the fact that it is user-friendly thanks to its intuitive graphical interface.

3.1.2 The used types of materials

SeismoStruct offers different material types to model the nonlinear behaviour of materials. All walls that have been modeled in this report with SeismoStruct use the nonlinear concrete model from Mander & al and the steel model from Menegotto-Pinto with the corresponding mechanical properties of each wall.

3.1.3 The used types of elements

Among the various types of elements that SeismoStruct proposes, only three of them are of our interest for modelling walls. Beams elements are either modeled by using inelastic force-based frame elements or inelastic displacement-based frame elements. Concerning the trusses elements, those are modeled in SeismoStruct by using inelastic truss elements.

3.2 Walls presentation

This section will present the geometry, the reinforcement layout and the material properties for walls WSH4 and TUB. Later in this chapter, it will also be presented how these walls were modeled using SeismoStruct software.

3.2.1 WSH4

3.2.1.1 Geometry and reinforcement layout

The wall WSH4 is a reinforced concrete wall that has a rectangular section. Its cross-section is shown in Figure 3.1. The properties and geometry of the wall have been taken from document [9] written by A. Dazio & al. (2009). WSH4 is 4.56 $[m]$ high, 2 $[m]$ long and 0.15 $[m]$ thick. It can be therefore deduced that this wall has a shear span ratio, i.e., the ratio between the height and the length of the wall, equal to 2.28.

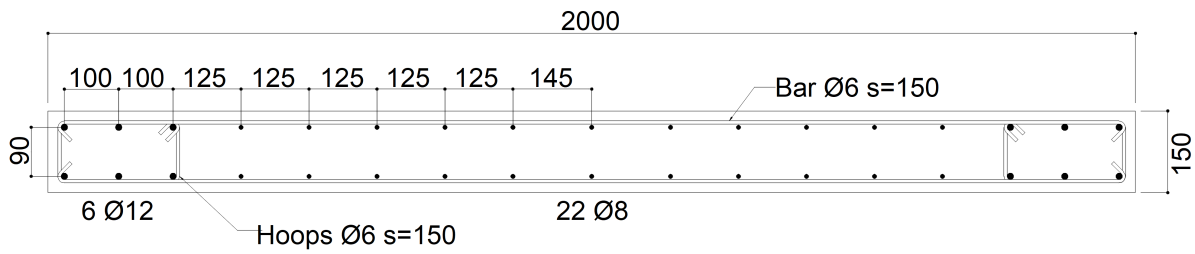

Figure 3.1: WSH4: Cross section and reinforcement detailing [Unit: mm].

Document [9] tell us that the axial load ratio (ALR) of wall WSH4 is equal to 0.057. This means that there is a constant vertical load (N) equal to 699.39 $[kN]$ applied at the top of the wall. This latter value of 699.39 $[kN]$ was obtained thanks to the following formula in which A_g is the gross cross-section area and f_c is the compressive concrete strength that makes up the wall:

$$ALR = \frac{N}{A_g \cdot f_c} \Rightarrow 0.057 = \frac{N}{(0.15 \cdot 2) \cdot (40.9 \cdot 10^6)} \Rightarrow N = 699.39\ [kN]$$

The reinforcement layout of WSH4 is made of 6 longitudinal steel bars, i.e., bars that cross the entire height of the wall, having a diameter of 12 $[mm]$ in each end of the wall. Between these two ends, there are 22 longitudinal bars having a diameter of 8 $[mm]$.

Concerning the transverse reinforcement, we can see in Figure 3.1 that the concrete in the extremities of the wall is confined by hoops, i.e., steel rings, of 6 $[mm]$ diameter spaced vertically along the height of the wall 150 $[mm]$ apart. This confinement allows the concrete inside the hoops to have a higher compressive strength. We can also see that there are 2 sets of 6 $[mm]$ diameter horizontal bars that cross the entire length of the wall. These latter are also spaced vertically along the height of the wall 150 $[mm]$ apart.

3.2.1.2 Material properties

Tables 3.1 and 3.2 list respectively the properties for the steel reinforcement and the concrete valid on the day of the wall test.

Steel Mechanical Properties					
		Rebar $\phi 6$	Rebar $\phi 8$	Rebar $\phi 12$	
Diameter	d	6	8	12	mm
Modulus of elasticity	E_s	200	200	200	GPa
Yield tensile strength	f_y	518.9	583.7	576	MPa
Ultimate tensile strength	f_u	558.7	714.4	674.9	MPa
Yield strain	ϵ_y	0.259	0.292	0.288	%
Ultimate strain	ϵ_u	10	10	10	%
Strain hardening parameter	α	0.204	0.673	0.509	%
Specific weight	γ	78	78	78	kN/m^3

Table 3.1: Steel mechanical properties.

Concrete Mechanical Properties			
Compressive concrete strength	f_c	40.9	MPa
Tensile concrete strength	f_t	2.5	MPa
Modulus of elasticity	E_c	30	GPa
Strain at peak stress	ϵ_c	0.2	%
Specific weight	γ	24	kN/m^3

Table 3.2: Concrete mechanical properties.

Note that for the steel mechanical properties presented in Table 3.1, the strain hardening parameter α was not directly given in document [9]. This parameter was therefore determined according to the following formula in which the parameters are defined in Tables 3.1 and 3.2:

$$\alpha = \frac{f_u - f_y}{\epsilon_u - \epsilon_y} \cdot E_s$$

3.2.2 TUB

3.2.2.1 Geometry and reinforcement layout

TUB is a U-section wall. Its cross-section is shown in Figure 3.2. The properties and geometry of the wall have been taken from document [3] written by K. Beyer & al. (2008). The length of both flanges of TUB is equal to 1050 $[mm]$ and the length of its web is equal to 1300 $[mm]$. Refer to Figure 3.2 to see where the flanges and the web are located. All along its section, the wall is 0.1 $[m]$ thick.

Concerning its height, TUB is 3350 $[mm]$ high. To apply horizontal loads in the North-South direction at the top of the wall, two actuators were placed at a height of 2950 $[mm]$. Another actuator was placed at a height of 3350 $[mm]$ in order to apply a load in the West-East direction.

Document [3] tell us that the axial load ratio (ALR) of wall TUB is equal to 0.04 which means that there is a constant vertical load (N) equal to 700.16 $[kN]$ applied at the top of the wall. This latter value of 700.16 $[kN]$ was obtained thanks to the following formula in which A_g is the gross cross-section area and f_c is the compressive concrete strength that makes up the wall:

$$ALR = \frac{N}{A_g \cdot f_c} \Rightarrow 0.04 = \frac{N}{(0.1 \cdot (2 \cdot 1.05 + 1.1)) \cdot (54.7 \cdot 10^6)} \Rightarrow N = 700.16\ [kN]$$

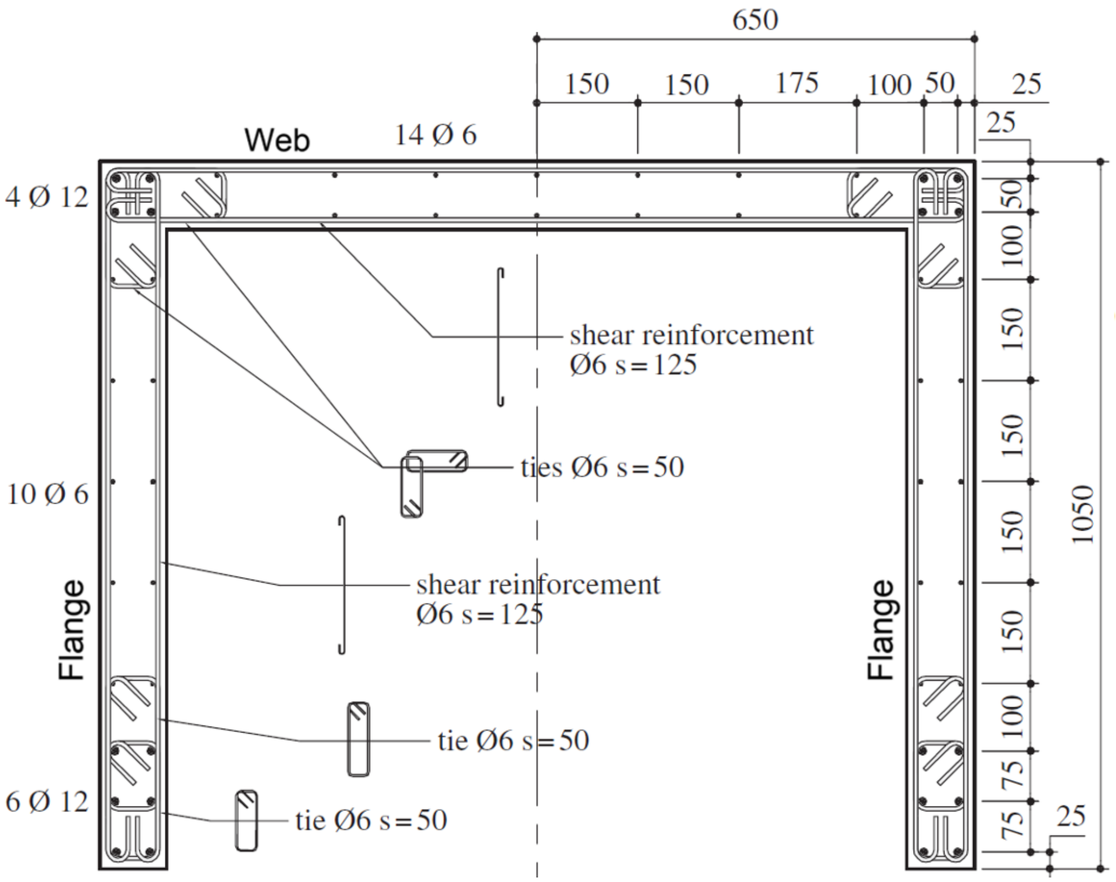

Figure 3.2: TUB: Cross section and reinforcement detailing from [3] [Unit: mm].

Regarding the reinforcement layout, we can see in Figure 3.2 that there are 10 longitudinal bars, i.e., bars that cross the entire height of the wall, having a diameter of 6 [mm] in each flange of TUB. There are also 14 longitudinal bars having a diameter of 6 [mm] in the web. In each corners, i.e., at both intersections between flanges and the web, there are 4 longitudinal bars having a diameter of 12 [mm]. In the South extremities of both flanges, there are also 6 longitudinal bars having a diameter of 12 [mm].

For the transverse reinforcement, we can see in Figure 3.1 that the concrete in the corners of the wall and in the South extremities of both flanges is confined by 2 sets of 6 [mm] diameter hoops, i.e., steel rings, spaced vertically along the height of the wall 50 [mm] apart. This allows to the concrete inside the hoops to have a higher compressive strength. We can also see that there are 2 sets of 6 [mm] diameter horizontal bars that cross the entire length of the web and both flanges. These latter are spaced vertically along the height of the wall 125 [mm] apart.

3.2.2.2 Material properties

Tables 3.3 and 3.4 list respectively the properties for the steel reinforcement and the concrete valid on the day of the wall test. Note that for the steel mechanical properties presented in Table 3.3, the strain hardening parameter α was not directly given in document [3]. This parameter was therefore determined according to the following formula in which the parameters are defined in Tables 3.3 and 3.4:

$$\alpha = \frac{f_u - f_y}{\epsilon_u - \epsilon_y} \cdot E_s$$

Steel Mechanical Properties				
		Rebar $\phi 6$	Rebar $\phi 12$	
Diameter	d	6	12	mm
Modulus of elasticity	E_s	200	200	GPa
Yield tensile strength	f_y	518	471	MPa
Ultimate tensile strength	f_u	681	574	MPa
Yield strain	ϵ_y	0.259	0.235	%
Ultimate strain	ϵ_u	8.4	12.7	%
Strain hardening parameter	α	1	0.413	%
Specific weight	γ	78	78	kN/m^3

Table 3.3: Steel mechanical properties.

Concrete Mechanical Properties			
Compressive concrete strength	f_c	54.7	MPa
Tensile concrete strength	f_t	2.2	MPa
Modulus of elasticity	E_c	34.8	GPa
Strain at peak stress	ϵ_c	0.2	%
Specific weight	γ	24	kN/m^3

Table 3.4: Concrete mechanical properties.

3.3 Stick model: Comparison

3.3.1 WSH4: Stick model

The stick model of wall WSH4 consists in representing the wall by only one vertical element of 4.56 $[m]$ high, i.e., the height of wall WSH4. This element was implemented in SeismoStruct [21] by using one inelastic force-based frame element with 5 integration sections and 150 fibres per section. This element has exactly the same shape and reinforcement layout as the one presented in Figure 3.1. Figure 3.3 shows the elevation view of the corresponding stick model.

Figure 3.3: Elevation view of the stick model for WSH4 [Unit: mm].

From this model, by making a pushover analysis, it can be obtained the base shear in the wall, i.e., the horizontal force at the bottom of the wall, as a function of the relative top displacement when WSH4 is loaded from the West to East direction. In Figure 3.4, the stick model results correspond to the red curve. We can make a comparison of between and the experimental data that correspond to the blue curve in Figure 3.4.

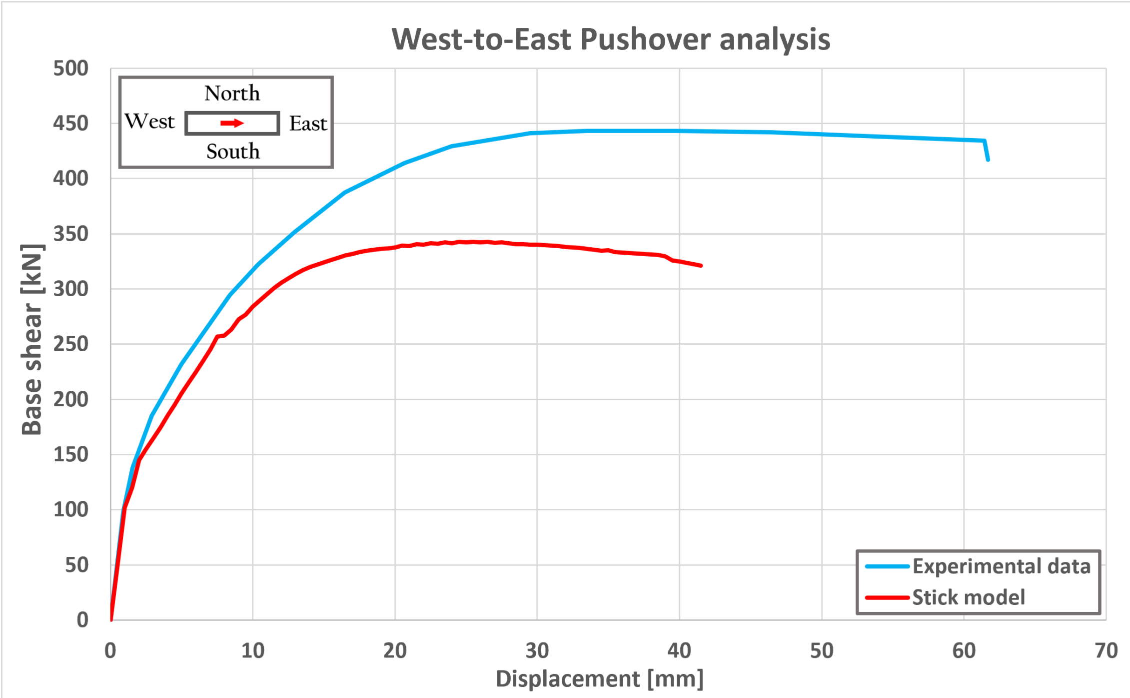

Figure 3.4: WSH4: Force-displacement relationship when loaded from West to East.

From Figure 3.4, it can be seen that the results from the stick model underestimate the base shear since the experimental data curve is much higher than the stick model curve after a top displacement of the wall equal to about 10 $[mm]$. However, the initial stiffness of both experimental data and stick model curves, i.e., the slope at the beginning of the curves, match really well. Note that the stick model curve has been stopped manually since after a top displacement of the wall equal to about 42 $[mm]$, the value of the base shear drops quickly.

3.3.2 TUB: Stick model

The TUB stick model consists to represent the wall by only one vertical element. The length of this element depends on the direction of the loading since, as previously stated, the actuators are not placed at the same height. So, if the wall is horizontally loaded in the North-South direction then its height is equal to 2.95 $[m]$ and if it is loaded in the West-East direction then its height is equal to 3.35 $[m]$. The element was implemented in SeismoStruct [21] by using one inelastic force-based frame element with 5 integration sections and 150 fibres per section. This element has exactly the same shape and reinforcement layout than the one presented in Figure 3.2. Figure 3.5 shows the elevation view of the corresponding stick model.

Figures 3.6, 3.7, 3.8 and 3.9 show the results of the TUB stick model when it is respectively loaded at the top of the wall in the South-to-North, North-to-South, West-to-East and East-to-West directions.

Figure 3.5: Elevation view of the stick model for TUB [Unit: *mm*].

In Figure 3.6, when TUB is loaded from the South to North direction, the results of the stick model are really good as the stick model curve approximate the experimental data closely. However, when the wall is loaded in the other three directions, the results of the stick model do not fit well with those from the experimental data. Indeed, in Figure 3.7, the stick model curve underestimates the base shear from the experimental data curve after a top displacement equal to about 30 [*mm*]. In both Figures 3.8 and 3.9, when the wall is horizontally loaded from the West to East and from the East to West directions, the stick model results overestimate the base shear of the experimental data.

Concerning the initial stiffness, we can see in Figures 3.6, 3.7, 3.8 and 3.9, that the slope at the beginning of each stick model curve is pretty much the same as the one from the corresponding experimental data curve, meaning that they have almost the same initial stiffness.

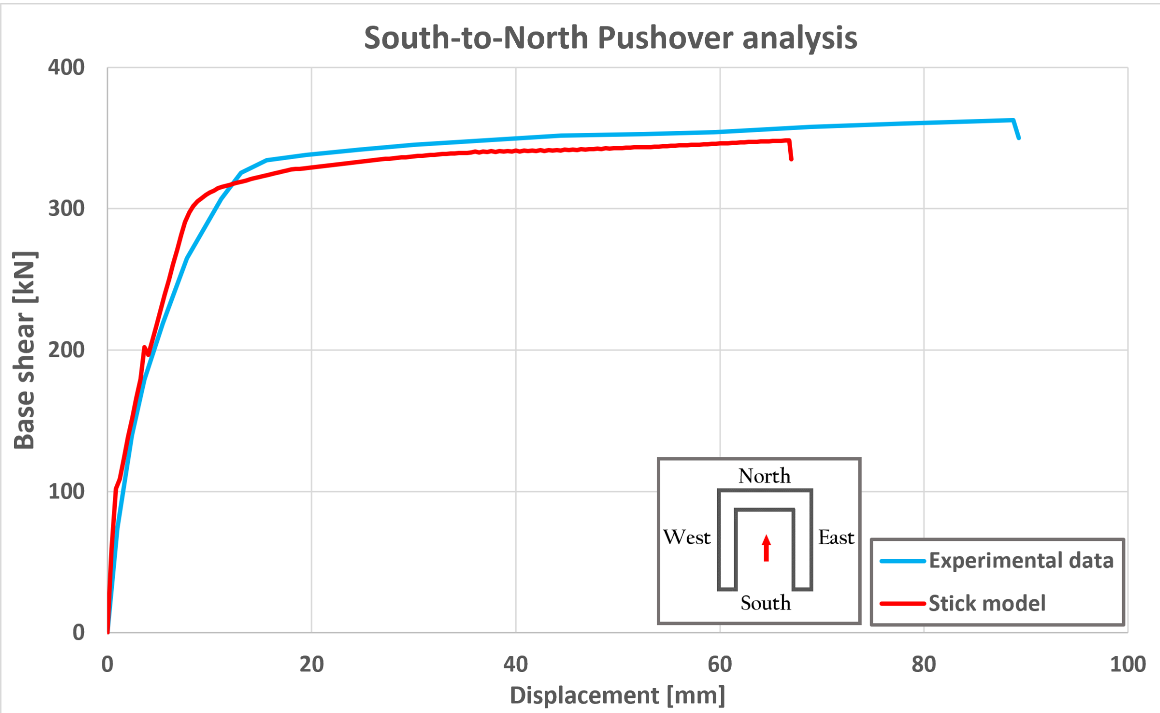

Figure 3.6: TUB: Force-displacement relationship when loaded from South to North.

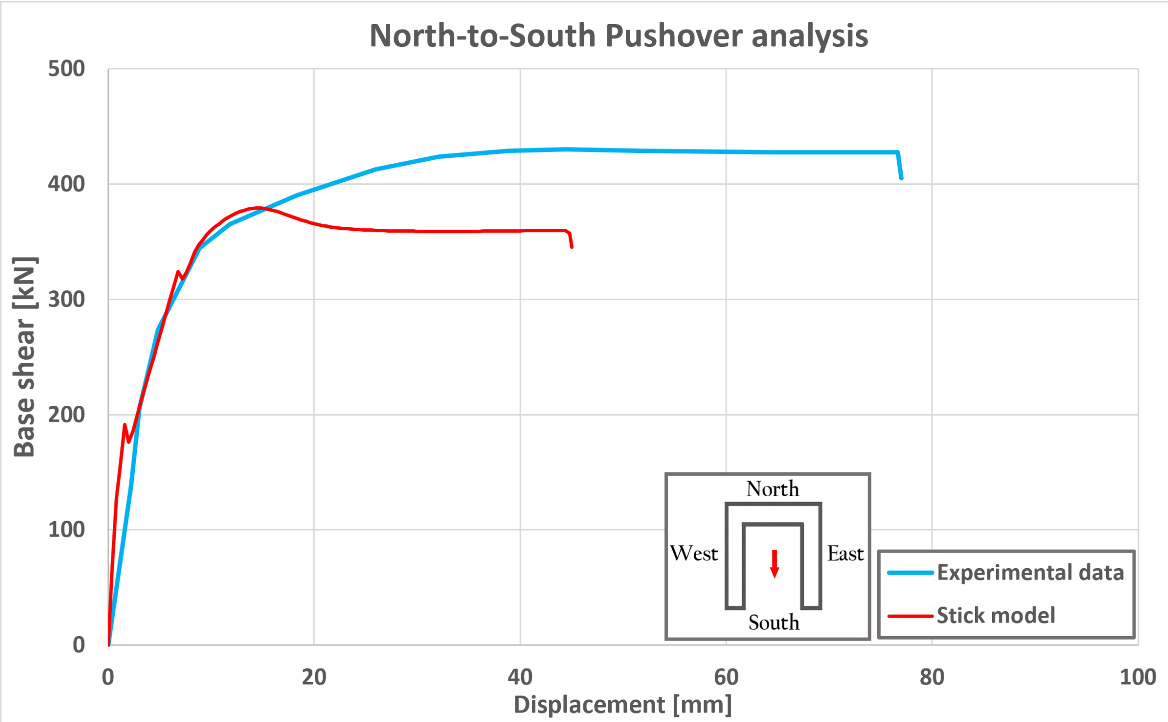

Figure 3.7: TUB: Force-displacement relationship when loaded from North to South.

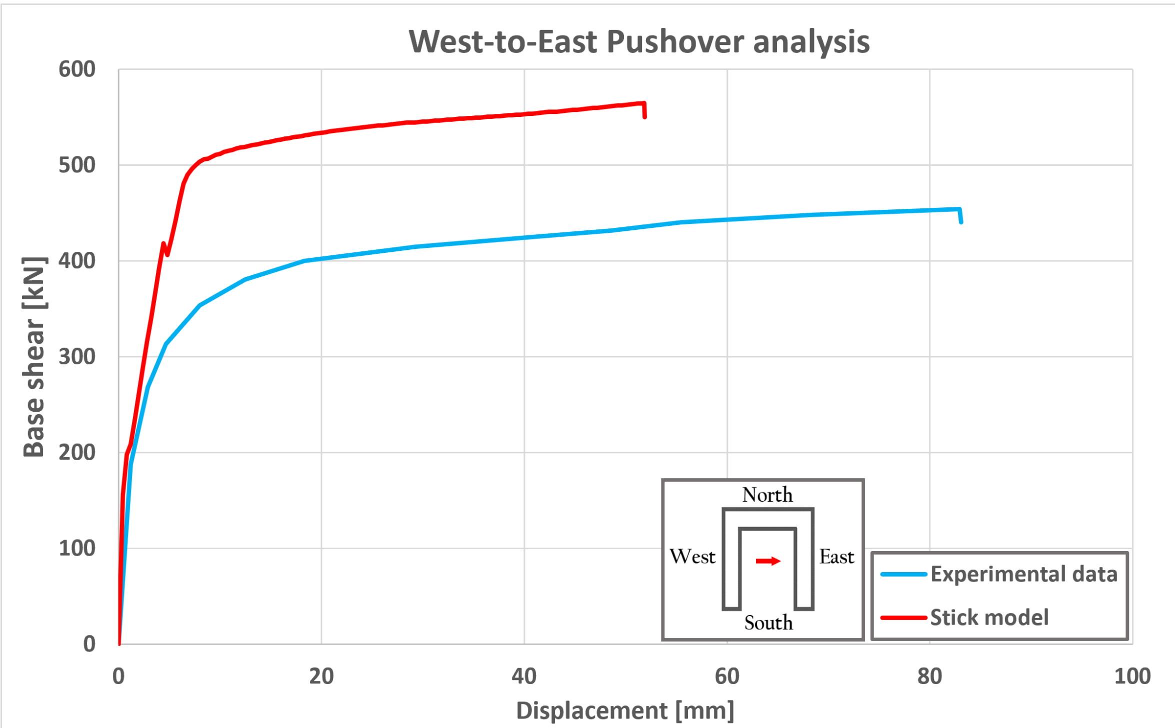

Figure 3.8: TUB: Force-displacement relationship when loaded from West to East.

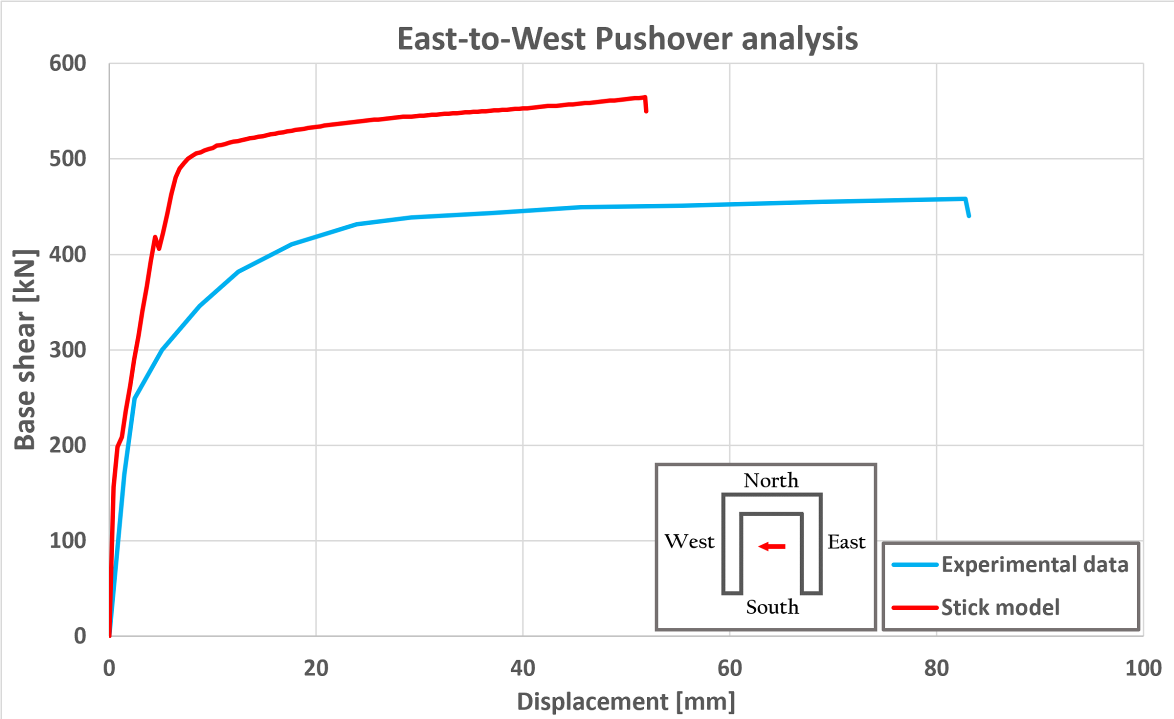

Figure 3.9: TUB: Force-displacement relationship when loaded from East to West.

3.4 Wide-column model: Comparison

3.4.1 WSH4: Wide-column model

The wide-column model of wall WSH4 consists in modelling it with 5 vertical elements that are placed one above the other. The length of each element is equal to 0.912 $[m]$, i.e., one fifth of the total height as explained in Section 2.3.2. The plan and elevation views of the wide-column model is represented in Figure 3.10. All the vertical elements were implemented in SeismoStruct [21] by using inelastic displacement-based frame elements.

From this wide-column model, by making a pushover analysis, it can be obtained the base shear in the wall, i.e., the horizontal force at the bottom of the wall, as a function of the relative top displacement when WSH4 is loaded from the West to East direction. In Figure 3.11, the wide-column model results correspond to the red curve. Those results can be compared to the experimental data which correspond to the blue curve in Figure 3.4. It can be seen that up to a top displacement of 10 $[mm]$, the results match quite well with the experimental data since the red curve is really close to the blue one. However, after a top displacement equal to 10 $[mm]$, the wide-column model start to underestimate the value of the base shear too much.

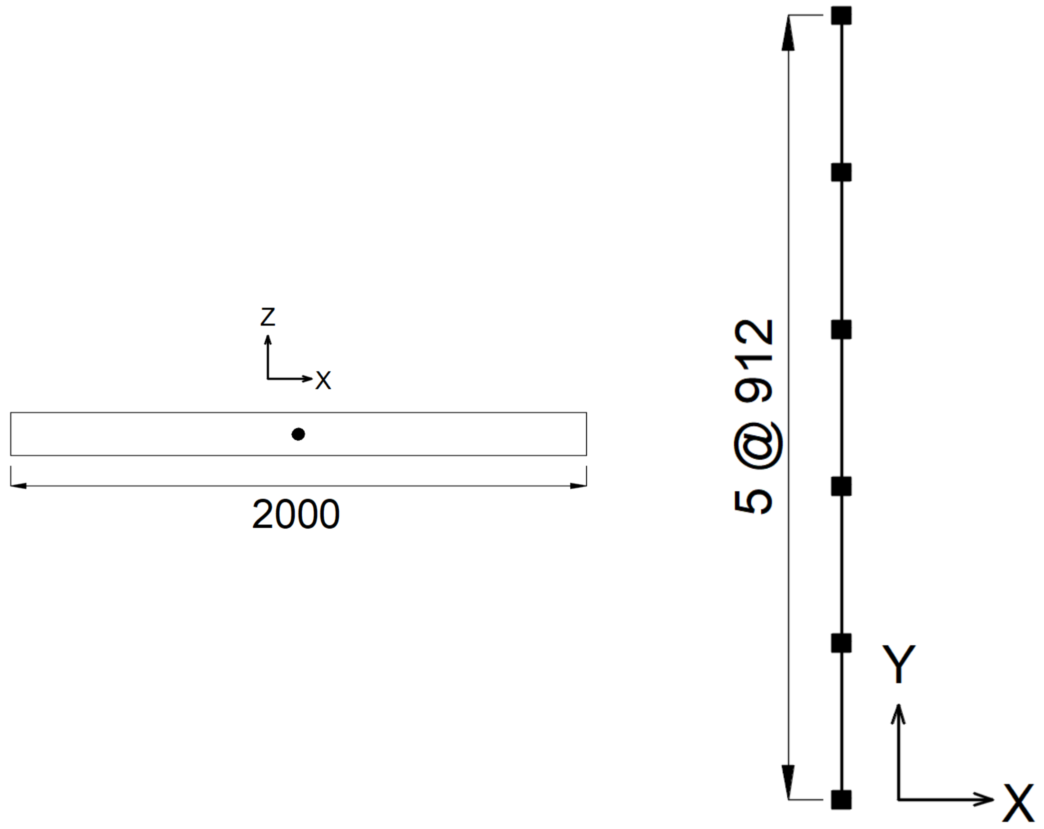

Figure 3.10: Plan and elevation views of the wide-column model for WSH4 [Unit: *mm*].

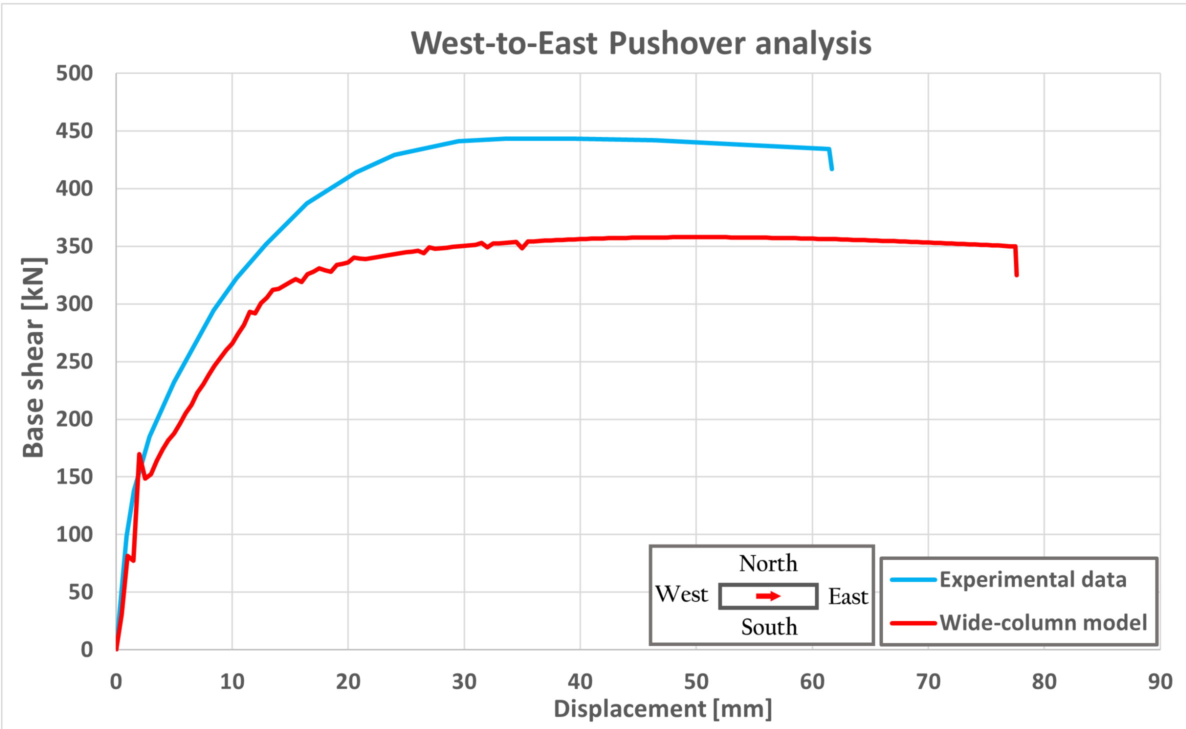

Figure 3.11: WSH4: Force-displacement relationship when loaded from West to East.

3.4.2 TUB: Wide-column model

The plan and perspective views of the wide-column model of wall TUB are shown in Figure 3.12. We can see in blue on Figure 3.12 that each part of the wall, i.e., the web and both flanges, are modeled by series of 5 verticals elements. The length of these elements depends on the direction in which the wall is pushed during the pushover analysis. Indeed, if the wall is horizontally loaded in the South-North direction, then the length of the vertical elements will be equal to 590 [mm], leading to a total height of 2950 [mm]. However, if TUB is loaded in the West-East direction, then the length of the vertical elements will be equal to 670 [mm], leading to a total height of 3350 [mm].

The vertical blue elements in Figure 3.12 are considered as beams elements. This is why they are modeled by inelastic displacement-based frame elements in SeismoStruct [21]. The horizontal elements in Figure 3.12 are, as explained in Section 2.3.2, rigid links that connect the vertical elements together. In Seismostruct software, these rigid elements are modeled by using elastic frame elements with a high flexural and shear rigidity.

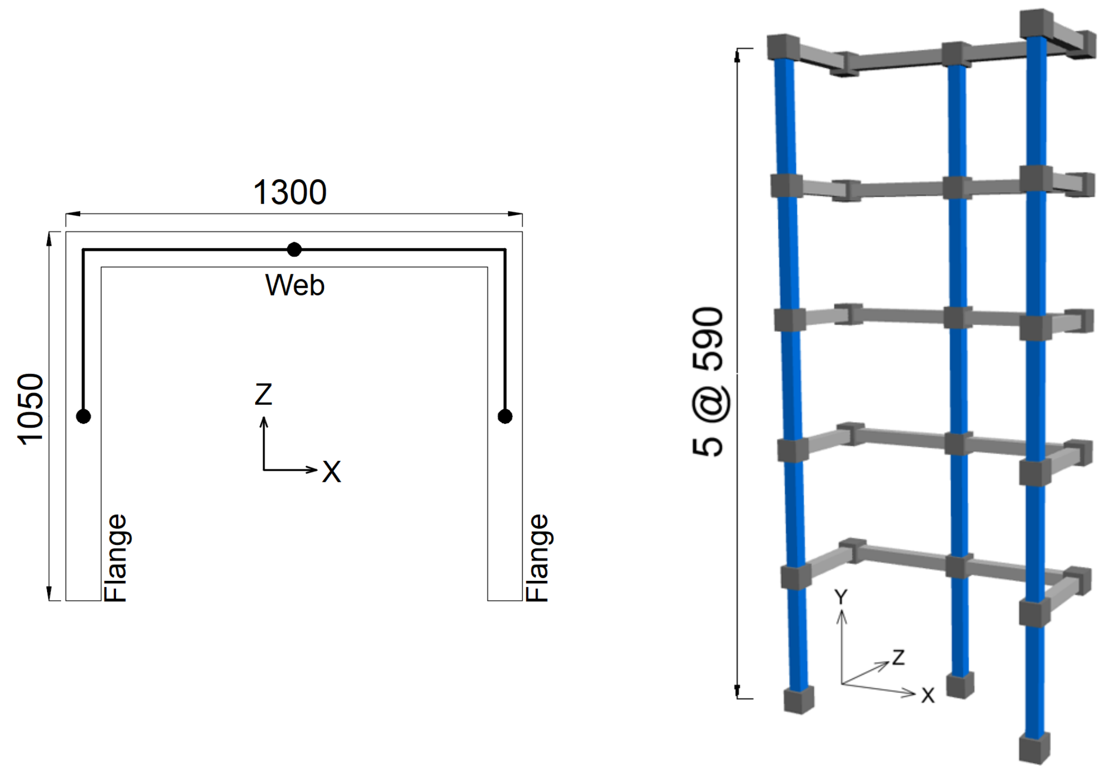

Figure 3.12: Plan and elevation views of the wide-column model for TUB [Unit: mm].

From this wide-column model, by making a pushover analysis it can be obtained the values of the base shear in the wall, i.e., the horizontal force at the bottom of the wall, as a function of the relative top displacement. In Figures 3.13, 3.14, 3.15 and 3.16, the red curves correspond to the wide-column model results of wall TUB when it is horizontally loaded in the South-to-North, North-to-South, West-to-East and East-to-West directions. Those results can be compared to the experimental data which correspond to the blue curves.

When loaded from the South to North direction, the wide-column model results of TUB in Figure 3.13 are really good up to a top displacement equal to about 10 [mm] since the red curve is very close to the blue one. However, after a top displacement equal to 10 [mm], the wide-column model of TUB begin to underestimate the base shear. In Figure 3.14, when the wall is loaded from the North to South direction, the wide-column model is again really good up to a top displacement equal to about 10 [mm]. After that, the model starts to overestimate the base shear. As it can be observed in Figures 3.15 and 3.16 when the wall is respectively loaded from the West to East and from the East to West direction, the wide-column model is everywhere underestimating the value of the base shear.

Concerning the initial stiffness, we can see in Figures 3.13 and 3.14, that the slope at the beginning of the wide-column model curve is pretty much the same as the one from the corresponding experimental data curve, meaning that they have almost the same initial stiffness. However, this is not the case when the wall is loaded from the West to East and the East to West direction as shown in Figures 3.15 and 3.16.

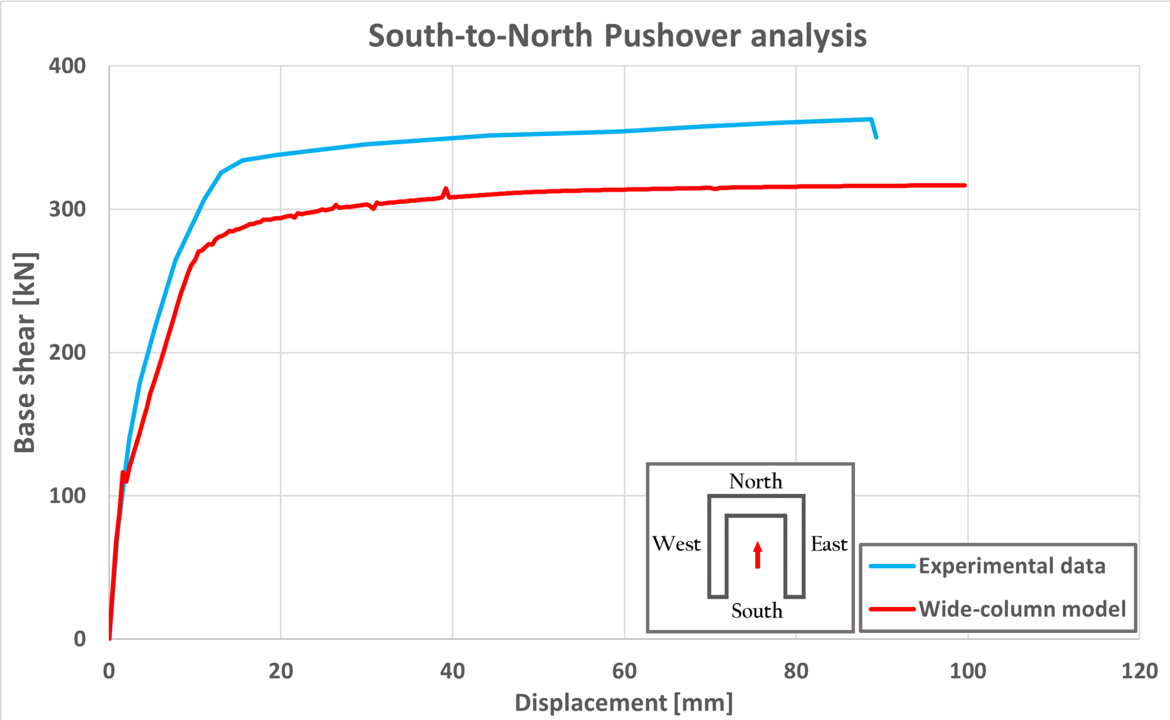

Figure 3.13: TUB: Force-displacement relationship when loaded from South to North.

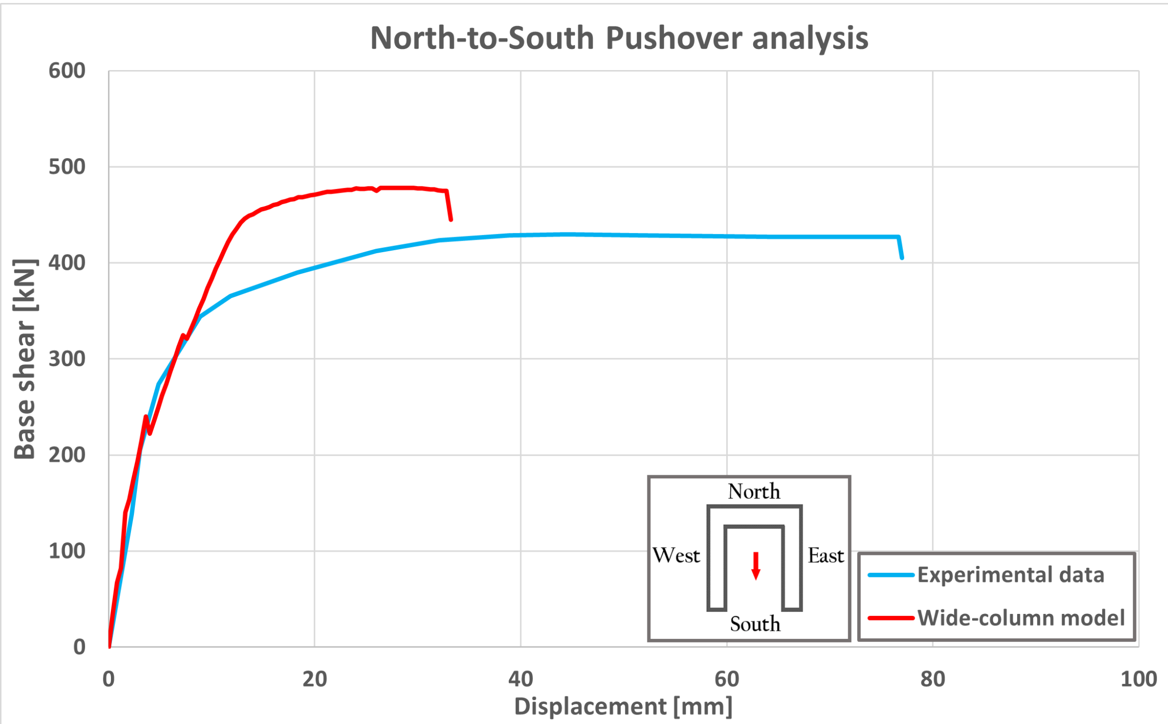

Figure 3.14: TUB: Force-displacement relationship when loaded from North to South.

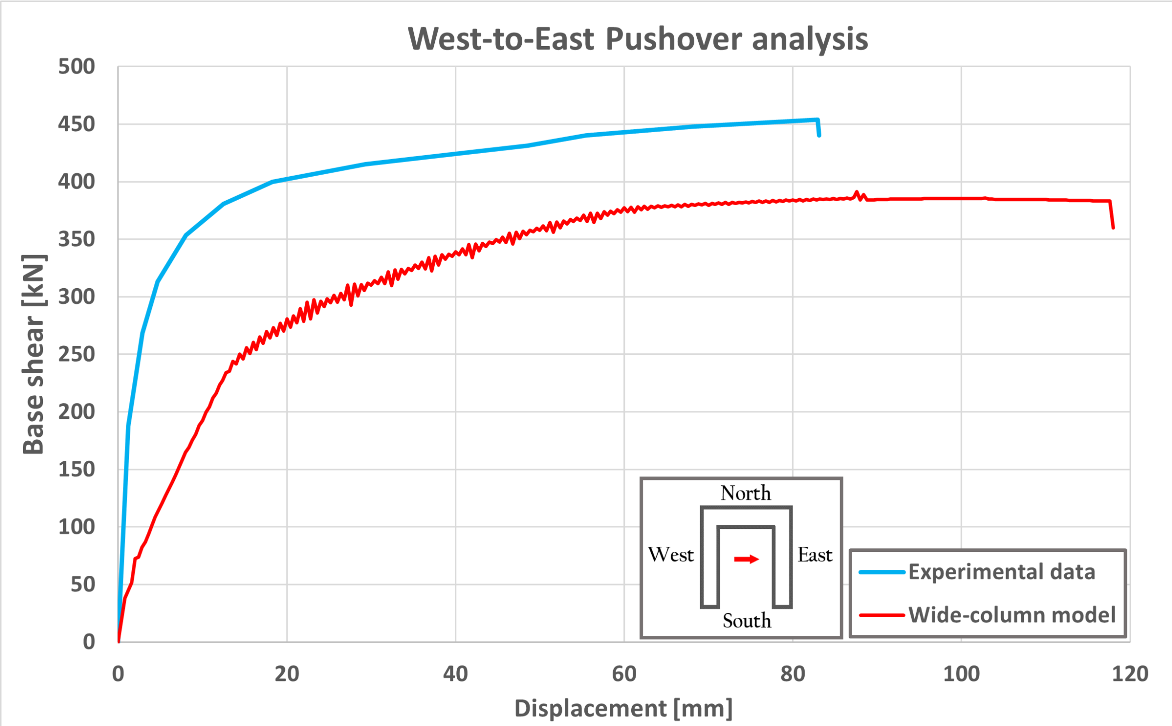

Figure 3.15: TUB: Force-displacement relationship when loaded from West to East.

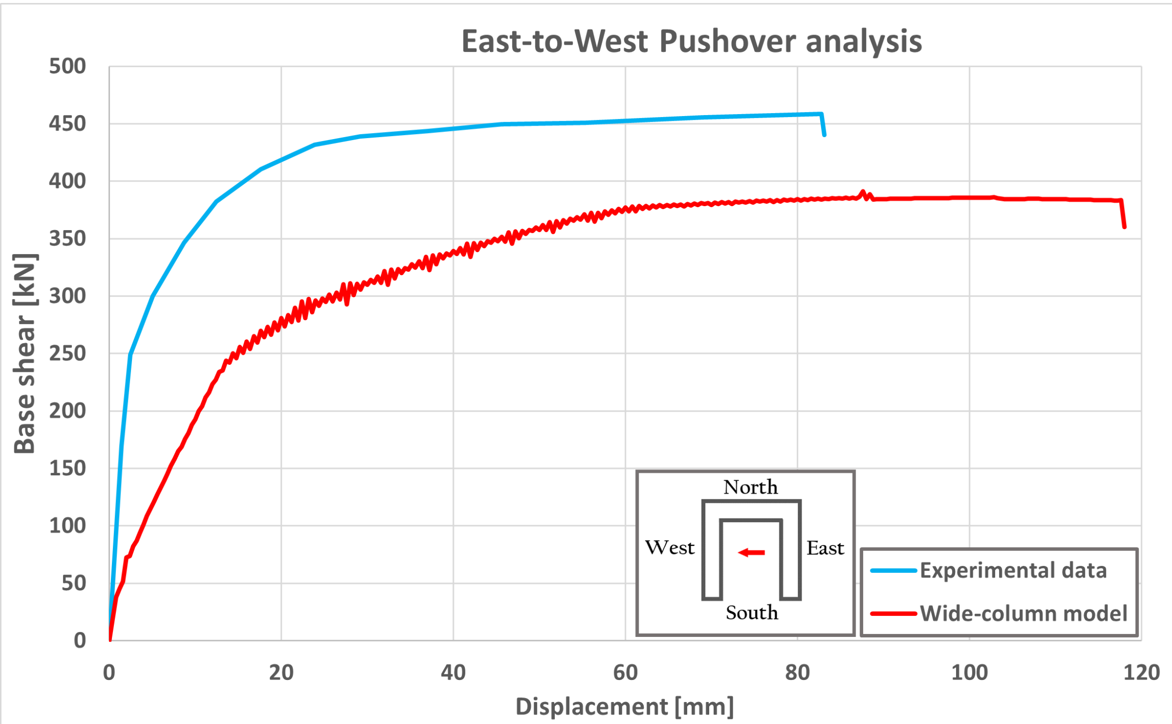

Figure 3.16: TUB: Force-displacement relationship when loaded from East to West.

3.5 Beam-truss model: Comparison

3.5.1 Definition of characteristic points

On each beam-truss model curve that will be presented in this report, some characteristic points will be indicated. The definitions of these points are as follows:

- The "Spalling of the vertical elements of concrete" is reached when the first vertical element of concrete in the beam-truss model has a compressive strain equal to 0.0035. The strain of an element can be defined as the ratio between the length of the element after a certain deformation and its initial length.
- The "Crushing of concrete" is reached when the first vertical element of confined concrete, i.e., concrete that is inside steel hoops, in the beam-truss model has a compressive strain equal to the following expression that was proposed by Paulay and Priestley (1992) [20]:

$$0.004 + \frac{1.4 \cdot \rho_s \cdot f_{ym} \cdot \epsilon_u}{f_{cm,c}}$$

  In the expression above, ρ_s is the volumetric ratio of the confining steel (hoops), i.e., the ratio between the volume of confining steel and the volume of concrete of the element, f_{ym} is the yield strength of the confining steel, ϵ_u corresponds to the ultimate tensile strain of the longitudinal bars and $f_{cm,c}$ is the confined compressive concrete strength. This latter value can be directly taken from the SeismoStruct software.

- The "Yielding of steel" is reached when the first longitudinal steel bar of the wall reaches its yield tensile strain. This value is given for each wall in their corresponding steel properties table and is denoted by ϵ_y.
- The "Fracture of steel" is achieved when the first longitudinal steel bar of the wall reaches 60 percent of its ultimate tensile strain. This ultimate tensile strain is given for each wall in their corresponding steel properties table and is denoted by ϵ_u.
- The "Spalling of the diagonal elements of concrete" is reached when the first diagonal element of concrete in the beam-truss model has a compressive strain equal to 0.0035.

3.5.2 WSH4: Beam-truss model

The plan and elevation views of the beam-truss model of wall WSH4 is represented in Figure 3.17. As we can see on the plan view of Figure 3.17, WSH4 cross-section is divided into 6 parts. Both extremities parts of the wall are modeled by using inelastic force-based frame vertical elements in SeismoStruct [21]. Indeed, as we can see in the elevation view of Figure 3.17, the two parts at each extremities of the wall use 14 vertical elements of 300 $[mm]$ length and 1 vertical element of 360 $[mm]$ length at the top of the wall. All the other elements that are used in the model, i.e., the vertical elements between those at the two extremities, the horizontal elements and the diagonal elements are modeled by using inelastic truss elements in SeismoStruct software [21].

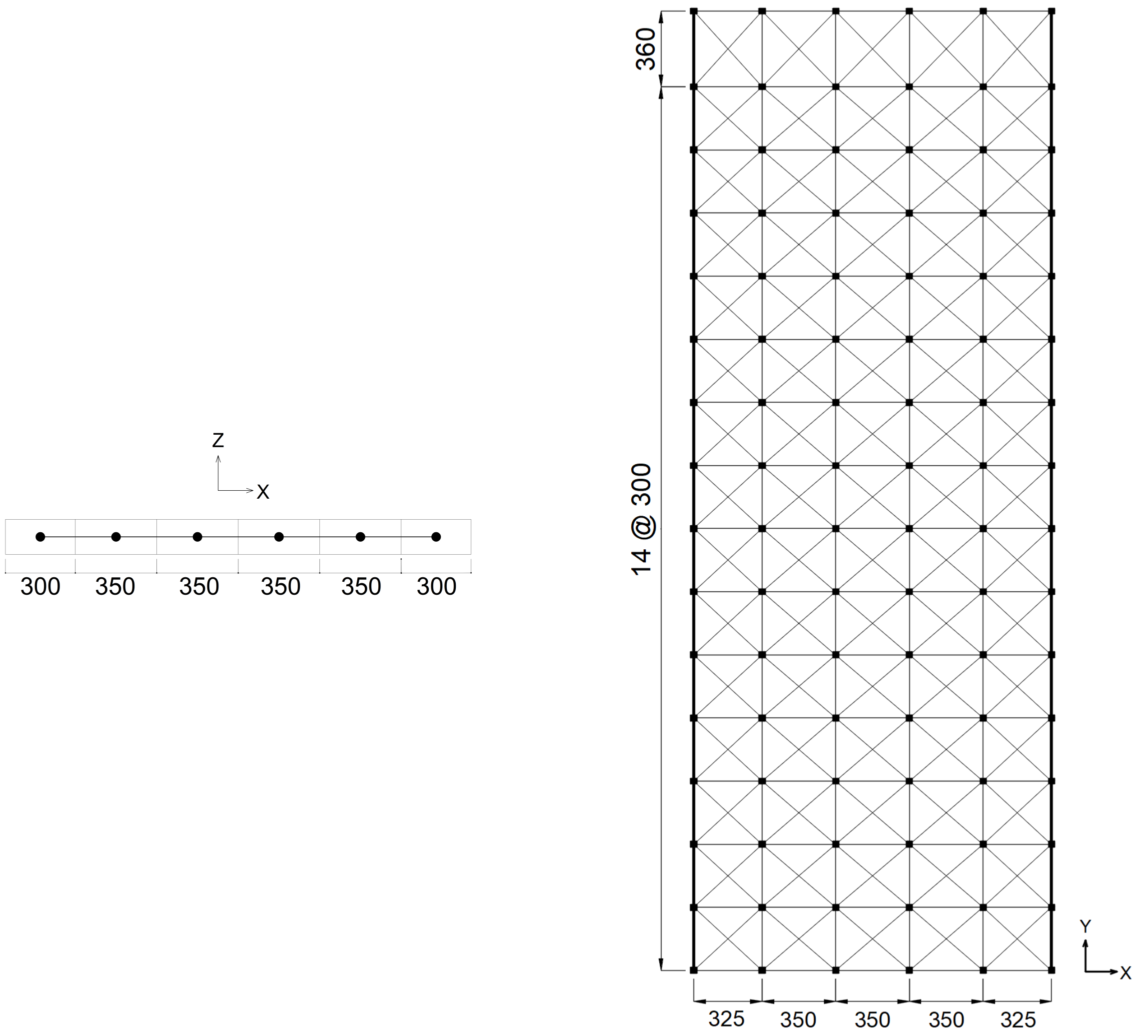

Figure 3.17: Plan and elevation views of the beam-truss model for WSH4 [Unit: *mm*].

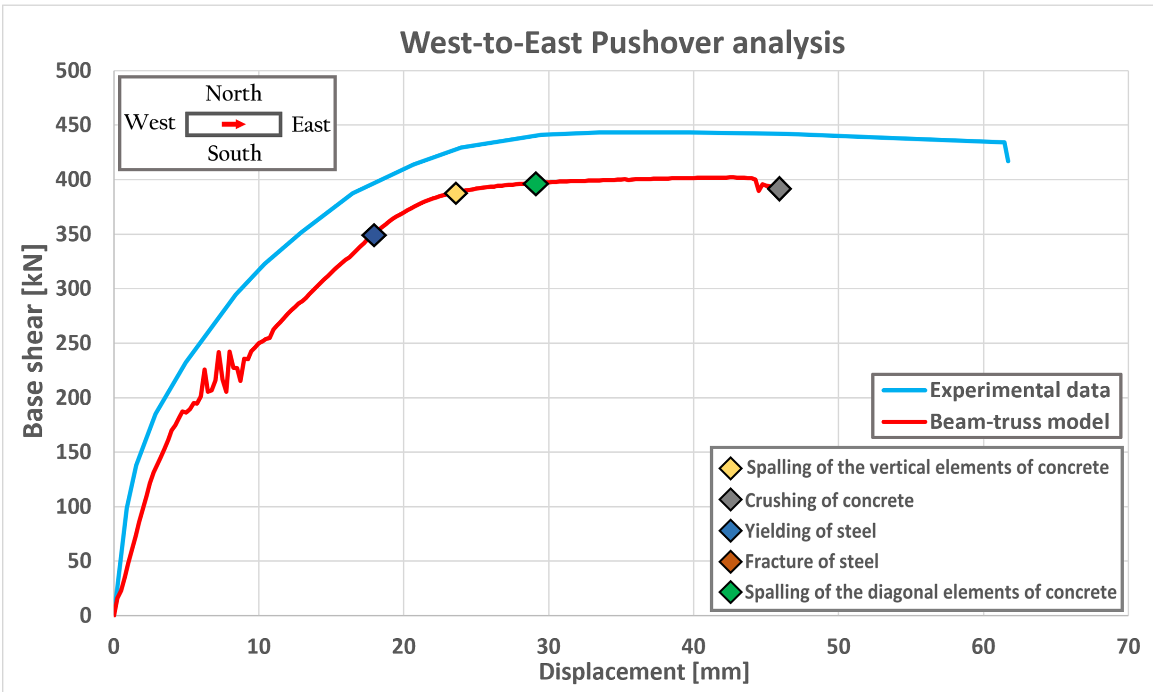

Figure 3.18: WSH4: Force-displacement relationship when loaded from West to East.

From this beam-truss model, it can be done a pushover analysis in the West-to-East direction of the wall. The results of the beam-truss model are shown in Figure 3.18 and are represented by the red curve. A comparison between these results and the experimental data that correspond to the blue curve in Figure 3.18. We can see that the base shear values obtained with the beam-truss model are underestimated compared to the one from the experimental data. However, those results are quite good since the maximum base shear difference between both beam-truss model and experimental data curves is equal to about 50 $[kN]$.

3.5.3 TUB: Beam-truss model

The plan and elevation views of the beam-truss model of wall TUB is represented in Figure 3.19. Indeed, the elevation views of the flange and the web of the wall is only valid when a pushover analysis in the South-North direction is done because the actuators that applied the horizontal forces in the South-North direction are placed at a height of 2950 $[mm]$. If the wall is loaded in the West-East direction, then instead of having 9 @ 328, i.e., 9 vertical elements of 328 $[mm]$ length, there will be 7 @ 478 in such a way that the total height of the model is equal to 3350 $[mm]$, i.e., the height where the West-East actuator is.

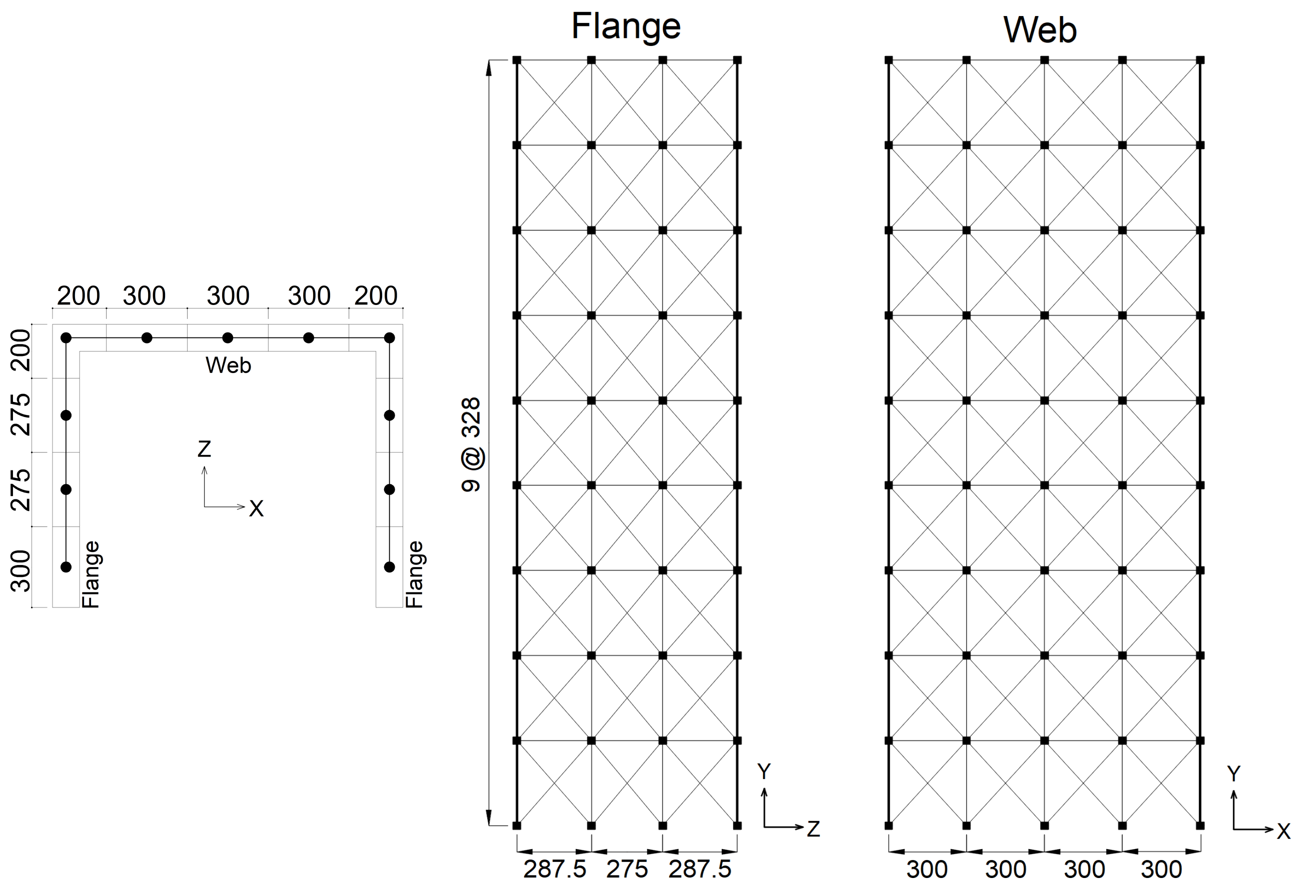

Figure 3.19: Plan and elevation views of the beam-truss model for TUB [Unit: mm].

As shown in Figure 3.19, the TUB cross-section is divided into 11 parts. All the vertical elements that modeled the two South extremities parts of flanges and the corner parts, i.e., the parts at the intersection between the flanges and the web, of the wall are modeled with inelastic force-based frame vertical elements in SeismoStruct [21]. All the other elements that are used in the model, i.e., the vertical elements between those that are force-based, the horizontal elements and the diagonal elements are modeled by using inelastic truss elements in SeismoStruct software [21].

Pushover analysis in the South-to-North, North-to-South, West-to-East and East-to-West directions were performed on wall TUB. Figures 3.20, 3.21, 3.22 and 3.23 show the evolution of the base shear as a function of the horizontal displacement at the top of the wall in each direction. The beam-truss model results correspond to the red curves and can be compared with the experimental data that correspond to the blue curves. In addition, the results can also be compared to the numerical data from paper which correspond to the green curves in Figures 3.20, 3.21, 3.22 and 3.23. Those numerical data from paper have been taken from document [16] written by Y. Lu & al. (2014) and that also modeled TUB like a beam-truss model.

In Figure 3.20, when TUB is loaded from the South to North direction, it can be seen that the beam-truss model curve approximates fairly well the experimental data curve. Indeed, the beam-truss model results are more accurate than the numerical data from paper after a top displacement equal to about 20 $[mm]$. When the wall is loaded from North to South, we can see in Figure 3.21 that the beam-truss model curve matches really well with the experimental data since the red curve is really close to the experimental data curve whereas the numerical data from paper do not. Finally, in Figures 3.22 and 3.23, when the wall is loaded either in the West to East direction or the East to West direction, the beam-truss model results underestimate the real base shear from the experimental data curve of a maximum value equal to about 50 $[kN]$.

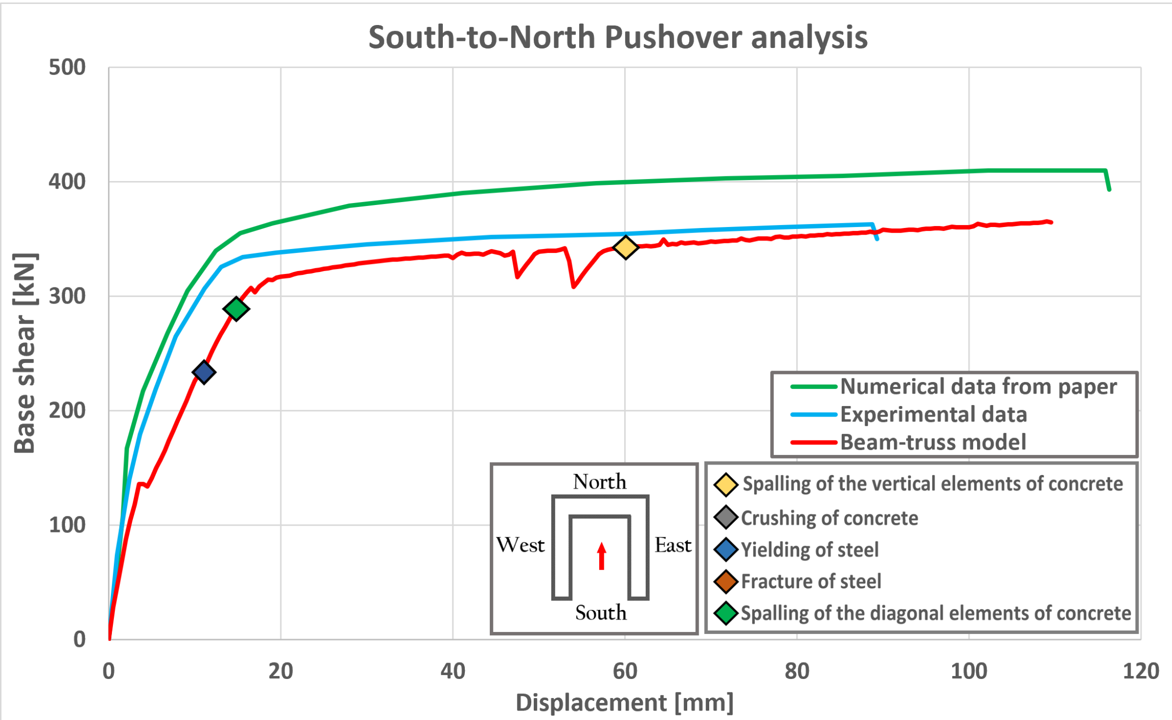

Figure 3.20: TUB: Force-displacement relationship when loaded from South to North.

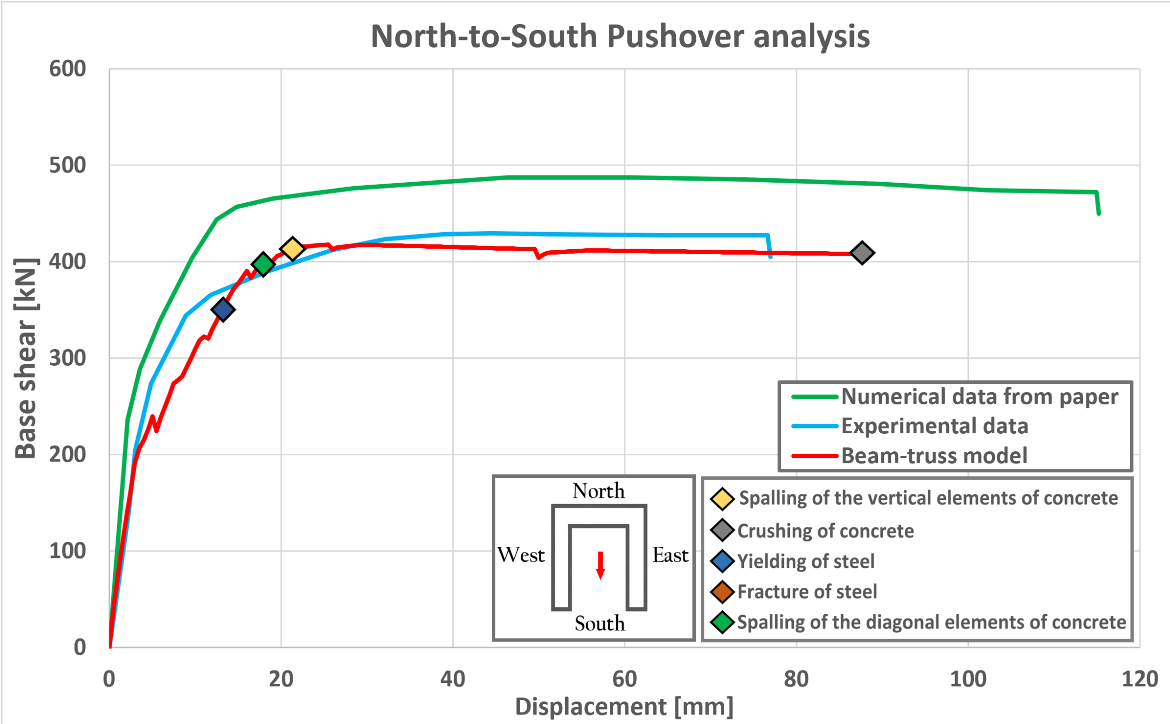

Figure 3.21: TUB: Force-displacement relationship when loaded from North to South.

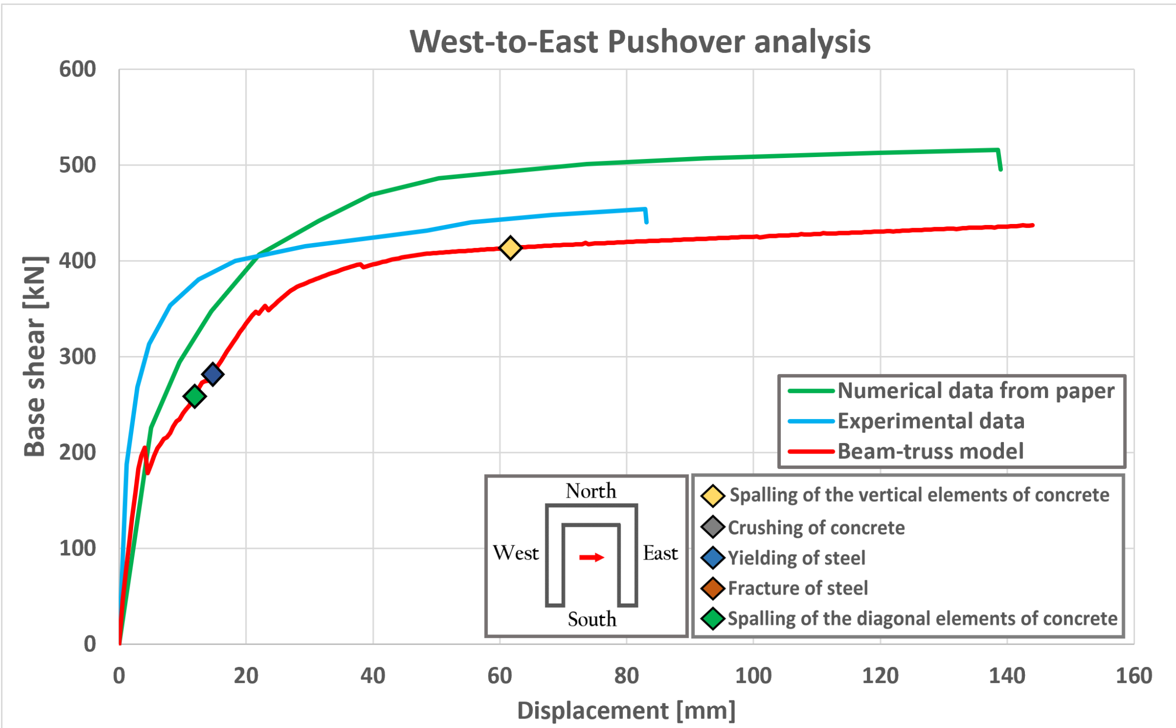

Figure 3.22: TUB: Force-displacement relationship when loaded from West to East.

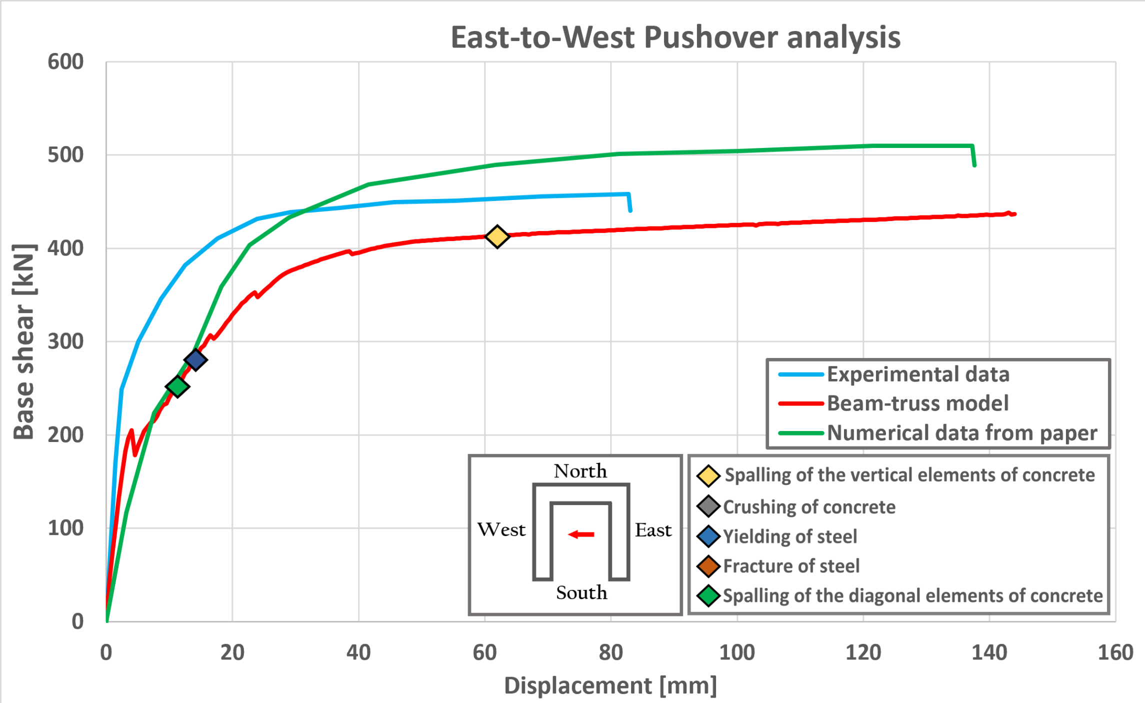

Figure 3.23: TUB: Force-displacement relationship when loaded from East to West.

3.6 Beam-truss model: Validation

Figure 3.24 shows a comparison between the pushover analysis results that were obtained with the stick model, wide-column model and beam-truss model of wall WSH4 when this latter is horizontally loaded from the West to East direction.

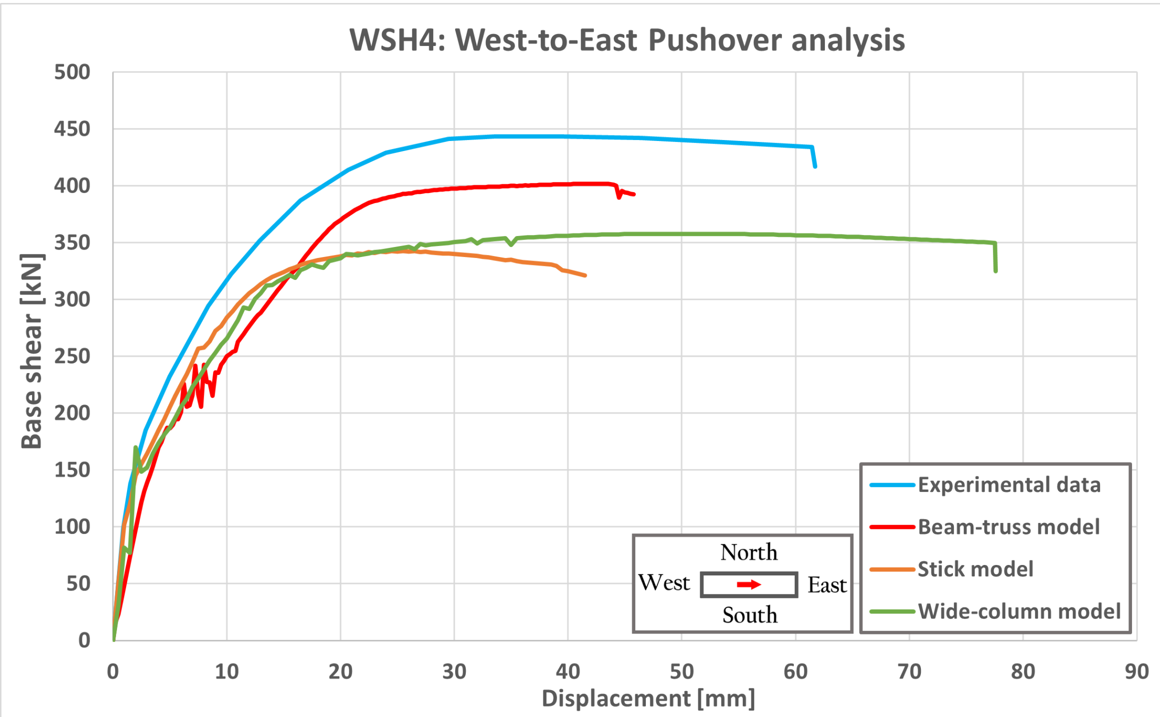

Figure 3.24: WSH4: Force-displacement relationship when loaded from West to East.

As shown in Figure 3.24, all model types give approximately the same result up to a value for the top displacement of the wall equal to about 17 [mm]. After this top displacement of 17 [mm], it is clearly the beam-truss model of wall WSH4 that gives the most accurate results since the red curve in Figure 3.24 is the one that is closest to the blue curve that represent the experimental data.

The same comparison can be done for wall TUB. Figure 3.25 shows the results obtained with the different model types when the wall is loaded from the North to South direction.

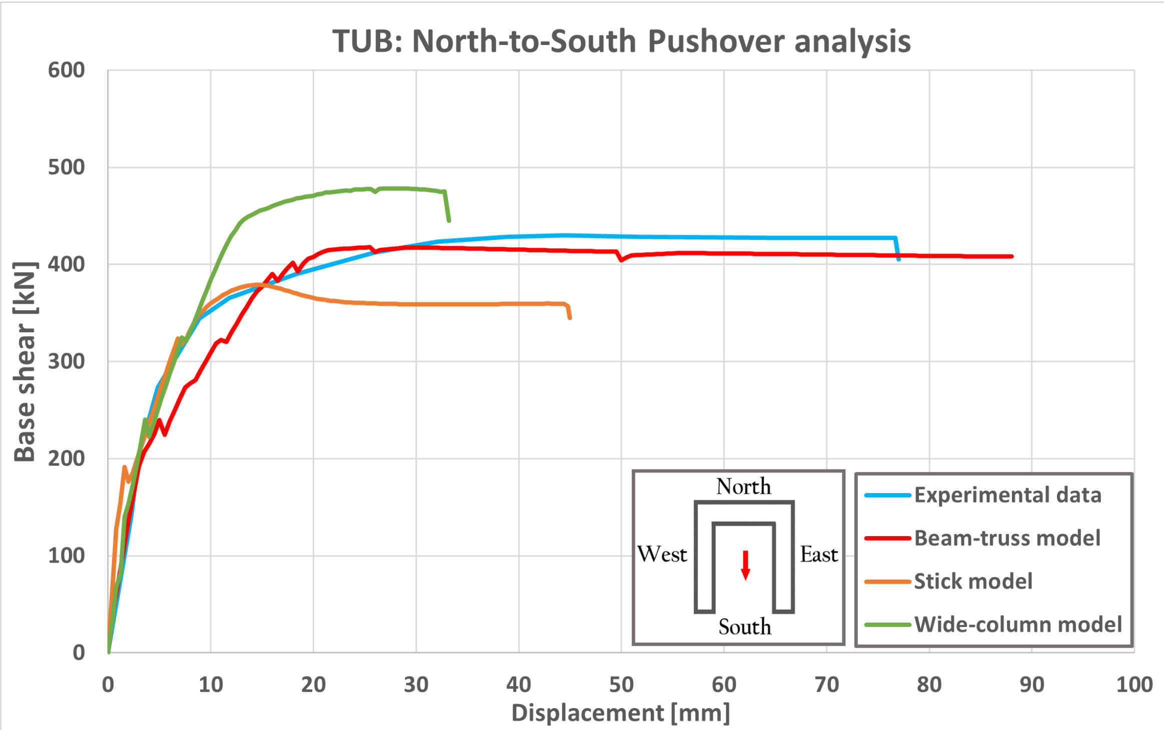

Figure 3.25: TUB: Force-displacement relationship when loaded from North to South.

We can see in Figure 3.25 that up to a displacement equal to about 5 [mm], all the model types of TUB give approximately the same results. For a top displacement that is range between 5 [mm] and 15 [mm], the stick and wide-column models have better results than the one obtained with the beam-truss model. However, after a top displacement of 15 [mm], it is the beam-truss model that gives the more accurate results since the red curve in Figure 3.25 is the one that is closest to the blue curve that represent the experimental data.

3.7 Conclusion

As a conclusion, all walls that will be analysed in Chapter 4 will be modeled with the beam-truss model approach since it seems the most accurate option. Another motivation for only building numerical models like beam-truss models is that these latter do not need for the designer to make many assumptions, opposed to the case of the wide-column models.

Chapter 4

Beam-truss modelling of complete database

This chapter aims at showing the numerical results coming from modelling rectangular and non-rectangular cross-sections walls. Note that these walls have a shear span ratio, i.e., the ratio between the height and the length of the wall, larger than 1.

4.1 Rectangular walls

4.1.1 Unit 1.0

4.1.1.1 Geometry

Unit 1.0 is a barbell-shaped section wall as shown in Figure 4.1. The properties and geometry of the wall are taken from document [17] written by J.M. Mestyanek (1986). Unit 1.0 is 2.5 [m] high and 2.5 [m] long. It can be therefore deduced that this wall has a shear span ratio, i.e., the ratio between the height and the length of the wall, equal to 1. The part of the wall between the barbels is 0.1 [m] thick. There is no axial load applied on top of the wall.

There are 8 longitudinal bars having a diameter of 12 [mm] in each barbel and there are 13 longitudinal bars having a diameter of 6 [mm] spaced 180 [mm] apart from each other between the two barbels. Regarding the transverse reinforcement, there are 6 [mm] diameter bars spaced 180 [mm] apart that cross the full length of the wall and hoops of 6 [mm] diameter spaced 70 [mm] apart in each barbel.

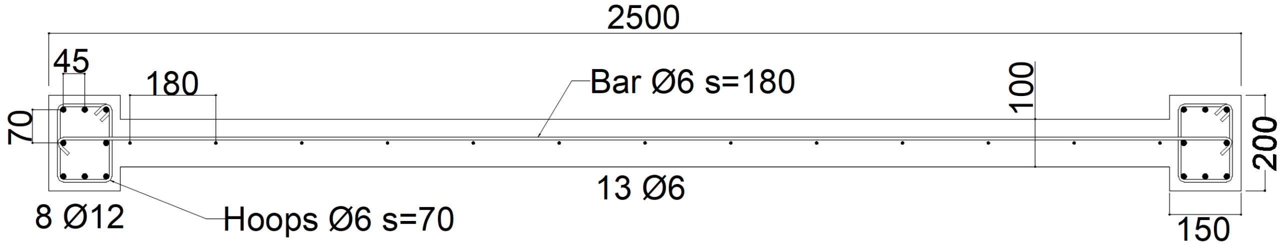

Figure 4.1: Unit 1.0: Cross section and reinforcement detailing [Unit: mm].

Figure 4.2 shows the plan and elevation views for the beam-truss model of the wall. As shown in the figure, the wall section is divided into 11 parts. The two parts at the extremities, i.e., the barbels, of the wall are modeled with inelastic displacement-based frame elements whereas the other vertical element are modeled with inelastic truss elements. The diagonal and horizontal elements are also modeled with inelastic truss elements.

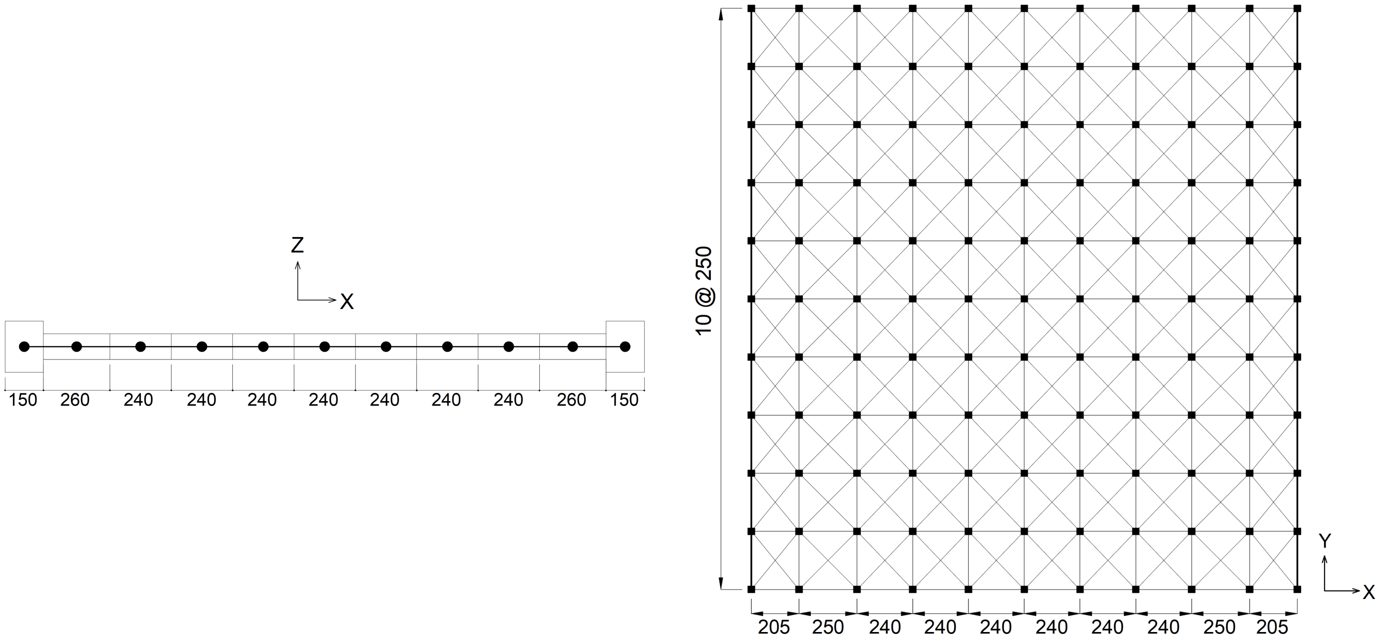

Figure 4.2: Plan and elevation views of the beam-truss model for Unit 1.0 [Unit: mm].

4.1.1.2 Material properties

Tables 4.1 and 4.2 list respectively the properties for the steel reinforcement and the concrete that are used in the beam-truss model. Note that the tensile strength of concrete is considered as equal to zero for diagonal and horizontal elements.

Steel Mechanical Properties				
		Rebar $\phi 6$	Rebar $\phi 12$	
Diameter	d	6	12	mm
Modulus of elasticity	E_s	190	193	GPa
Yield tensile strength	f_y	472	451	MPa
Ultimate tensile strength	f_u	658	608	MPa
Yield strain	ϵ_y	0.248	0.234	%
Ultimate strain	ϵ_u	20	29	%
Strain hardening parameter	α	0.496	0.283	%
Specific weight	γ	78	78	kN/m^3

Table 4.1: Steel mechanical properties.

Concrete Mechanical Properties			
Compressive concrete strength	f_c	27	MPa
Tensile concrete strength	f_t	3.15	MPa
Modulus of elasticity	E_c	24.41	GPa
Strain at peak stress	ϵ_c	0.2	%
Specific weight	γ	24	kN/m^3

Table 4.2: Concrete mechanical properties.

4.1.1.3 Analysis output

Pushover analyses in the West-to-East direction and in the East-to-West direction were performed on Unit 1.0. The results of those tests are presented in Figures 4.3 and 4.4 in which the displacements correspond to the displacements at the top of the wall.

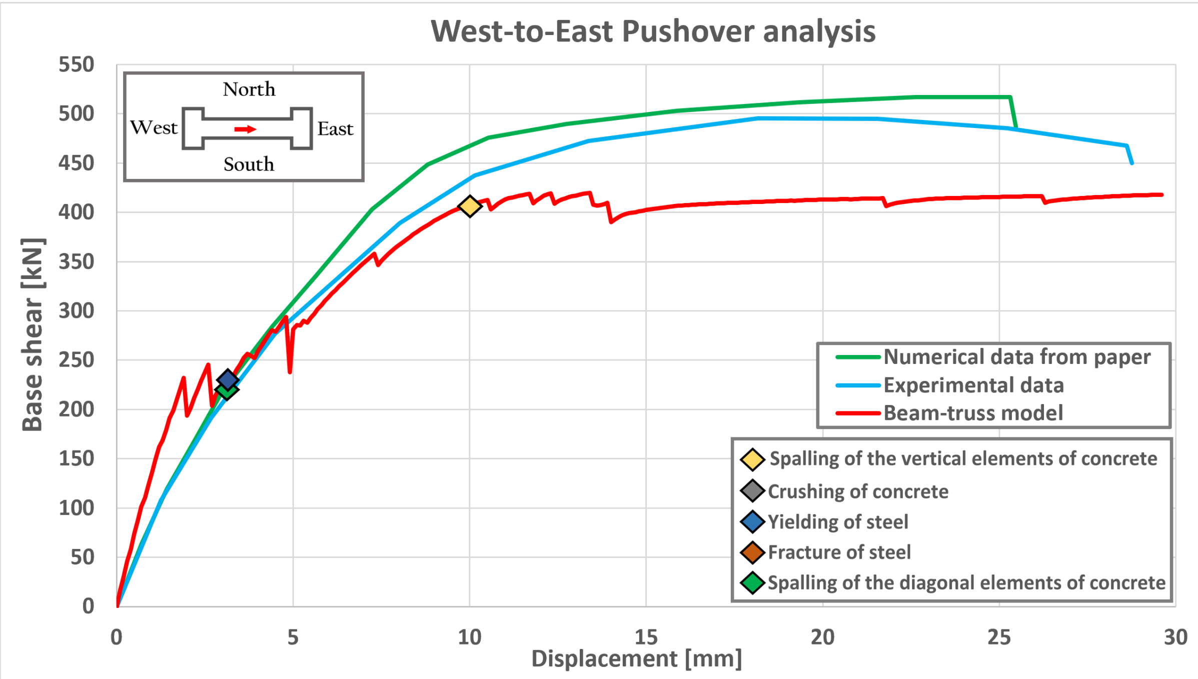

Figure 4.3: Unit 1.0: Force-displacement relationship when loaded from West to East.

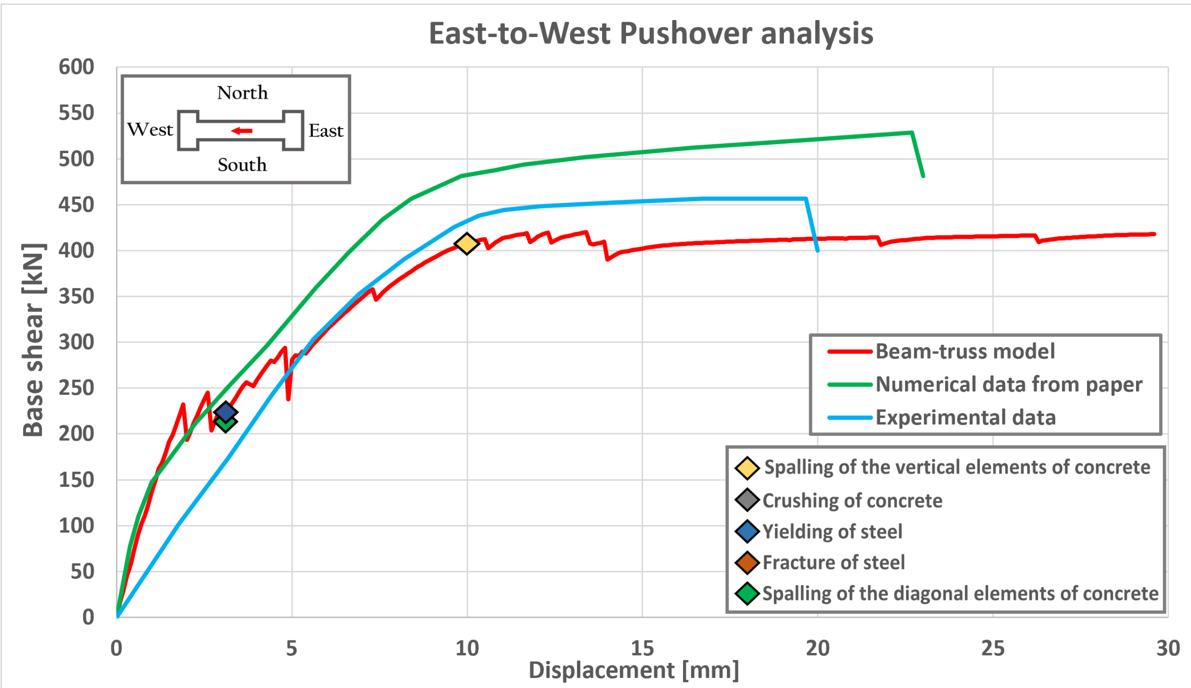

Figure 4.4: Unit 1.0: Force-displacement relationship when loaded from East to West.

The results for the beam-truss model that has been presented, which correspond to the red curves in Figures 4.3 and 4.4, were obtained using the SeismoStruct software. The numerical data from paper, which correspond to the green curves in Figures 4.3 and 4.4, have been taken from document [16] written by Y. Lu & al. (2014) and that also modeled the wall using the beam-truss model.

For both graphs depicted in Figures 4.3 and 4.4, the results of the beam-truss model are the same since the wall is symmetrical. In Figure 4.4, when loaded from East to West, we can see that globally the result of the beam-truss model is more accurate than the numerical data from paper made by Y. Lu & al. as the red curve is closer to the experimental data curve. This is not the case when the wall is loaded from West to East.

Concerning the initial stiffness, we can see in Figure 4.3 that the numerical data from paper is more accurate than the beam-truss model curve since its initial slope is close to the one from the experimental data. However, in Figure 4.4, the initial stiffness is almost the same for both beam-truss model curve and numerical data from paper curve.

Finally, note that on both graphs, the yielding of steel and spalling of concrete occur at the same time.

4.1.2 Unit 2.0

4.1.2.1 Geometry

Unit 2.0 is a barbell-shaped section wall as shown in Figure 4.5. The properties and geometry of the wall have been taken from document [17] written by J.M. Mestyanek (1986). Unit 2.0 is 2.5 $[m]$ high and 1.25 $[m]$ long. Its shear span ratio, i.e., the ratio between the height and the length of the wall, is therefore equal to 2. The part of the wall between the barbels is 0.1 $[m]$ thick. There is no axial load applied on top of the wall.

There are 4 longitudinal bars having a diameter of 10 $[mm]$ and 4 one having a diameter of 16 $[mm]$ in each barbel. Between the two barbels, there are 6 longitudinal bars having a diameter of 6 $[mm]$ spaced 180 $[mm]$ apart from each other. Concerning the transverse reinforcement, there are 6 $[mm]$ diameter bars spaced 180 $[mm]$ apart that cross the full length of the wall and hoops of 6 $[mm]$ diameter spaced 90 $[mm]$ apart in each barbel.

Figure 4.6 illustrates the plan and elevation views for the beam-truss model of the wall. The wall section is divided into 9 parts. The two parts at the extremities, i.e., the barbels, of the wall are modeled with inelastic displacement-based frame elements whereas the other vertical elements are modeled with inelastic truss elements. The diagonal and horizontal elements are also modeled with inelastic truss elements.

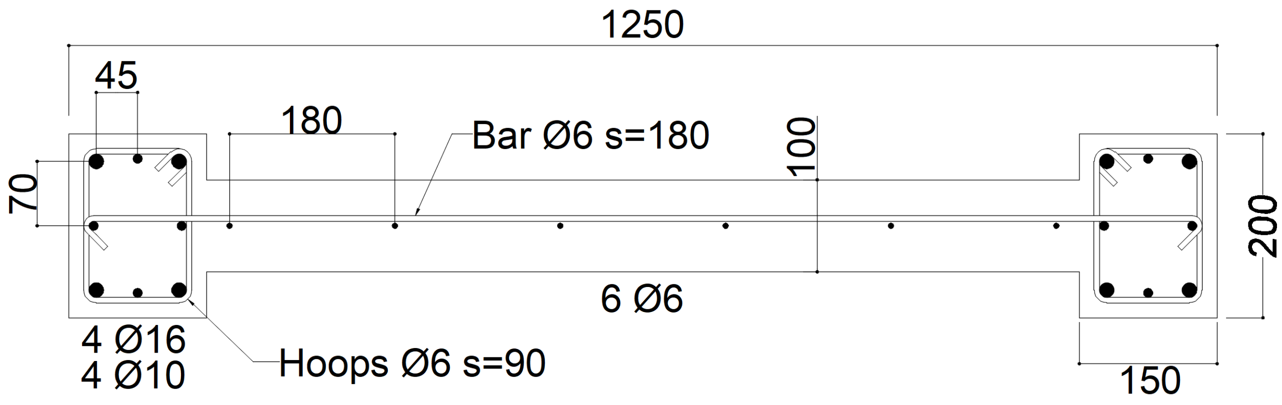

Figure 4.5: Unit 2.0: Cross section and reinforcement detailing [Unit: *mm*].

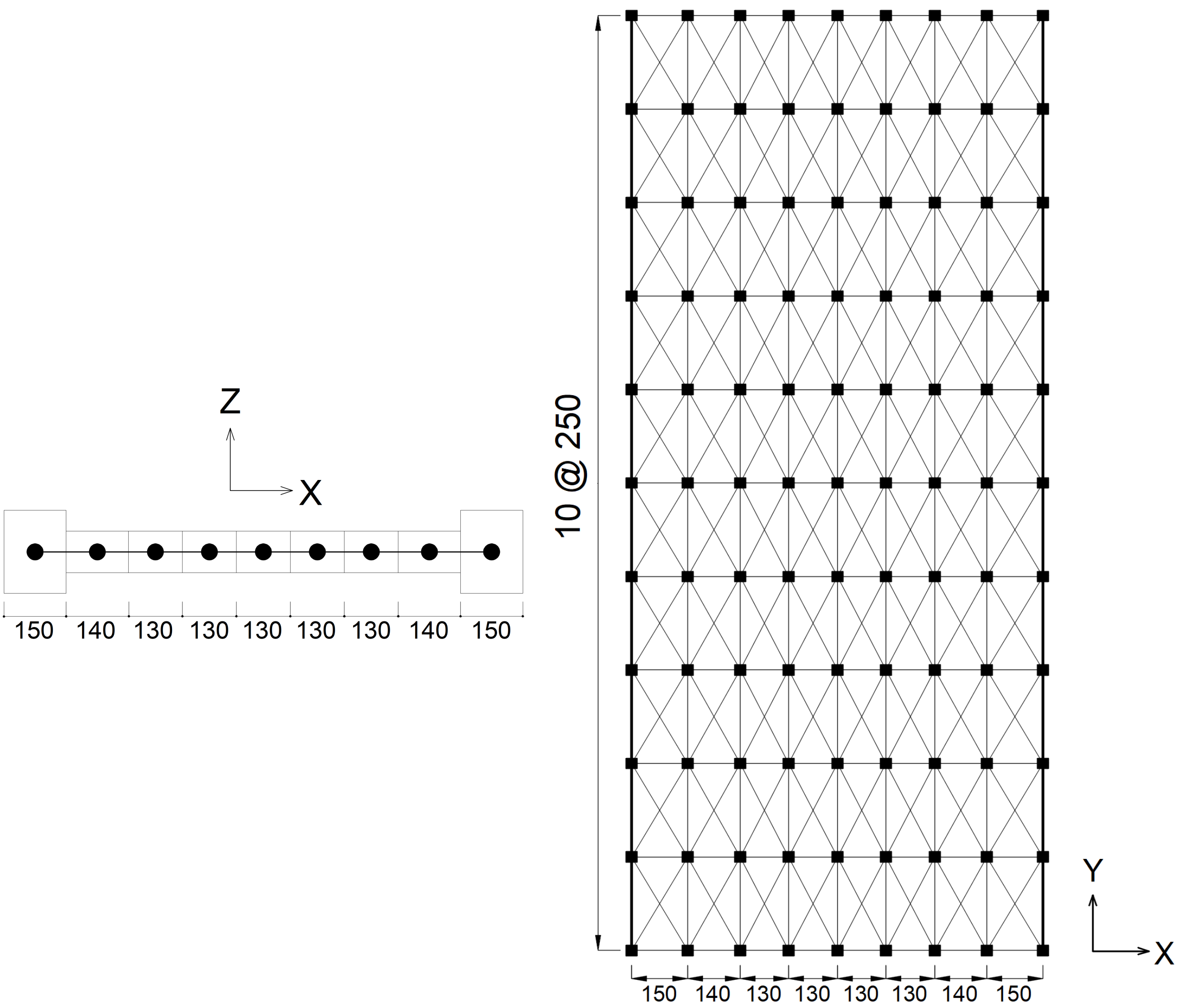

Figure 4.6: Plan and elevation views of the beam-truss model for Unit 2.0 [Unit: *mm*].

4.1.2.2 Material properties

Tables 4.3 and 4.4 present respectively the properties for the steel reinforcement and the concrete that are used in the beam-truss model. Be aware that the tensile strength of concrete is considered as equal to zero for diagonal and horizontal elements.

Steel Mechanical Properties					
		Rebar $\phi 6$	Rebar $\phi 10$	Rebar $\phi 16$	
Diameter	d	6	10	16	mm
Modulus of elasticity	E_s	190	190	198	GPa
Yield tensile strength	f_y	472	443	465	MPa
Ultimate tensile strength	f_u	658	576	638	MPa
Yield strain	ϵ_y	0.248	0.233	0.235	%
Ultimate strain	ϵ_u	20	31	26	%
Strain hardening parameter	α	0.496	0.228	0.339	%
Specific weight	γ	78	78	78	kN/m^3

Table 4.3: Steel mechanical properties.

Concrete Mechanical Properties			
Compressive concrete strength	f_c	26.5	MPa
Tensile concrete strength	f_t	3.3	MPa
Modulus of elasticity	E_c	24.19	GPa
Strain at peak stress	ϵ_c	0.2	%
Specific weight	γ	24	kN/m^3

Table 4.4: Concrete mechanical properties.

4.1.2.3 Analysis output

Pushover analyses in the West-to-East direction and in the East-to-West direction were performed on Unit 2.0. The results of those tests can be seen in Figures 4.7 and 4.8 in which the displacements correspond to the displacements at the top of the wall.

The results for the beam-truss model that we had just explained, which correspond to the red curves in Figures 4.7 and 4.8, were obtained using the SeismoStruct software. The numerical data from paper, which correspond to the green curves in Figures 4.7 and 4.8, have been taken from document [16] written by Y. Lu & al. (2014) and that also modeled the wall using the beam-truss model.

For both graphs depicted in Figures 4.7 and 4.8, the results of the beam-truss model are the same since the wall is symmetrical. In Figure 4.7, when loaded from West to East, we can see that the result of the beam-truss model is more accurate than the numerical data from paper. since the red curve is closer to the experimental data curve. The beam-truss model curve in Figure 4.8 begins to have a really good match with the experimental curve after a top displacement equal to about 12 [mm].

Regarding the initial stiffness, we can see in Figure 4.7 that the beam-truss model curve is more accurate than the numerical data from paper curve since its initial slope is close to the one from the experimental data. However, in Figure 4.8, the initial stiffness of the beam truss model curve is further away than the one of the experimental curve whereas the numerical data from paper curve is a good approximation of the experimental curve.

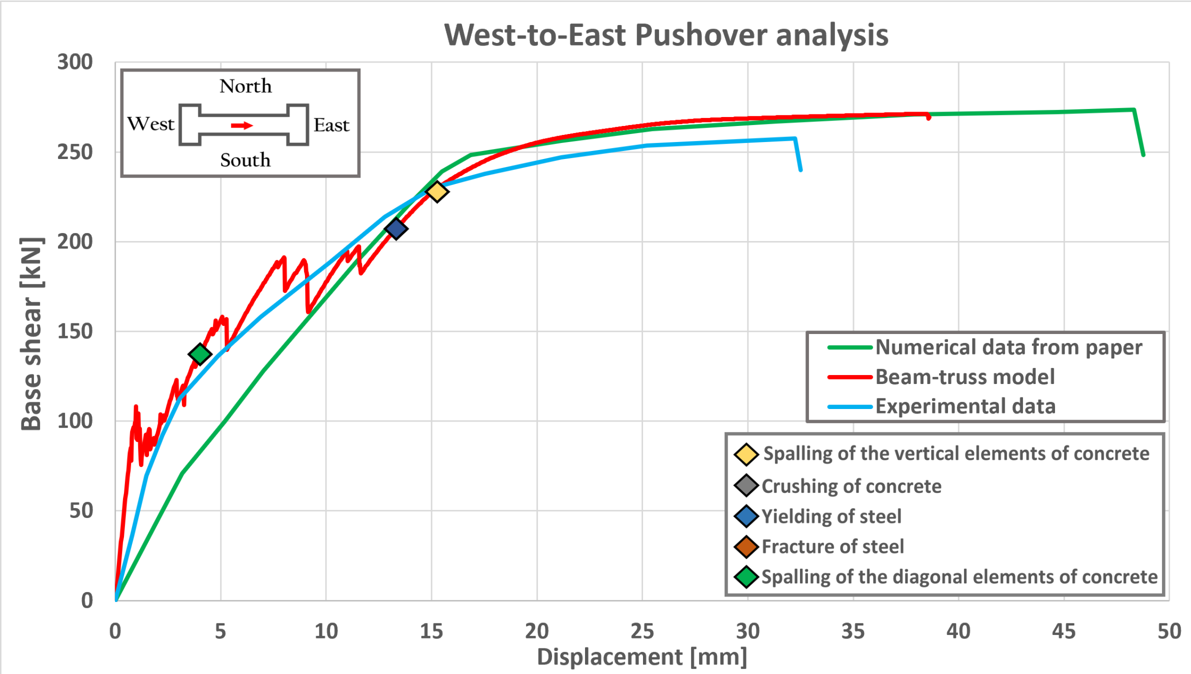

Figure 4.7: Unit 2.0: Force-displacement relationship when loaded from West to East.

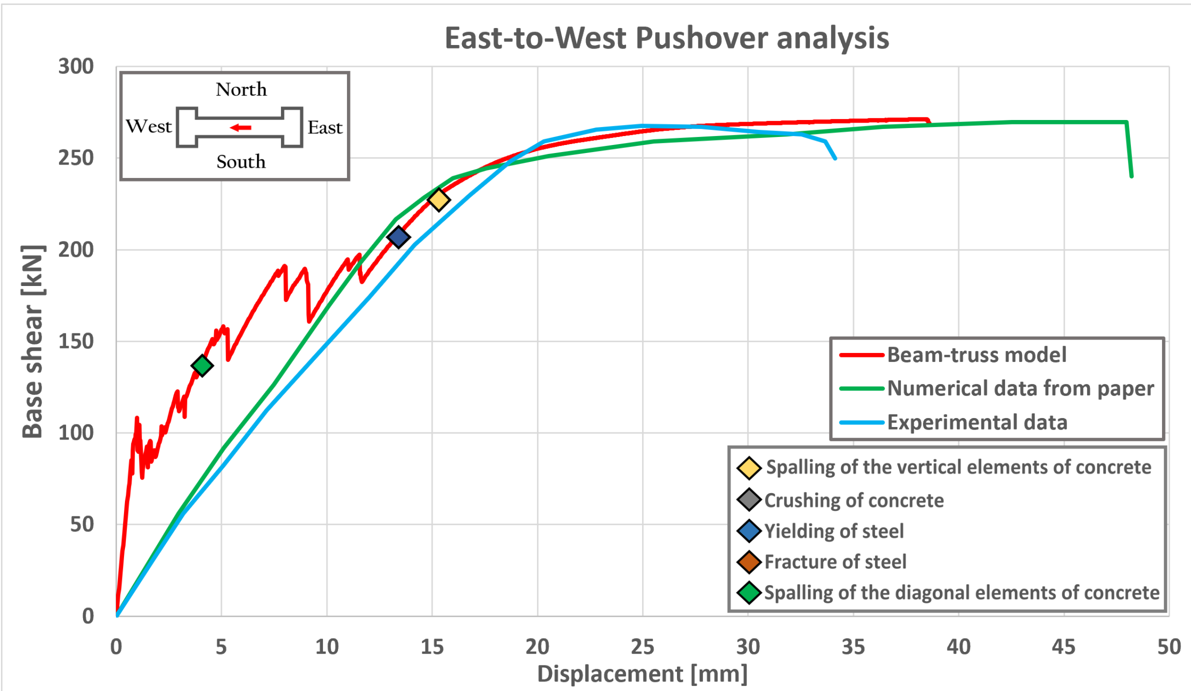

Figure 4.8: Unit 2.0: Force-displacement relationship when loaded from East to West.

4.1.3 RW2

4.1.3.1 Geometry

RW2 is a rectangular section wall as shown in Figure 4.9. The properties and geometry of the wall have been taken from document [25] written by J. H. Thomsen & al. (2004). RW2 is 3.65 $[m]$ high and 1.2 $[m]$ long. It can be therefore deduced that this wall has a shear span ratio, i.e., the ratio between the height and the length of the wall, equal to 3.04. RW2 is 0.1 $[m]$ thick. The axial load ratio of the wall is equal to 7 [%] which means that there is a total axial load of 367 $[kN]$ applied at the top of the wall.

RW2 is confined in each of its extremities by hoops of 4.8 $[mm]$ diameter spaced 51 $[mm]$ apart. In those confined boundaries, there are 8 longitudinal bars having a diameter of 9.5 $[mm]$. In the unconfined zone of the wall, there are 8 longitudinal bars having a diameter of 6.4 $[mm]$. Regarding the transverse reinforcement, there are two sets of 6.4 $[mm]$ diameter bars spaced 190 $[mm]$ apart that cross the full length of the wall.

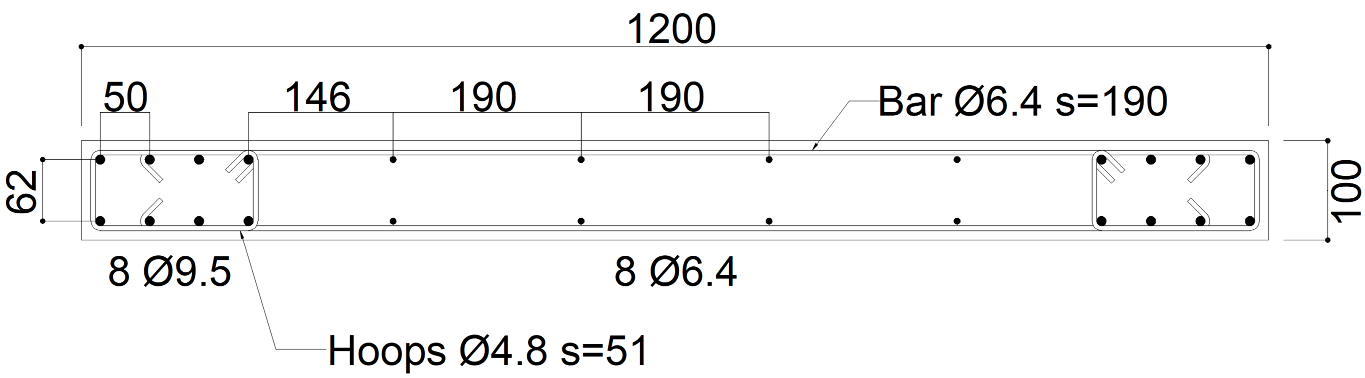

Figure 4.9: RW2: Cross section and reinforcement detailing [Unit: mm].

Figure 4.10 shows the plan and elevation views for the beam-truss model of the wall. The wall section is divided into 5 parts. The two vertical parts at the extremities of the wall are modeled with inelastic displacement-based frame elements whereas the other vertical elements are modeled with inelastic truss elements. The diagonal and horizontal elements are also modeled with inelastic truss elements.

4.1.3.2 Material properties

Tables 4.5 and 4.6 present respectively the properties for the concrete and the steel reinforcement that are used in the beam-truss model. Note that the tensile strength of concrete is considered as equal to zero for diagonal and horizontal elements.

Concrete Mechanical Properties			
Compressive concrete strength	f_c	43.7	MPa
Tensile concrete strength	f_t	2.13	MPa
Modulus of elasticity	E_c	31	GPa
Strain at peak stress	ϵ_c	0.2	%
Specific weight	γ	24	kN/m^3

Table 4.5: Concrete mechanical properties.

Steel Mechanical Properties					
		Rebar $\phi 4.8$	Rebar $\phi 6.4$	Rebar $\phi 9.5$	
Diameter	d	4.8	6.4	9.5	mm
Modulus of elasticity	E_s	200	200	200	GPa
Yield tensile strength	f_y	448	448	434	MPa
Ultimate tensile strength	f_u	483	586	641	MPa
Yield strain	ϵ_y	0.224	0.224	0.217	%
Ultimate strain	ϵ_u	6	8	10	%
Strain hardening parameter	α	0.3	0.89	1.06	%
Specific weight	γ	78	78	78	kN/m^3

Table 4.6: Steel mechanical properties.

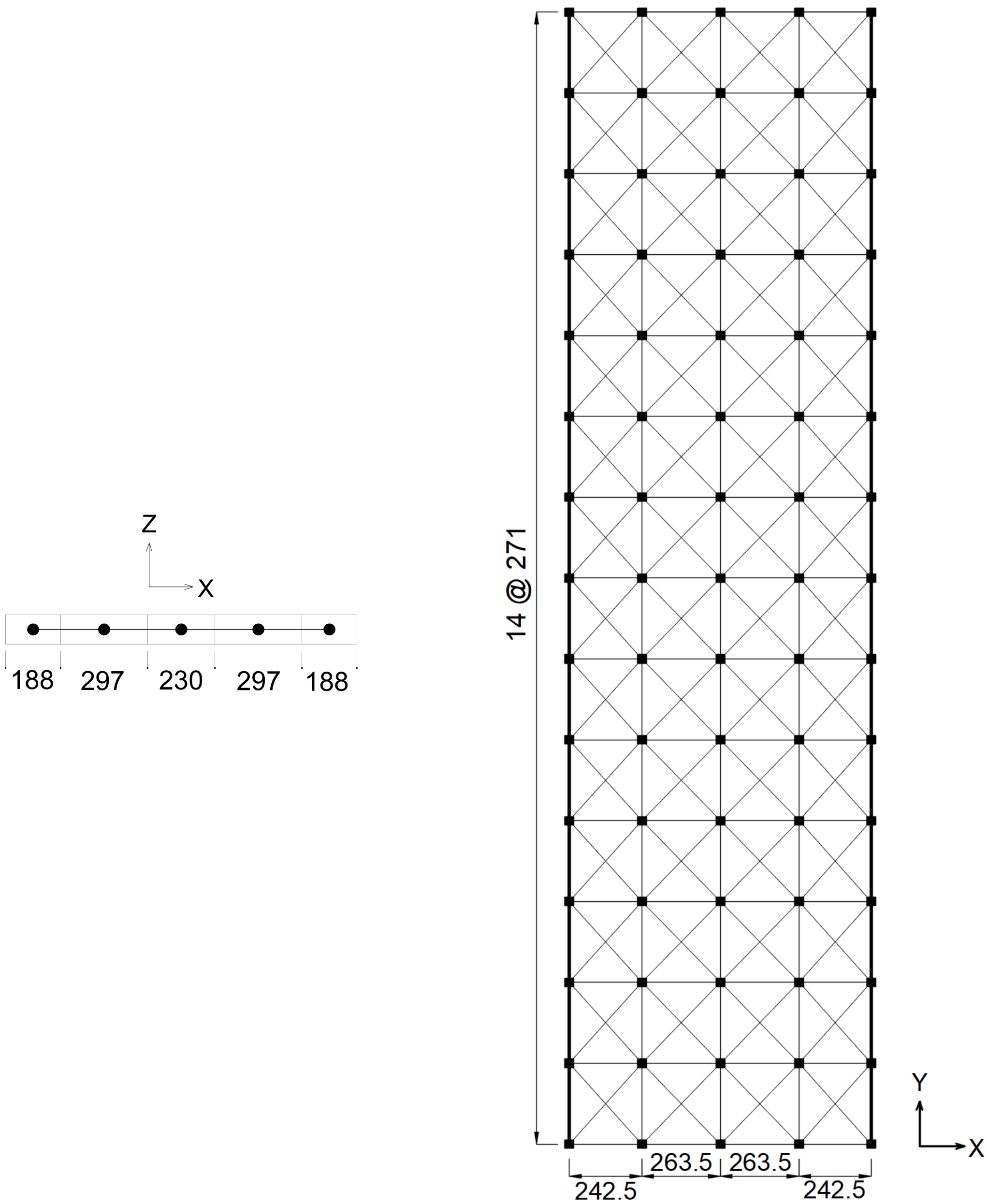

Figure 4.10: Plan and elevation views of the beam-truss model for RW2 [Unit: mm].

4.1.3.3 Analysis output

Pushover analyses in the West-to-East direction and in the East-to-West direction were performed on RW2. The results of those tests can be seen in Figures 4.11 and 4.12 in which the displacements correspond to the displacements at the top of the wall.

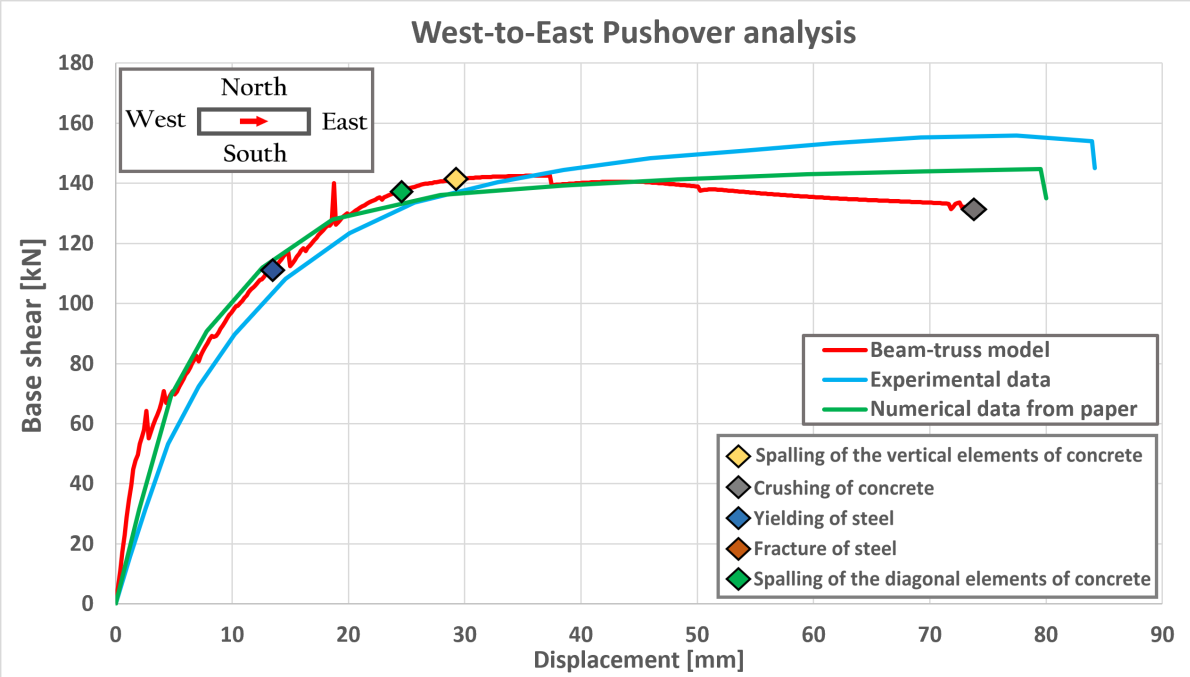

Figure 4.11: RW2: Force-displacement relationship when loaded from West to East.

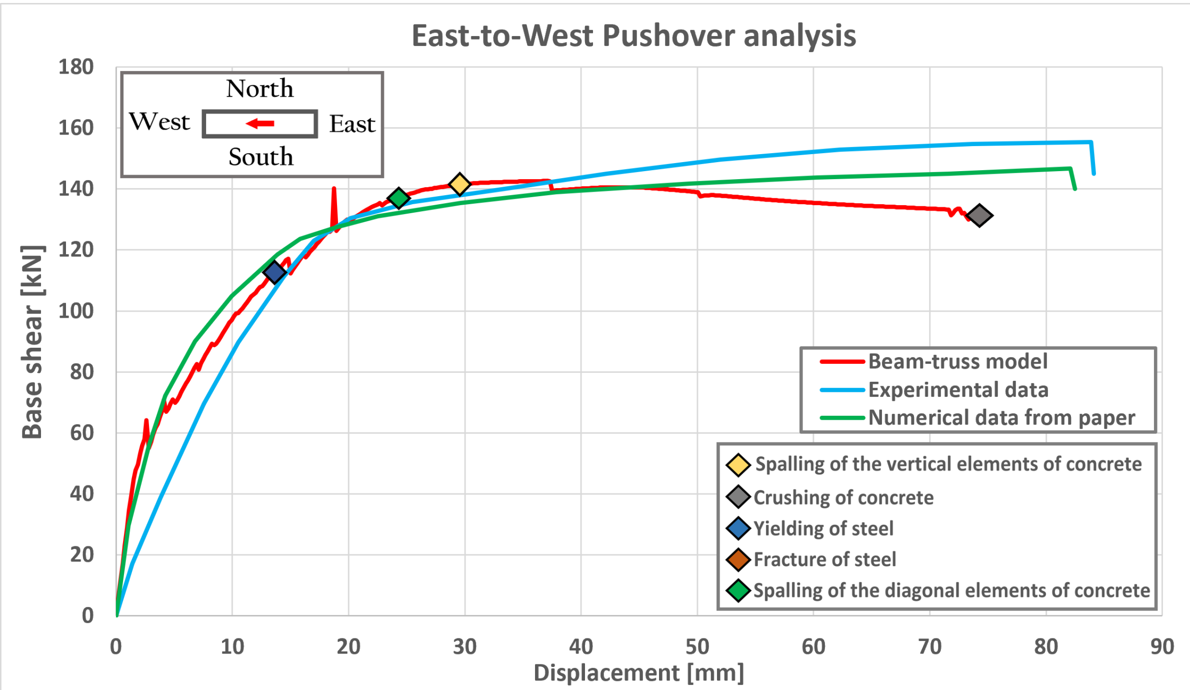

Figure 4.12: RW2: Force-displacement relationship when loaded from East to West.

The results for the beam-truss model that has been presented, which correspond to the red curves in Figures 4.11 and 4.12, were obtained using the SeismoStruct software. The numerical data from paper, which correspond to the green curves in Figures 4.11 and 4.12, have been taken from document [1] written by C. Arteta & al. (2019) and that also modeled the wall using the beam-truss model.

For both graphs depicted in Figures 4.11 and 4.12, the results of the beam-truss model are the same since the wall is symmetrical. Both beam truss model curve and numerical data from paper curve have a good approximation of the experimental result curve. The beam-truss model curves stop due to crushing of concrete in the vertical elements located at the extremities of the wall.

4.2 I-shaped walls

4.2.1 F1

4.2.1.1 Geometry

F1 is an I-section wall. Its cross-section is illustrated in Figure 4.13. The properties and geometry of the wall have been taken from document [18] written by Oesterle & al. (1976). The height of the wall is equal to 4.56 [m]. The length of the web taking into account the thickness of both flanges is equal to 1905 [mm]. The length of each flange is equal to 914 [mm]. The shear span ratio of the wall, i.e., the ratio between the height and the length of the web, is therefore equal to 2.4. Each part of the wall is 102 [mm] thick. There is no axial load applied on top of the wall.

In the web of the wall, there are 16 longitudinal bars having a diameter of 6.4 [mm]. In each flange, there are 28 longitudinal bars having a diameter of 12.7 [mm]. Concerning the transverse reinforcement, each extremities of the flanges are confined by hoops of 6.4 [mm] diameter spaced 89 [mm] apart. There are also two sets of 6.4 [mm] diameter bars spaced 89 [mm] apart that cross the full length of the web and the flanges of the wall.

Figure 4.14 shows the plan and elevation views for the beam-truss model of the wall. The wall section is divided into 11 parts. The three vertical elements in each flange of the wall are modeled with inelastic displacement-based frame elements whereas the other vertical elements in the web are modeled with inelastic truss elements. The diagonal and horizontal elements are also modeled with inelastic truss elements.

4.2.1.2 Material properties

Tables 4.7 and 4.8 present respectively the properties for the steel reinforcement and the concrete that are used in the beam-truss model. Be aware that the tensile strength of concrete is considered as equal to zero for diagonal and horizontal elements.

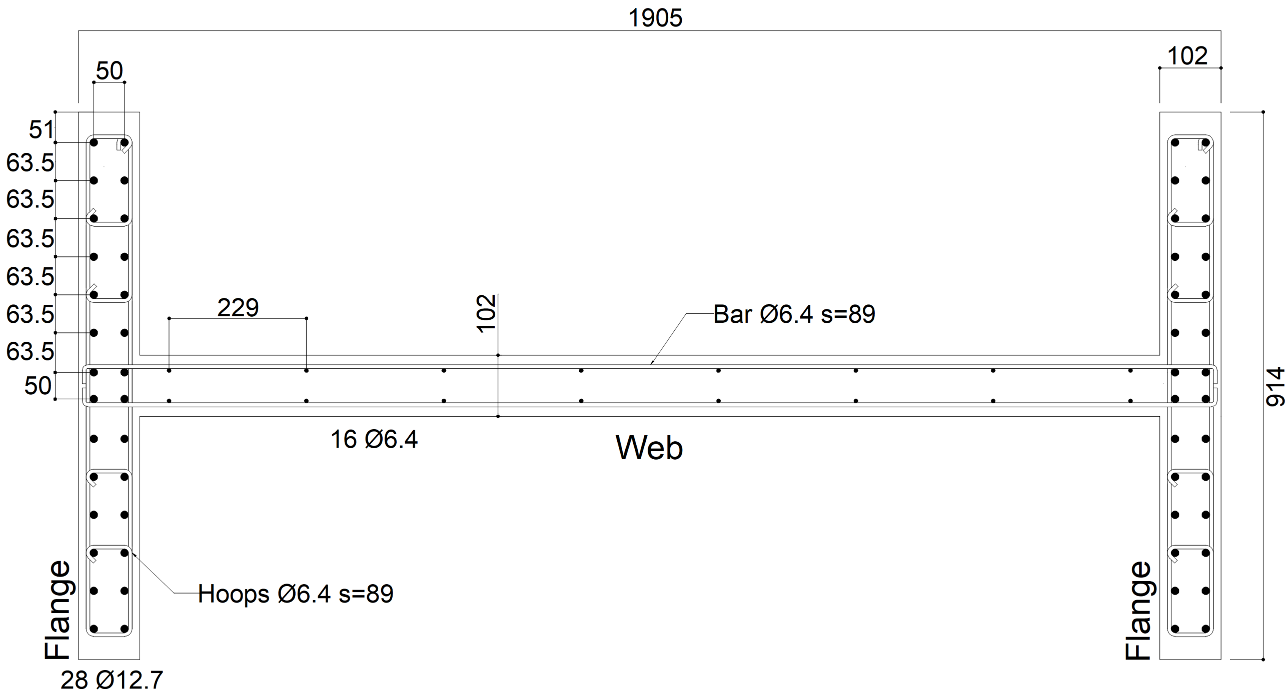

Figure 4.13: F1: Cross section and reinforcement detailing [Unit: *mm*].

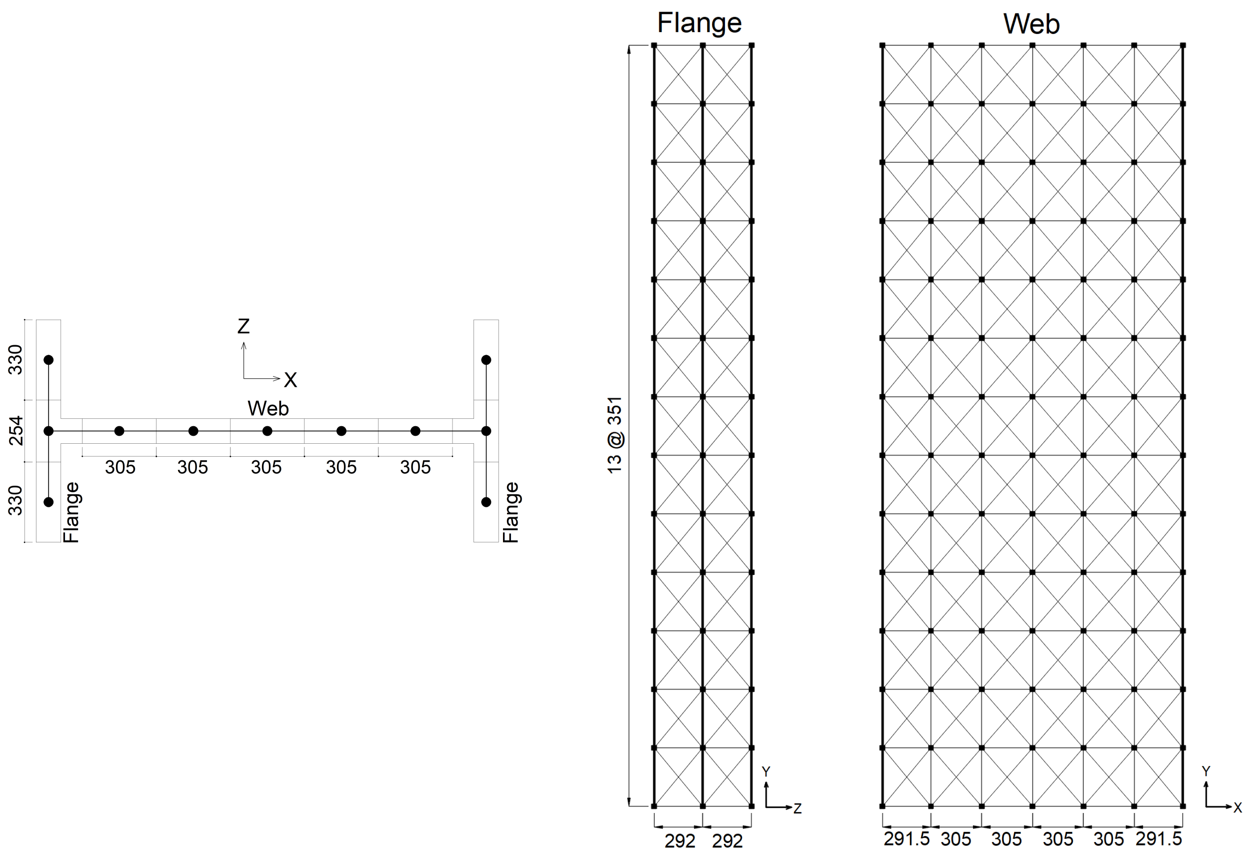

Figure 4.14: Plan and elevation views of the beam-truss model for F1 [Unit: *mm*].

Steel Mechanical Properties				
		Rebar $\phi 6.4$	Rebar $\phi 12.7$	
Diameter	d	6.4	12.7	mm
Modulus of elasticity	E_s	200	200	GPa
Yield tensile strength	f_y	525	445	MPa
Ultimate tensile strength	f_u	705	707	MPa
Yield strain	ϵ_y	0.2625	0.2225	%
Ultimate strain	ϵ_u	10.4	11.5	%
Strain hardening parameter	α	0.888	1.16	%
Specific weight	γ	78	78	kN/m^3

Table 4.7: Steel mechanical properties.

Concrete Mechanical Properties			
Compressive concrete strength	f_c	38.6	MPa
Tensile concrete strength	f_t	2.06	MPa
Modulus of elasticity	E_c	29.2	GPa
Strain at peak stress	ϵ_c	0.2	%
Specific weight	γ	24	kN/m^3

Table 4.8: Concrete mechanical properties.

4.2.1.3 Analysis output

Pushover analyses in the West-to-East direction and in the East-to-West direction were performed on F1. The results of those tests can be seen in Figures 4.15 and 4.16 in which the displacements correspond to the displacements at the top of the wall.

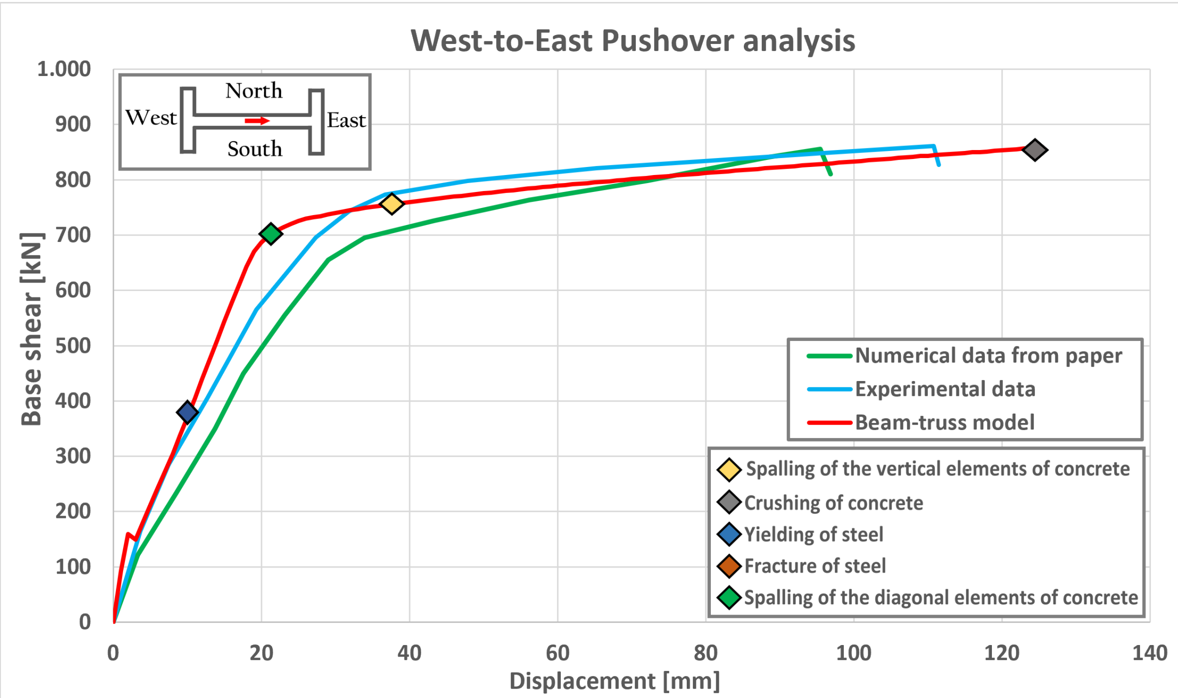

Figure 4.15: F1: Force-displacement relationship when loaded from West to East.

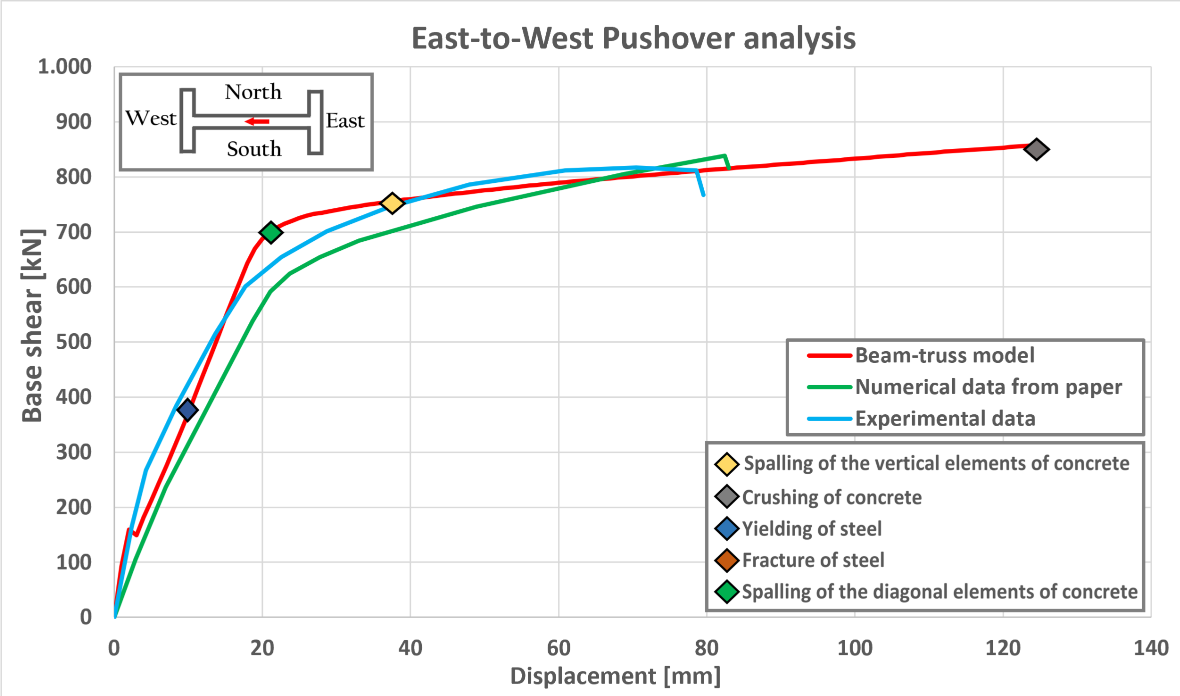

Figure 4.16: F1: Force-displacement relationship when loaded from East to West.

The results for the beam-truss model that has been presented, which correspond to the red curves in Figures 4.15 and 4.16, were obtained using the SeismoStruct software. The numerical data from paper, which correspond to the green curves in Figures 4.15 and 4.16, have been taken from document [16] written by Y. Lu & al. (2014) and that also modeled the wall using the beam-truss model.

For both graphs depicted in Figures 4.15 and 4.16, the results of the beam-truss model are the same since the wall is symmetrical. In both Figures 4.15 and 4.16, we can see that globally the result of the beam-truss model is more accurate than the numerical data from paper made by Y. Lu & al. as the red curve is closer to the experimental data curve.

Regarding the initial stiffness, we can see in Figures 4.15 and 4.16 that both numerical data from paper curve and beam-truss model curve have almost the same initial slope than the experimental data curve meaning that they have a good approximation of the initial stiffness.

Finally, the beam-truss model curve in both Figures 4.15 and 4.16 stops due to crushing of concrete in the vertical elements.

4.3 T-shaped walls

4.3.1 TW2

4.3.1.1 Geometry

TW2 is an T-section wall as illustrated in Figure 4.17. The properties and geometry of the wall have been taken from document [25] written by J. H. Thomsen & al. (2004). The height of the wall is equal to 3.66 [m]. The length of the web and the flange is equal to 1219 [mm]. The shear span ratio of the wall, i.e., the ratio between the height and the length of the wall, is therefore equal to 3 in both direction. Each part of the wall is 102 [mm] thick. The axial load ratio of the wall is equal to 7.4 [%] which means that there is a total axial load of 730 [kN] applied at the top of the wall.

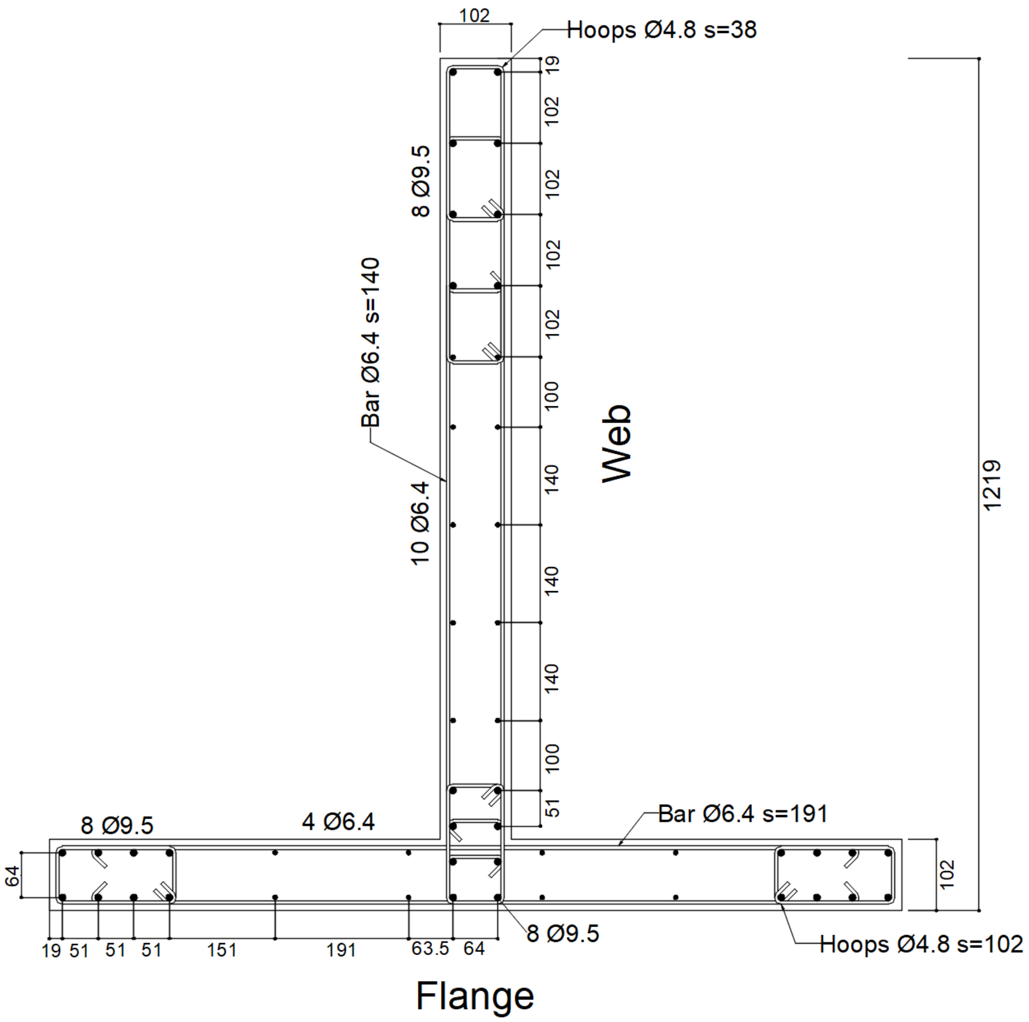

Figure 4.17: TW2: Cross section and reinforcement detailing [Unit: mm].

There are 10 longitudinal bars having a diameter of 6.4 [mm] in the web and 8 longitudinal bars having also a diameter of 6.4 [mm] in the flange. In each confined extremities of the web and the flange, there are 8 longitudinal bars having a diameter of 9.5 [mm]. Concerning the transverse reinforcement, there are hoops of 4.8 [mm] diameter spaced 102 [mm] apart in the confined extremities of the flange and in the intersection between the flange and the web. In the North extremity of the web, there are hoops of 4.8 [mm]

diameter spaced 38 [mm] apart. There are also two sets of 6.4 [mm] diameter bars spaced 140 [mm] apart that cross the full length of the web and there are also two sets of 6.4 [mm] diameter bars spaced 191 [mm] apart that cross the full length of the flange of the wall.

Figure 4.18 shows the plan and elevation views for the beam-truss model of the wall. The wall section is divided into 9 parts. Each vertical elements located at the extremities of the wall and at the intersection between the web and the flange are modeled with inelastic displacement-based frame elements whereas the other vertical elements are modeled with inelastic truss elements. The diagonal and horizontal elements are also modeled with inelastic truss elements.

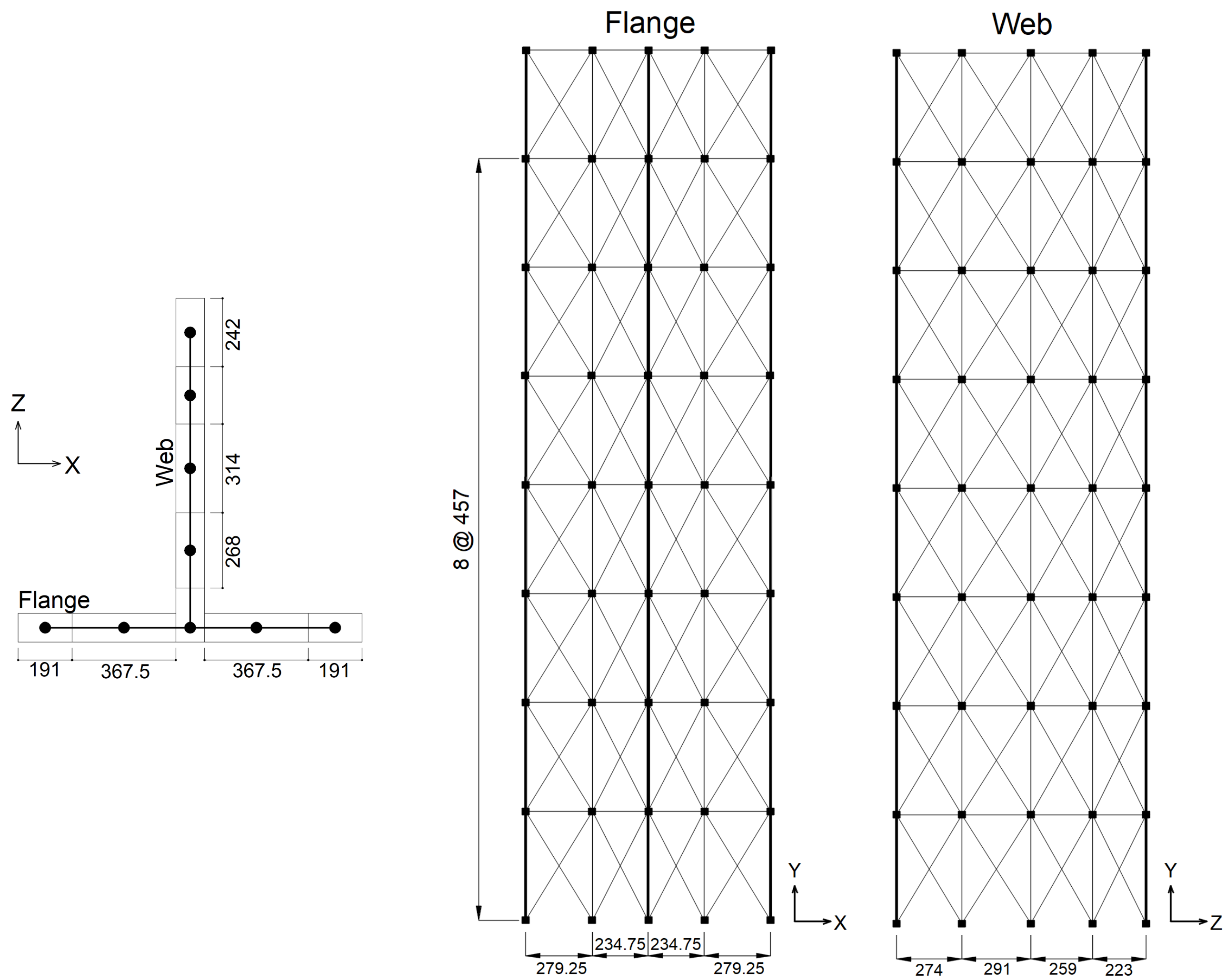

Figure 4.18: Plan and elevation views of the beam-truss model for TW2 [Unit: mm].

4.3.1.2 Material properties

Tables 4.9 and 4.10 present respectively the properties for the steel reinforcement and the concrete that are used in the beam-truss model. Note that the tensile strength of concrete is considered as equal to zero for diagonal and horizontal elements.

Steel Mechanical Properties

		Rebar $\phi 4.8$	Rebar $\phi 6.4$	Rebar $\phi 9.5$	
Diameter	d	4.8	6.4	9.5	mm
Modulus of elasticity	E_s	200	200	200	GPa
Yield tensile strength	f_y	448	448	434	MPa
Ultimate tensile strength	f_u	483	586	641	MPa
Yield strain	ϵ_y	0.224	0.224	0.217	%
Ultimate strain	ϵ_u	6	8	10	%
Strain hardening parameter	α	0.3	0.89	1.06	%
Specific weight	γ	78	78	78	kN/m^3

Table 4.9: Steel mechanical properties.

Concrete Mechanical Properties

Compressive concrete strength	f_c	41.4	MPa
Tensile concrete strength	f_t	2.13	MPa
Modulus of elasticity	E_c	30.2	GPa
Strain at peak stress	ϵ_c	0.2	%
Specific weight	γ	24	kN/m^3

Table 4.10: Concrete mechanical properties.

4.3.1.3 Analysis output

Pushover analyses in the South-to-North direction and in the North-to-South direction were performed on TW2. The results of those tests can be seen in Figures 4.19 and 4.20 in which the displacements correspond to the displacements at the top of the wall.

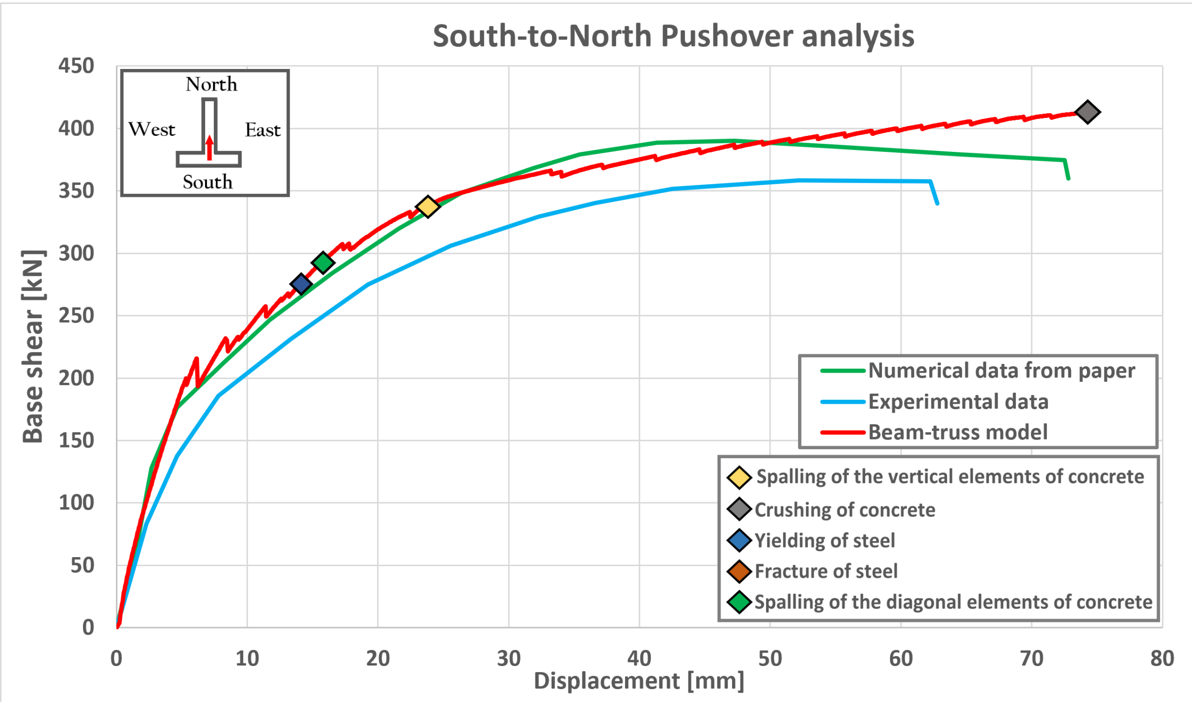

Figure 4.19: TW2: Force-displacement relationship when loaded from South to North.

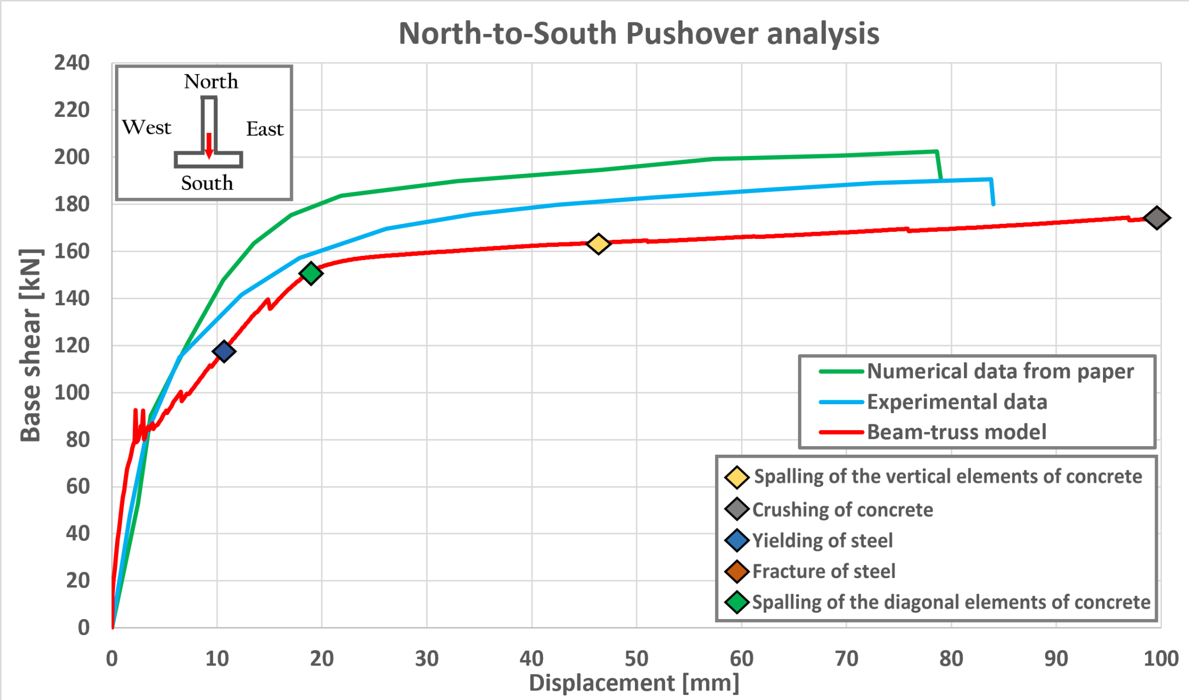

Figure 4.20: TW2: Force-displacement relationship when loaded from North to South.

The results for the beam-truss model that has been explained, which correspond to the red curves in Figures 4.19 and 4.20, were obtained using the SeismoStruct software. The numerical data from paper, which correspond to the green curves in Figures 4.19 and 4.20, have been taken from document [16] written by Y. Lu & al. (2014) and that also modeled the wall using the beam-truss model.

In Figure 4.19, the beam-truss model curve is constantly above the experimental data one. However, there is a good match between the beam-truss model curve and the numerical data from paper curve. In Figure 4.20, the beam-truss model curve is most of the time below the experimental data curve whereas the numerical data from paper curve is most of the time higher than the experimental data one.

Regarding the initial stiffness, we can see in Figure 4.19 that both the numerical data from paper curve and beam-truss model curve have the same initial slope than the experimental data curve meaning that they correctly approximate the initial stiffness.

Finally, on both graphs 4.19 and 4.20, the beam-truss model curves stop due to crushing of concrete in the vertical elements.

4.3.2 NTW1

4.3.2.1 Geometry

NTW1 is an T-section wall. Its cross-section is shown in Figure 4.21. The properties and geometry of the wall have been taken from document [4] written by B. L. Brueggen & al. (2017). The height of the wall is equal to 7.32 [m]. The length of the web and the flange are respectively equal to 2.29 [m] and 1.83 [m]. The shear span ratio of the wall, i.e., the ratio between the height and the length of the wall, is therefore equal to 3.2 when taking the length of the web and equal to 4 when taking the length of the flange. Each part of the wall is 152 [mm] thick. The axial load ratio of the wall is equal to 2.8 [%] which means that there is a total axial load of 830 [kN] applied at the top of the wall.

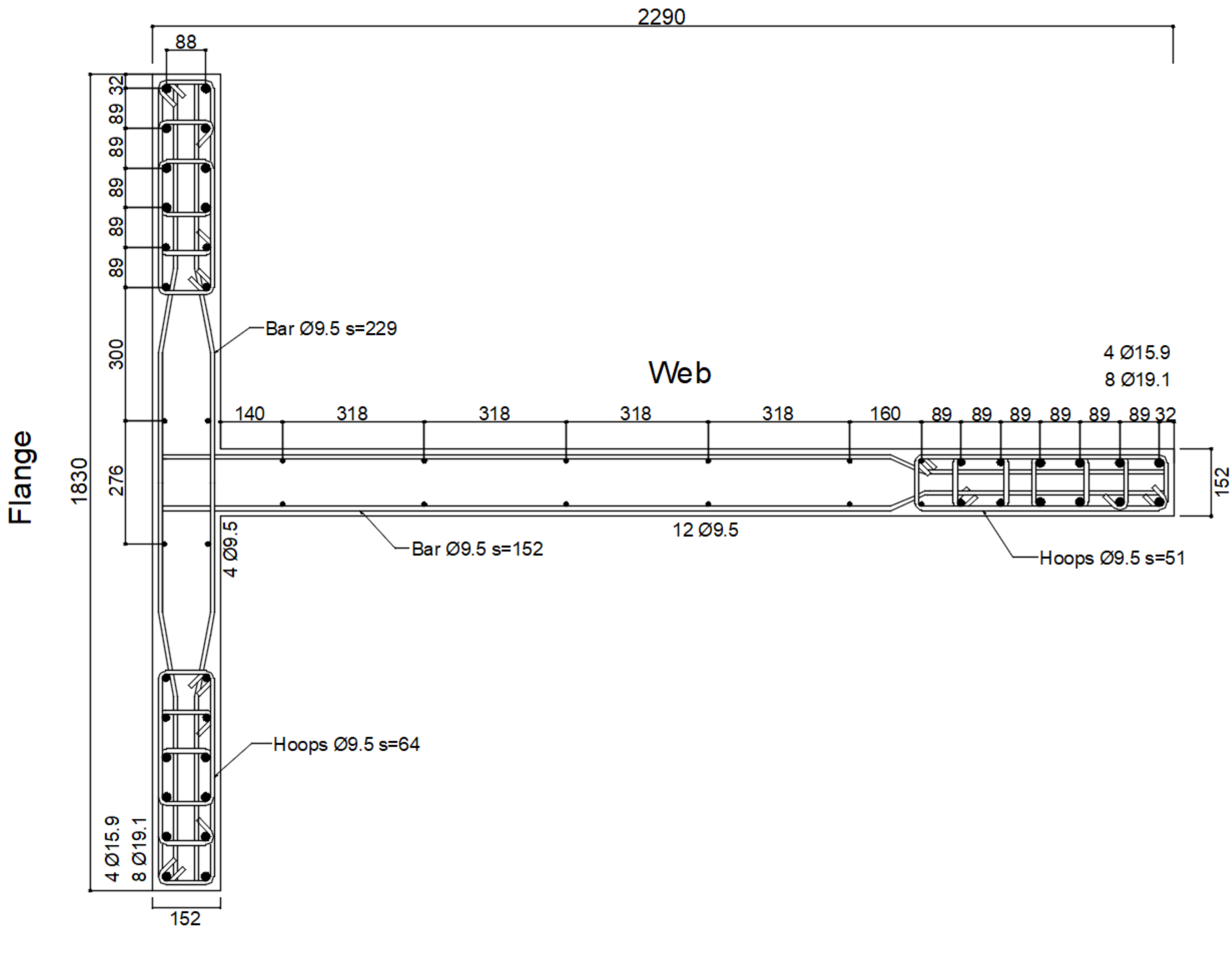

Figure 4.21: NTW1: Cross section and reinforcement detailing [Unit: mm].

There are 12 longitudinal bars having a diameter of 9.5 [mm] in the web and 4 longitudinal bars having also a diameter of 9.5 [mm] in the flange. In each confined extremities of the web and the flange, there are 8 longitudinal bars having a diameter of 19.1 [mm] and 4 longitudinal bars having a diameter of 15.9 [mm]. Regarding the transverse reinforcement, there are hoops of 9.5 [mm] diameter spaced 64 [mm] apart in the confined extremities of the flange. In the East extremity of the web, there are hoops of 9.5 [mm] diameter spaced

51 [mm] apart. There are also two sets of 9.5 [mm] diameter bars spaced 152 [mm] apart that cross the full length of the web and there are also two sets of 9.5 [mm] diameter bars spaced 229 [mm] apart that cross the full length of the flange of the wall.

Figure 4.22 shows the plan and elevation views for the beam-truss model of the wall. The wall section is divided into 15 parts. The vertical elements located at both extremities of the flange and the web are modeled with inelastic displacement-based frame elements whereas the other vertical elements are modeled with inelastic truss elements. The diagonal and horizontal elements are also modeled with inelastic truss elements.

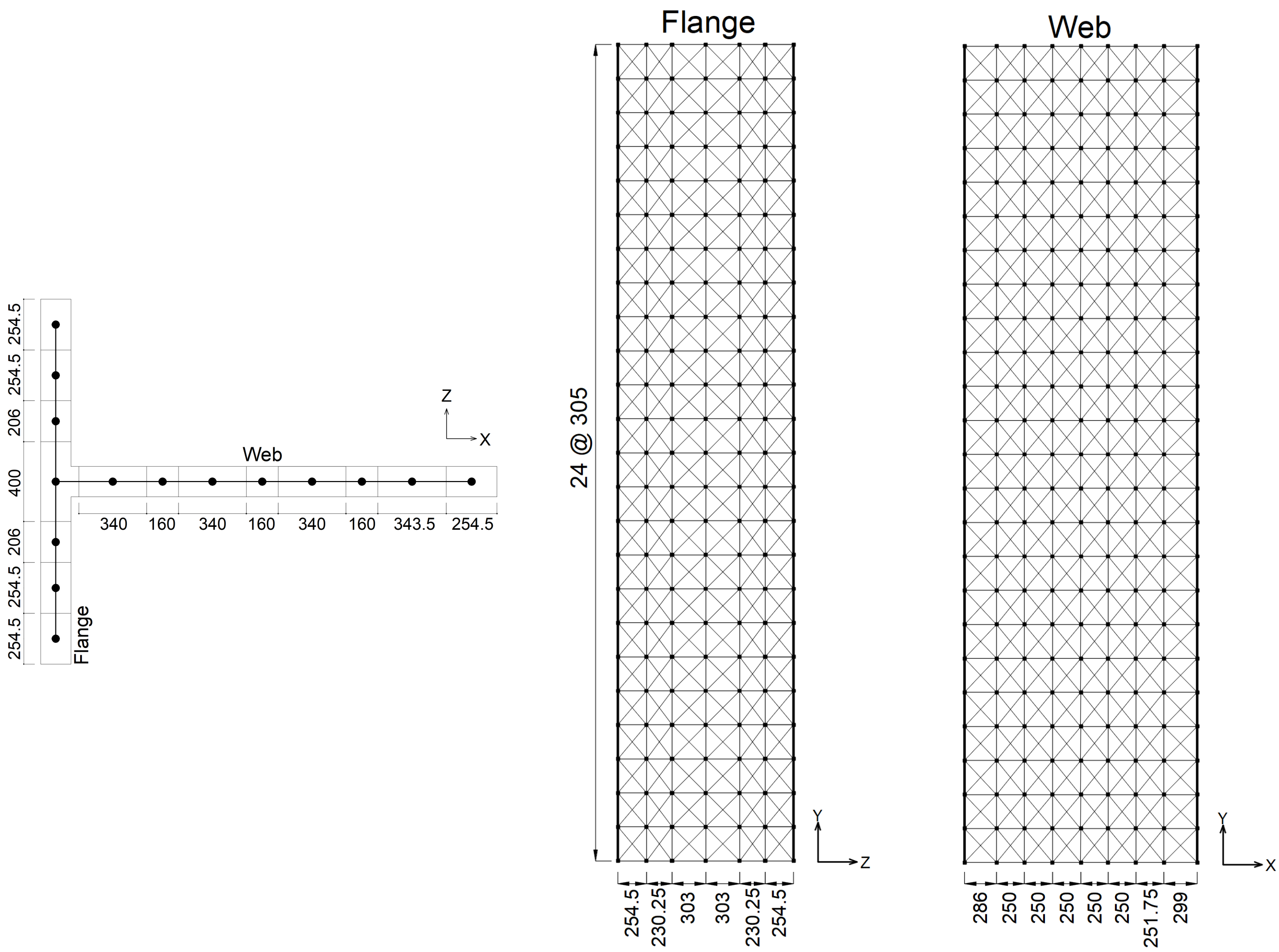

Figure 4.22: Plan and elevation views of the beam-truss model for NTW1 [Unit: mm].

4.3.2.2 Material properties

Tables 4.11 and 4.12 present respectively the properties for the steel reinforcement and the concrete that are used in the beam-truss model. Note that the tensile strength of concrete is considered as equal to zero for diagonal and horizontal elements.

Steel Mechanical Properties					
		Rebar $\phi 9.5$	Rebar $\phi 15.9$	Rebar $\phi 19.1$	
Diameter	d	9.5	15.9	19.1	mm
Modulus of elasticity	E_s	200	193	198	GPa
Yield tensile strength	f_y	503	434	439	MPa
Ultimate tensile strength	f_u	727	631	636	MPa
Yield strain	ϵ_y	0.251	0.225	0.222	%
Ultimate strain	ϵ_u	10	10	10	%
Strain hardening parameter	α	1.15	1.04	1.02	%
Specific weight	γ	78	78	78	kN/m^3

Table 4.11: Steel mechanical properties.

Concrete Mechanical Properties			
Compressive concrete strength	f_c	49.3	MPa
Tensile concrete strength	f_t	2.2	MPa
Modulus of elasticity	E_c	33	GPa
Strain at peak stress	ϵ_c	0.2	%
Specific weight	γ	24	kN/m^3

Table 4.12: Concrete mechanical properties.

4.3.2.3 Analysis output

Pushover analyses in the West-to-East direction, East-to-West direction and in the North-to-South direction were performed on NTW1. The results of those tests can be seen in Figures 4.23, 4.24 and 4.25 in which the displacements correspond to the displacements at half the height of the wall.

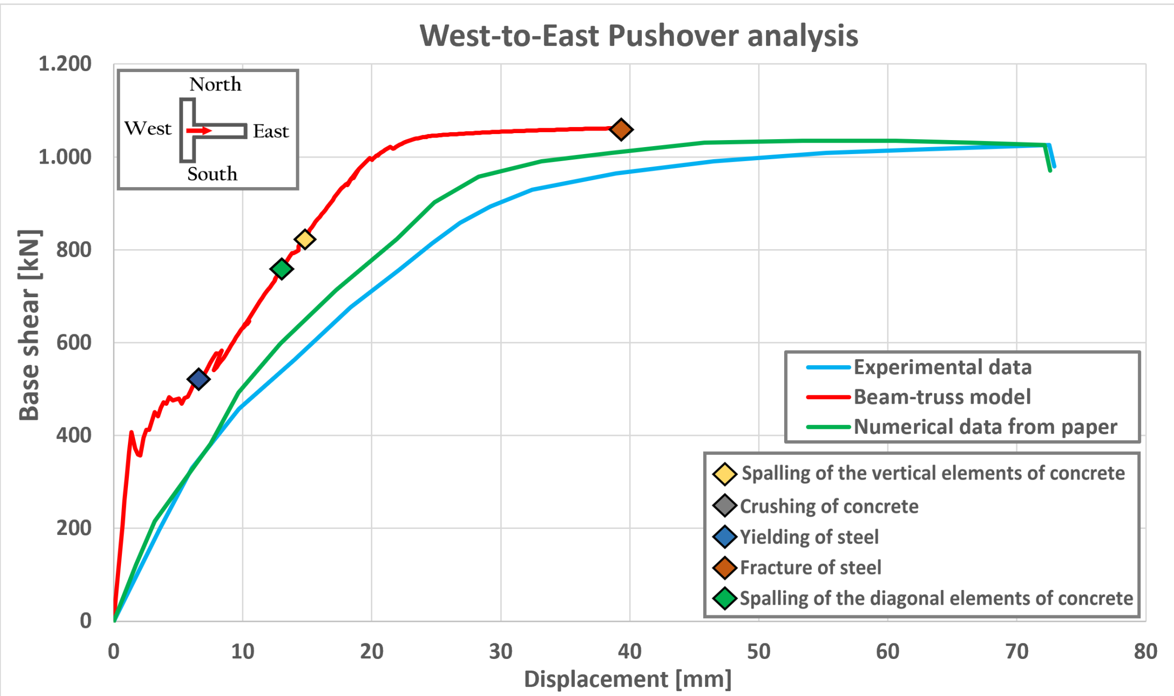

Figure 4.23: NTW1: Force-displacement relationship when loaded from West to East.

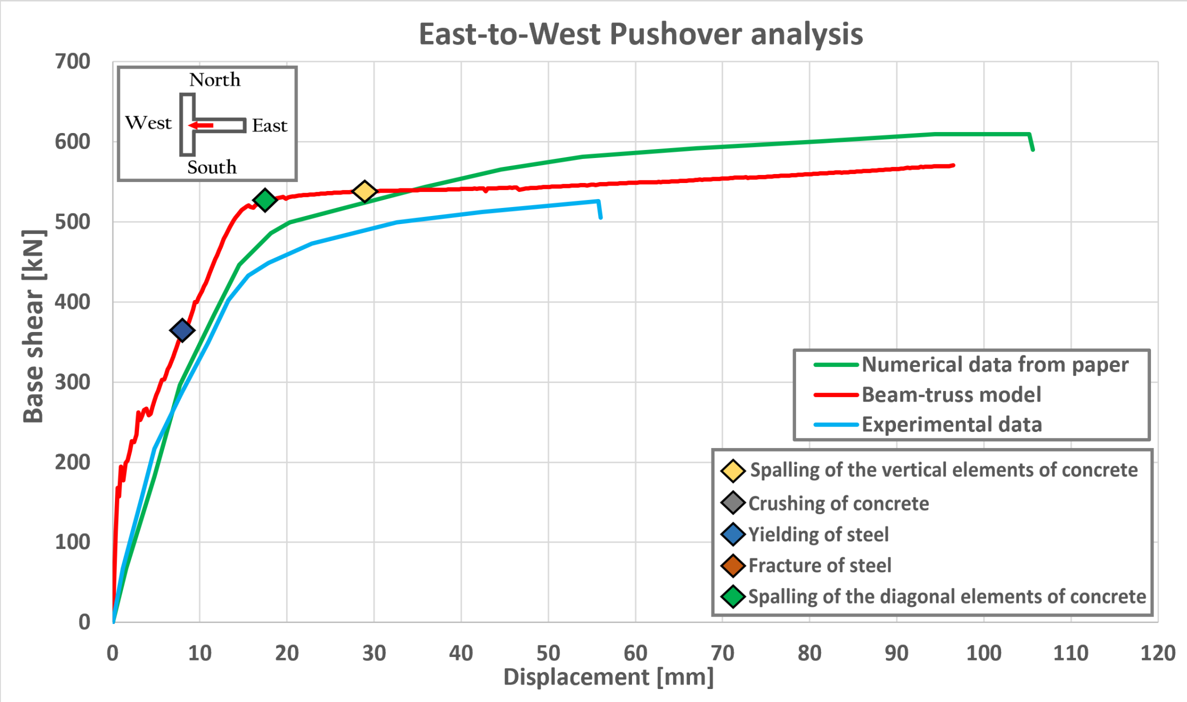

Figure 4.24: NTW1: Force-displacement relationship when loaded from East to West.

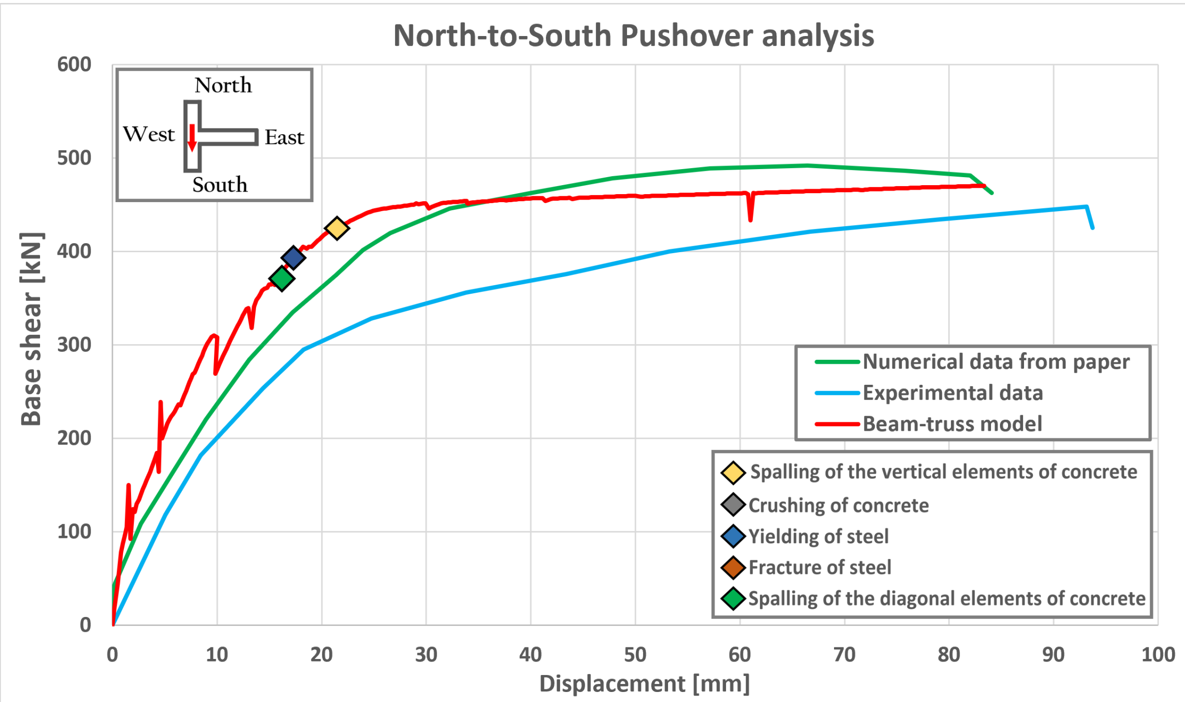

Figure 4.25: NTW1: Force-displacement relationship when loaded from North to South.

The results for the beam-truss model that has been presented, which correspond to the red curves in Figures 4.23, 4.24 and 4.25, were obtained using the SeismoStruct software. The numerical data from paper, which correspond to the green curves in Figures 4.23, 4.24 and 4.25, have been taken from document [16] written by Y. Lu & al. (2014) and that also modeled the wall using the beam-truss model.

In Figures 4.23, 4.24 and 4.25, the beam-truss model curves are constantly above the experimental data curves. The beam-truss model curve in Figure 4.23 does not manage to correctly approximate the experimental data curve whereas the numerical data from paper does. Indeed, we can see a big difference of about 300 $[kN]$ for the base shear when the displacement at mid height of the wall is equal to 20 $[mm]$. When the wall is loaded from East to West in Figure 4.24, the beam-truss model curve approximate properly the experimental data curve and it is even better than the numerical data from paper curve after a displacement at mid height of the wall equal to 34 $[mm]$. In Figure 4.25, when the wall is loaded from North to South, the beam-truss model curve is at times quite far from the experimental data curve but it is globally close to the numerical data from paper curve.

Regarding the initial stiffness, we can clearly see in Figures 4.23 and 4.24 that the beginning of the beam-truss model curve is very steep compared to numerical data from paper curve and experimental data curve. However, in Figure 4.25, the beginning of the beam-truss model curve is also steep compared to the experimental data curve but has a good match with the one of the numerical data from paper curve.

Finally, in Figure 4.23, the beam-truss model curve stops due to the fracture of the longitudinal steel bars in the vertical elements of the model.

4.4 U-shaped walls

4.4.1 TUA

4.4.1.1 Geometry

TUA is a U-section wall. Its cross-section is shown in Figure 4.26. The properties and geometry of the wall have been taken from document [3] written by K. Beyer & al. (2008). The length of both flanges is equal to 1050 $[mm]$ and the length of the web is equal to 1300 $[mm]$. The wall is 0.15 $[m]$ thick in the web and flanges. When the wall is loaded in the North-South direction, its height is considered as equal to 2950 $[mm]$ since the North-South actuators, i.e, the system allowing to apply a horizontal displacement on the wall, are placed at this level. If the wall is loaded in the East-West direction, then the height of the wall is equal to 3350 $[mm]$. The shear span ratio when the wall is loaded in the North-South and in the East-West direction is respectively equal to 2.81 and 2.58. The axial load ratio of the wall is equal to 2 [%] which means that there is a total axial load of 725 $[kN]$ applied at the top of the wall.

In each flange of the wall, there are 8 longitudinal bars having a diameter of 6 $[mm]$. In the web, there are 12 longitudinal bars having also a diameter of 6 $[mm]$. In both corners of the wall, i.e., at the two intersections between the web and the flanges, there are 4 longitudinal bars having a diameter of 12 $[mm]$. In both South extremities of the flanges, there are 7 longitudinal bars having a diameter of 12 $[mm]$. Concerning the transverse reinforcement, there are 2 sets of hoops of 6 [*mm*] diameter spaced 50 [*mm*] apart in each corner of the wall. In the South extremities of the flanges, there are hoops and diamond stirrups, i.e., hoops having a triangular shape, of 6 [*mm*] diameter spaced 50 [*mm*] apart. There are also two sets of 6 [*mm*] diameter bars spaced 125 [*mm*] apart that cross the full length of the web and flanges.

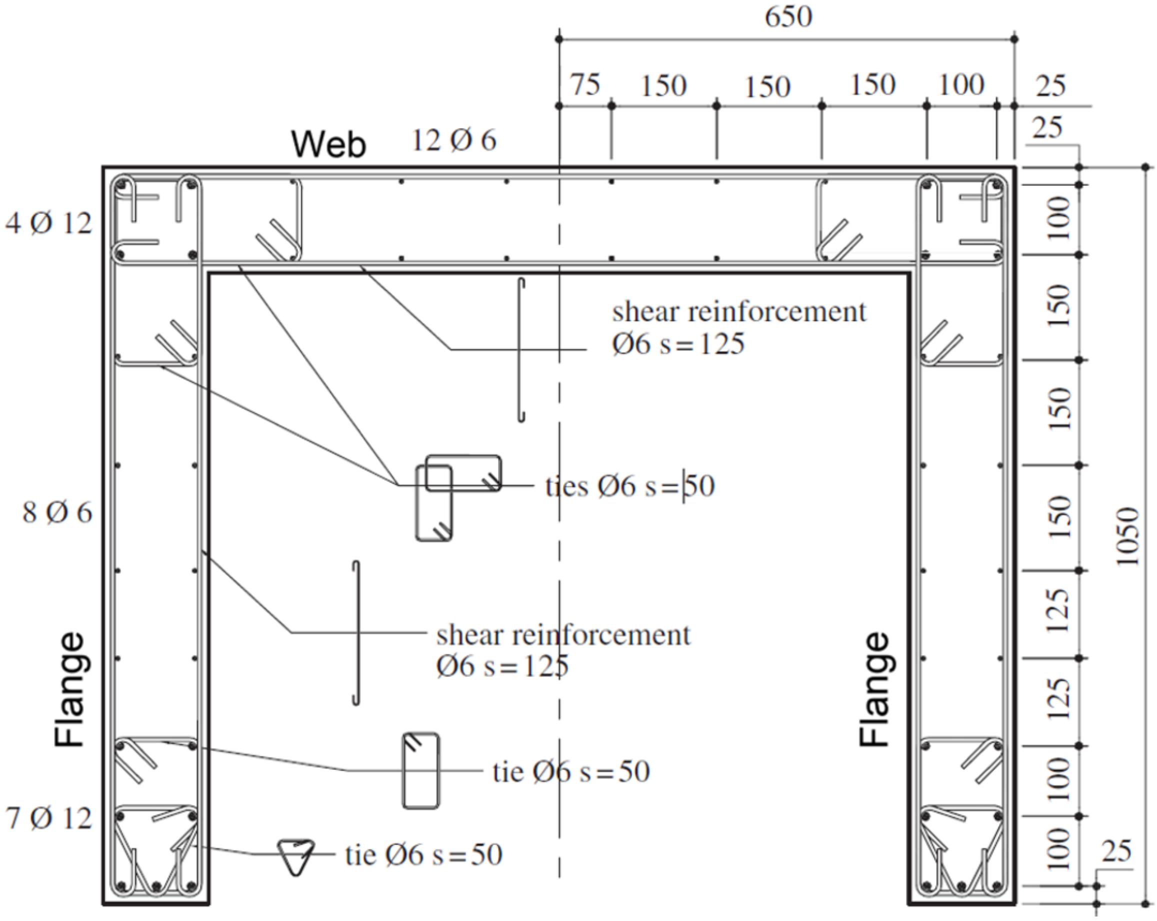

Figure 4.26: TUA: Cross section and reinforcement detailing from [3] [Unit: *mm*].

Figure 4.27 shows the plan and elevation views for the beam-truss model of the wall when it is loaded in the North-South direction. The wall section is divided into 11 parts. When loaded in the East-West direction, the plan view of the beam-truss model illustrated in Figure 4.27 remains the same but the elevation view changes. Instead of having 11 vertical elements with a height of 250 [*mm*] each, there are 12 of them and instead of the last vertical elements at the top of the model being 200 [*mm*] high, they become 350 [*mm*] high. The vertical elements located at both South extremities of the flanges and the ones in the corners are modeled with inelastic displacement-based frame elements whereas the other vertical elements are modeled with inelastic truss elements. The diagonal and horizontal elements are also modeled with inelastic truss elements.

4.4.1.2 Material properties

Tables 4.13 and 4.14 list respectively the properties for the steel reinforcement and the concrete that are used in the beam-truss model. Note that the tensile strength of concrete is considered as equal to zero for diagonal and horizontal elements.

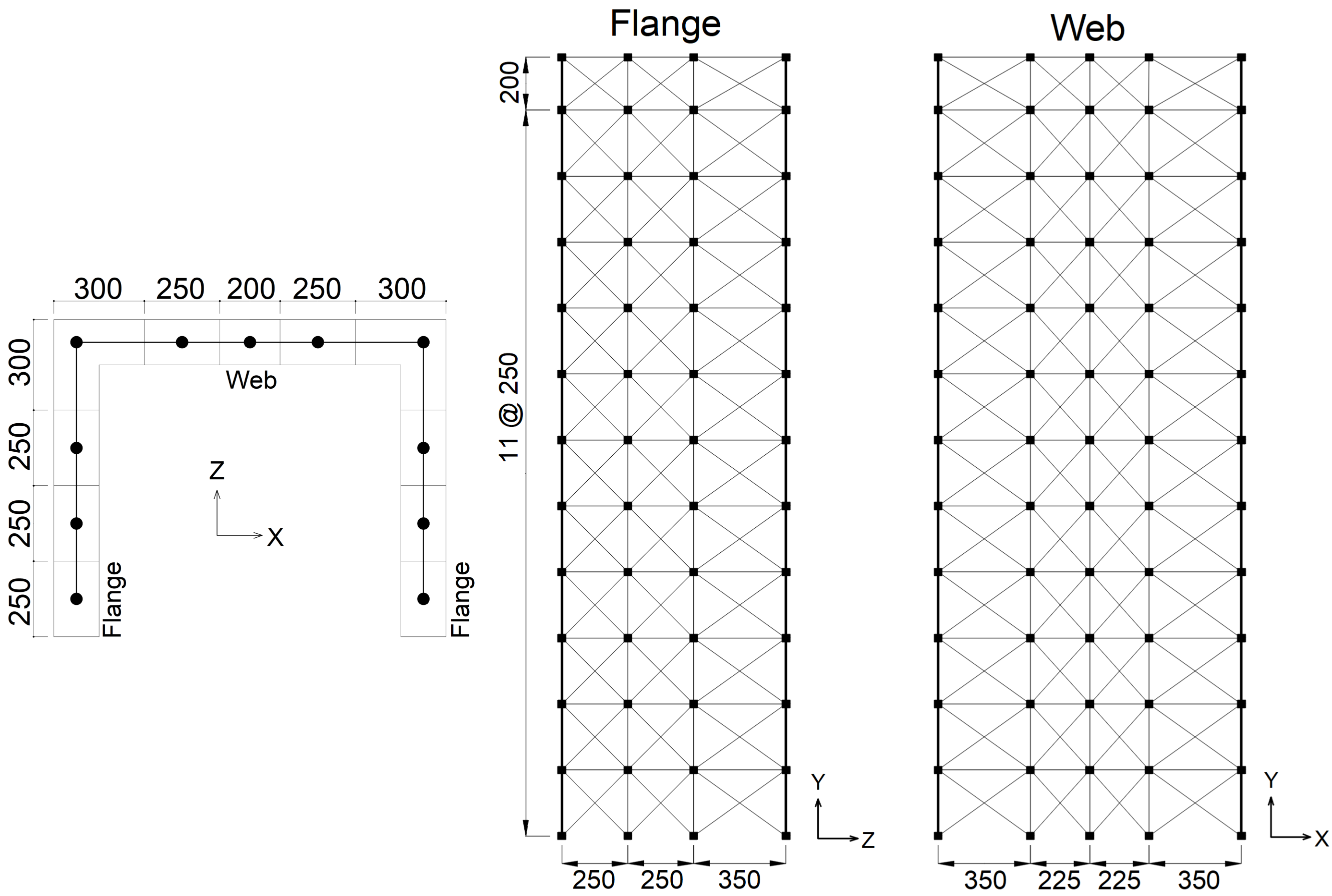

Figure 4.27: Plan and elevation views of the beam-truss model for TUA [Unit: mm].

Steel Mechanical Properties

		Rebar $\phi 6$	Rebar $\phi 12$	
Diameter	d	6	12	mm
Modulus of elasticity	E_s	200	200	GPa
Yield tensile strength	f_y	518	488	MPa
Ultimate tensile strength	f_u	681	595	MPa
Yield strain	ϵ_y	0.259	0.244	%
Ultimate strain	ϵ_u	8.4	12.6	%
Strain hardening parameter	α	1	0.433	%
Specific weight	γ	78	78	kN/m^3

Table 4.13: Steel mechanical properties.

Concrete Mechanical Properties

Compressive concrete strength	f_c	77.9	MPa
Tensile concrete strength	f_t	2.2	MPa
Modulus of elasticity	E_c	41.5	GPa
Strain at peak stress	ϵ_c	0.2	%
Specific weight	γ	24	kN/m^3

Table 4.14: Concrete mechanical properties.

4.4.1.3 Analysis output

Pushover analyses in the West-to-East direction, South-to-North direction and in the North-to-South direction were performed on TUA. The results of those tests can be seen in Figures 4.28, 4.29 and 4.30 in which the displacements correspond to the displacements at the top of the wall.

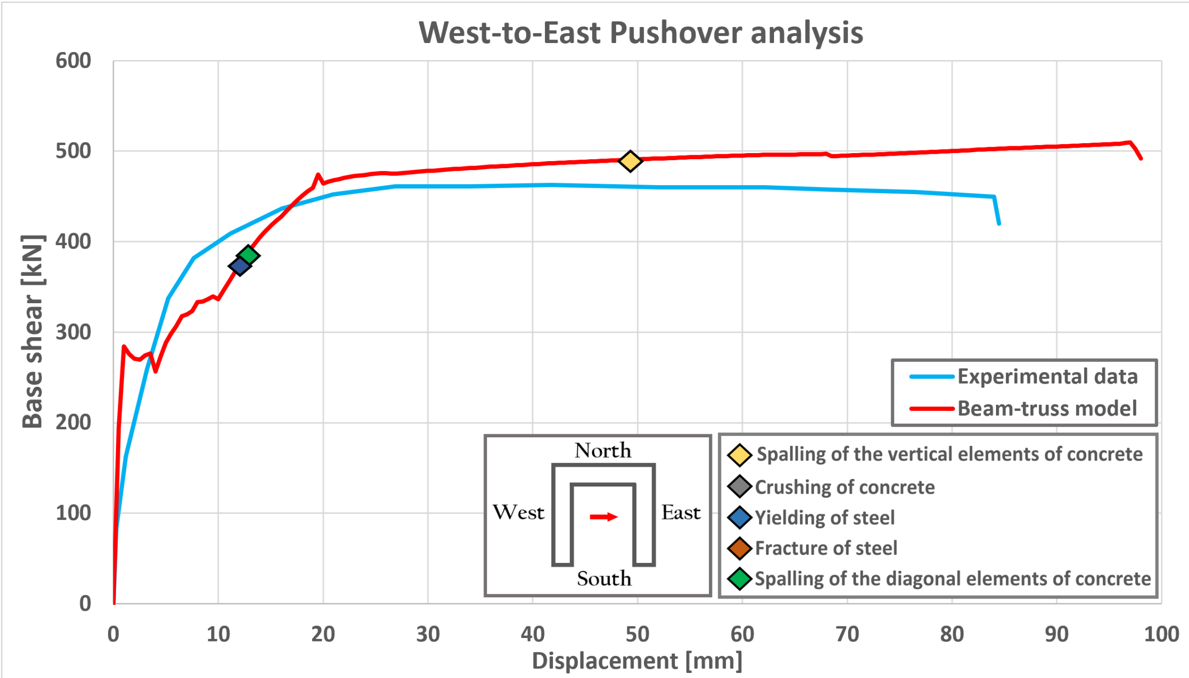

Figure 4.28: TUA: Force-displacement relationship when loaded from West to East.

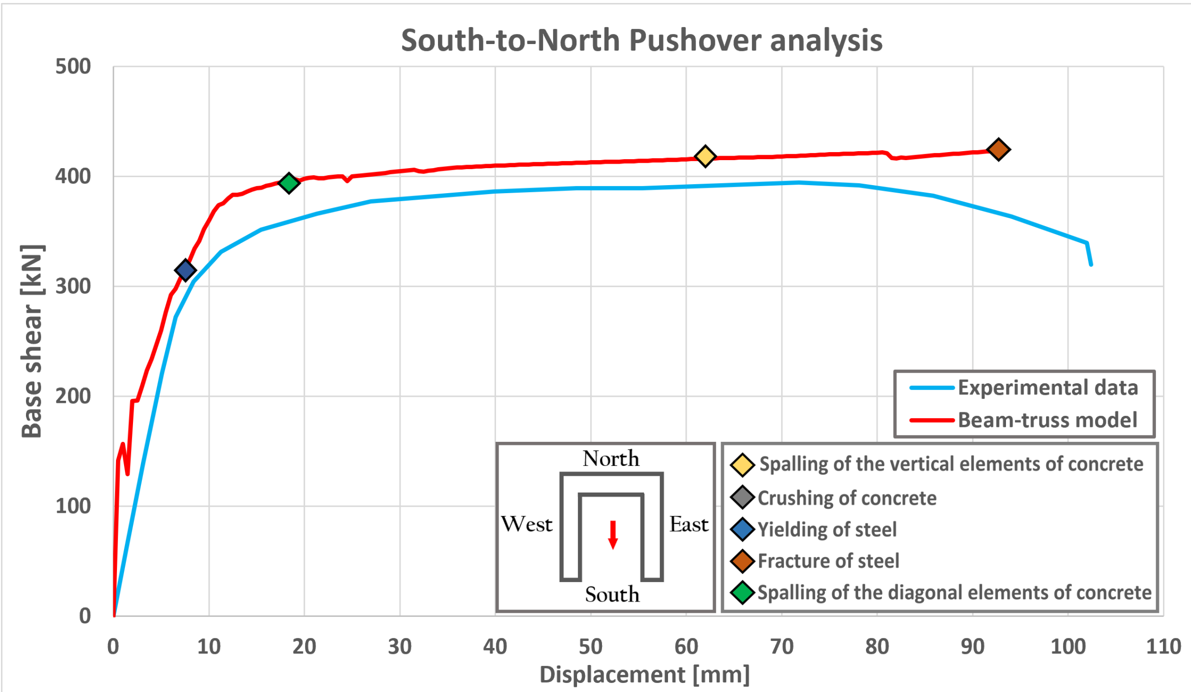

Figure 4.29: TUA: Force-displacement relationship when loaded from South to North.

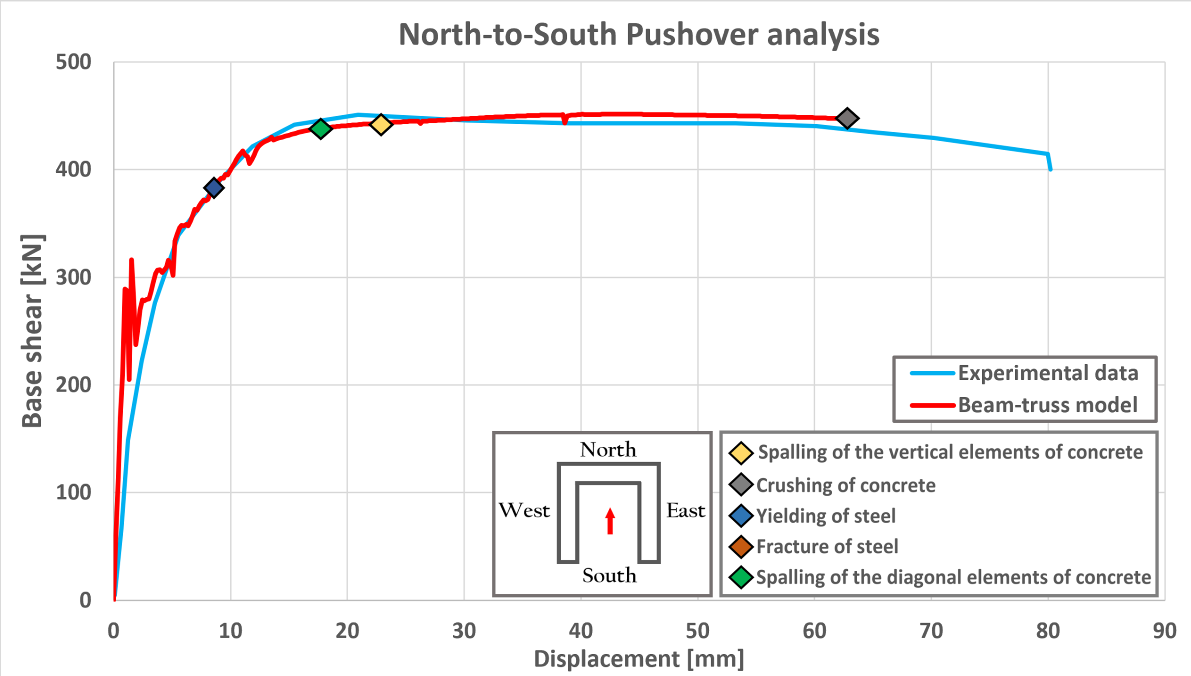

Figure 4.30: TUA: Force-displacement relationship when loaded from North to South.

The results for the beam-truss model that has been presented, which correspond to the red curves in Figures 4.28, 4.29 and 4.30, were obtained using the SeismoStruct software. We can see that those curves have a really good match with the experimental data curves, especially when the wall is loaded from North to South in Figure 4.30. In fact, the beam-truss model curves in Figures 4.28 and 4.29 are most of the time slightly above the experimental data curves.

Regarding the initial stiffness, we can see in Figures 4.28 and 4.30 that the initial slope of the beam-truss model curve match really well with the experimental data one, meaning that they have almost the same initial stiffness. However, when loaded from South-to-North in Figure 4.29, the initial slope of the beam-truss model curve is steeper than the one of experimental data.

Finally, we can see in Figure 4.29 that the beam-truss model curve stops due to fracture of the longitudinal steel bars that are situated at the South extremities of the flanges. When the wall is loaded from North-to-South, in Figure 4.30, the beam-truss model curve stops due to the crushing of concrete in the corners of the wall.

In addition, some cyclic loading tests were performed on wall TUA in both West-East and North-South directions. The results of those tests are presented in Figures 4.31 and 4.32 where we can see that the beam-truss model curves are following properly the experimental data curves meaning that the behaviour of the wall is well captured by the beam-truss model.

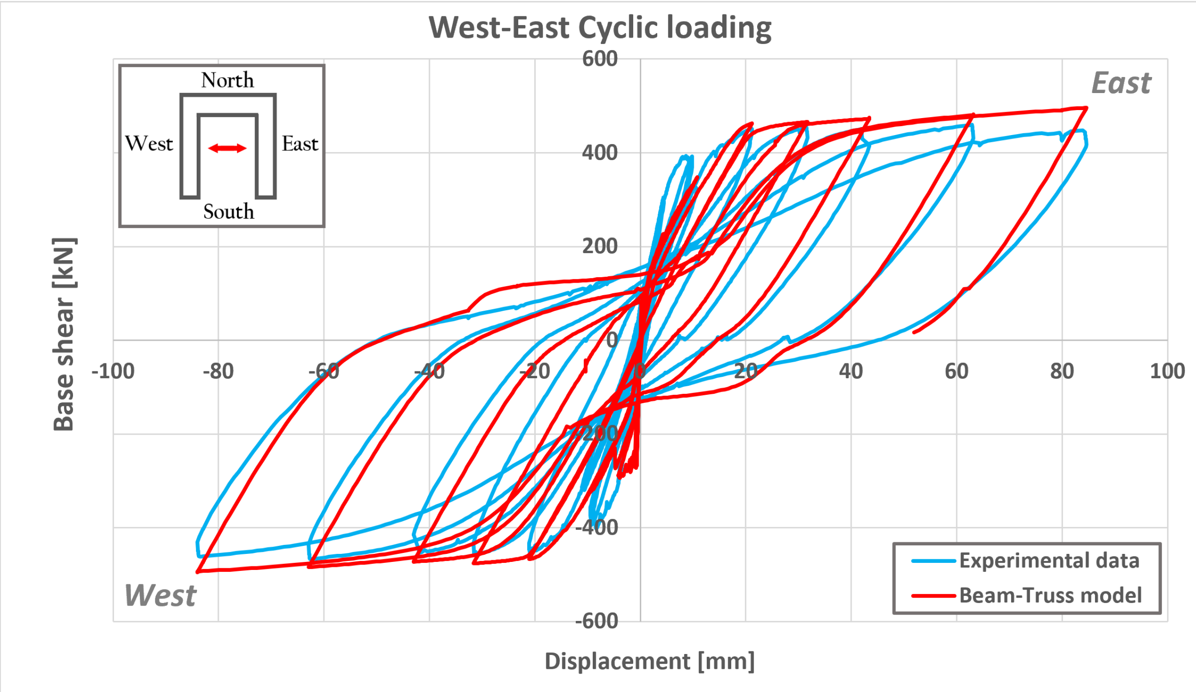

Figure 4.31: TUA: Force-displacement relationship during West-East cyclic loading.

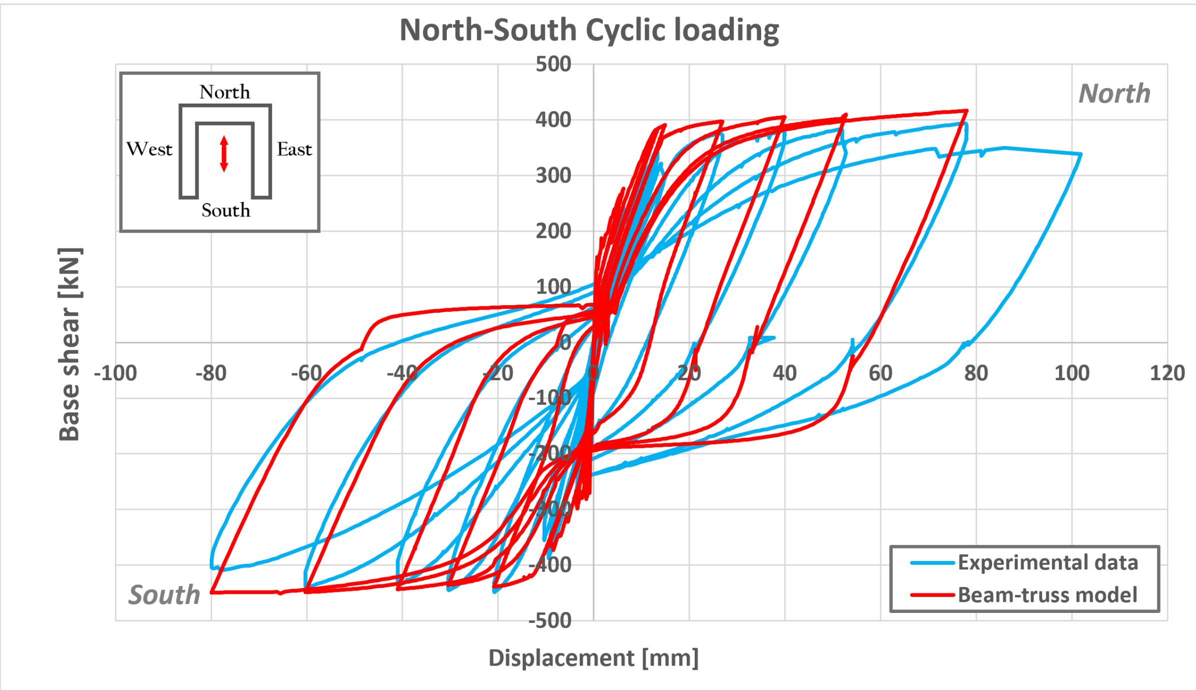

Figure 4.32: TUA: Force-displacement relationship during North-South cyclic loading.

4.4.2 TUC

4.4.2.1 Geometry

TUC is a U-section wall as shown in Figure 4.33. The properties and geometry of the wall have been taken from document [6] written by R. Constantin & al. (2016). The length of both flanges is equal to 1050 [mm] and the length of the web is equal to 1300 [mm]. The wall is 0.1 [m] thick in the web and flanges. The height of the wall is equal to 2950 [mm]. The axial load ratio of the wall is equal to 6 [%] which means that there is a total axial load of 806 [kN] applied at the top of the wall.

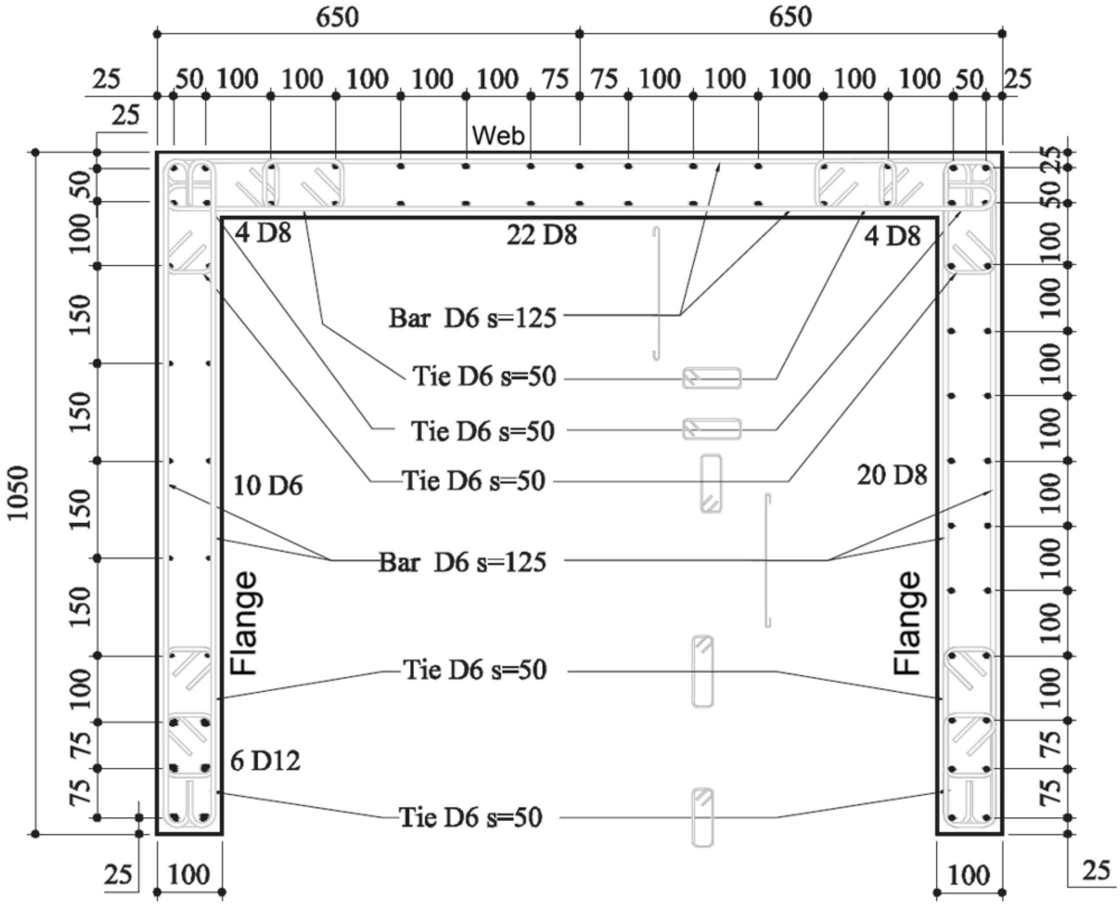

Figure 4.33: TUC: Cross section and reinforcement detailing from [6] [Unit: mm].

In the left flange of Figure 4.33, there are 10 longitudinal bars having a diameter of 6 [mm]. In the right flange, there are 20 longitudinal bars having a diameter of 8[mm]. There are also 22 longitudinal bars having a diameter of 8 [mm] in the web of the wall. The South extremity of the left flange contains 6 longitudinal bars having a diameter of 12 [mm]. In both corners of the wall, i.e., the intersections between the flanges and the web, there are 4 longitudinal bars having a diameter of 8 [mm]. Regarding the transverse reinforcement, there are 3 sets of hoops of 6 [mm] diameter spaced 50 [mm] apart in each corner of the wall. In the South extremities of both flanges, there are 2 sets of hoops of 6 [mm] diameter spaced 50 [mm] apart. There are also two sets of 6 [mm] diameter bars spaced 125 [mm] apart that cross the full length of the web and flanges.

Figure 4.34 shows the plan and elevation views for the beam-truss model of the wall. The wall section is divided into 11 parts. The vertical elements located at both South extremities of the flanges and the ones in the corners are modeled with inelastic displacement-based frame elements whereas the other vertical elements are modeled with inelastic truss elements. The diagonal and horizontal elements are also modeled with inelastic truss elements.

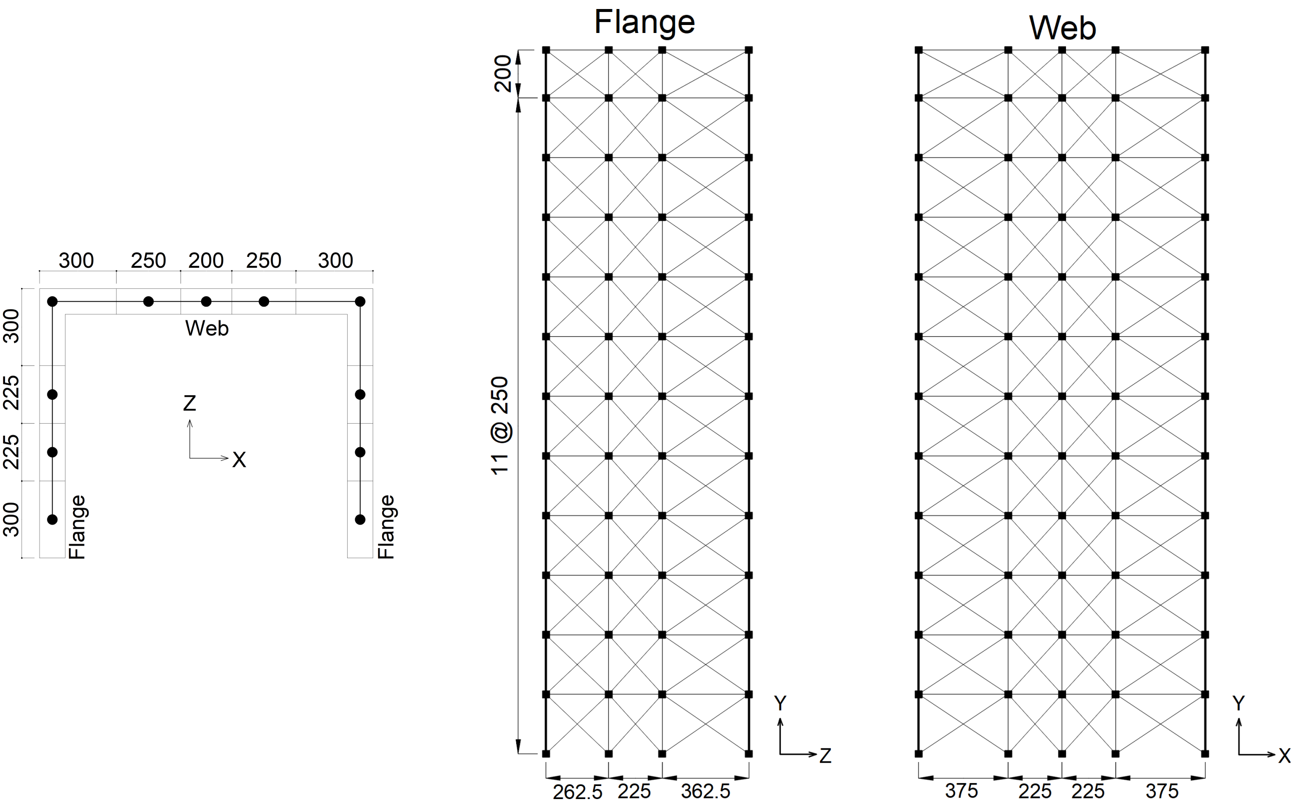

Figure 4.34: Plan and elevation views of the beam-truss model for TUC [Unit: mm].

4.4.2.2 Material properties

Tables 4.15 and 4.16 list respectively the properties for the steel reinforcement and the concrete that are used in the beam-truss model. Note that the tensile strength of concrete is considered as equal to zero for diagonal and horizontal elements.

Steel Mechanical Properties

		Rebar $\phi 6$	Rebar $\phi 8$	Rebar $\phi 12$	
Diameter	d	6	8	12	mm
Modulus of elasticity	E_s	200	200	200	GPa
Yield tensile strength	f_y	492	563	529	MPa
Ultimate tensile strength	f_u	623	663	633	MPa
Yield strain	ϵ_y	0.246	0.2815	0.2645	%
Ultimate strain	ϵ_u	6.8	7.9	9.6	%
Strain hardening parameter	α	1	0.66	0.56	%
Specific weight	γ	78	78	78	kN/m^3

Table 4.15: Steel mechanical properties.

Concrete Mechanical Properties			
Compressive concrete strength	f_c	42	MPa
Tensile concrete strength	f_t	3.2	MPa
Modulus of elasticity	E_c	31.6	GPa
Strain at peak stress	ϵ_c	0.2	$\%$
Specific weight	γ	24	kN/m^3

Table 4.16: Concrete mechanical properties.

4.4.2.3 Analysis output

Pushover analyses in the diagonal directions were performed on TUC. The results of those analyses in the Southeast-to-Northwest, Southwest-to-Northeast, Northeast-to-Southwest and in the Northwest-to-Southeast directions are respectively presented in Figures 4.35, 4.36, 4.37 and 4.38. In fact, the wall was loaded at the same time in both South-North and West-East directions in such a way that a resulting diagonal displacement was applied on top of the wall. In order to represent the data in a single graph, the base shear-displacement data were calculated thanks to the square root of the sum of the squares (SRSS) procedure. Therefore, at each pushover step, we calculate the square root of the sum of the squares of the base shear in the South-North direction and in the West-East direction. The same procedure is done for the displacements.

The results for the beam-truss model that has been explained, which correspond to the red curves in Figures 4.35, 4.36, 4.37 and 4.38, were obtained using the SeismoStruct software. We can see in Figures 4.35 and 4.36 that the beam-truss model curves have a really good match with the experimental data curves. The beam-truss model curves in Figures 4.37 and 4.38 are globally above the experimental data curves but they approximate them more or less correctly.

Regarding the initial stiffness, we can see in Figures 4.35, 4.36, 4.37 and 4.38 that the initial slope of the beam-truss model curves match really well with the experimental data one, meaning that they have almost the same initial stiffness.

Finally, we can see in Figure 4.36 that the beam-truss model curve stops due to fracture of the longitudinal steel bars that are situated at the South extremities of the left flange. For Figures 4.35, 4.37 and 4.38, the beam-truss model curve stops due to the crushing of concrete in the vertical elements of the model.

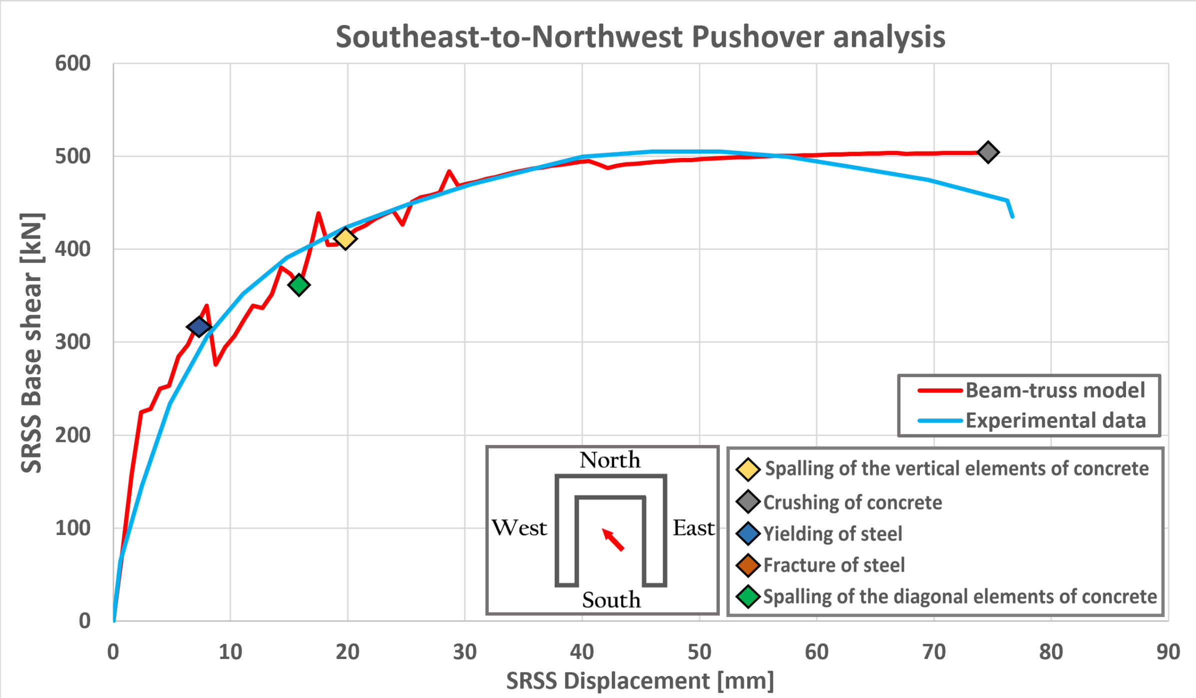

Figure 4.35: TUC: Force-displacement relationship when loaded from Southeast to Northwest.

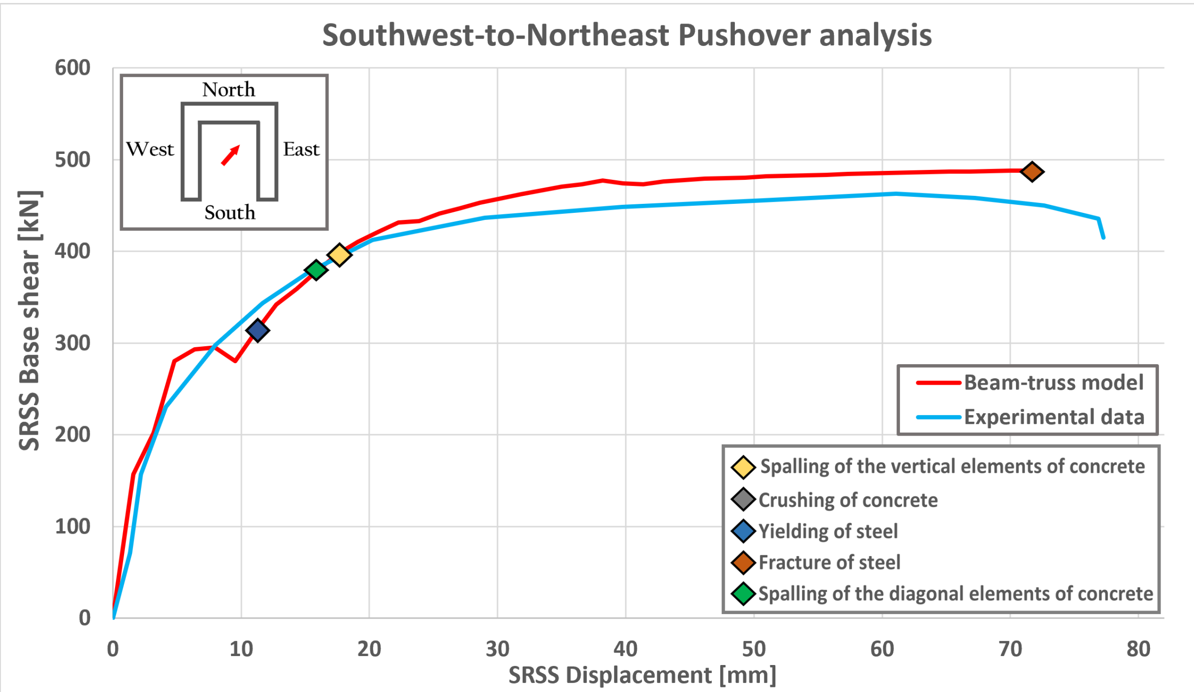

Figure 4.36: TUC: Force-displacement relationship when loaded from Southwest to Northeast.

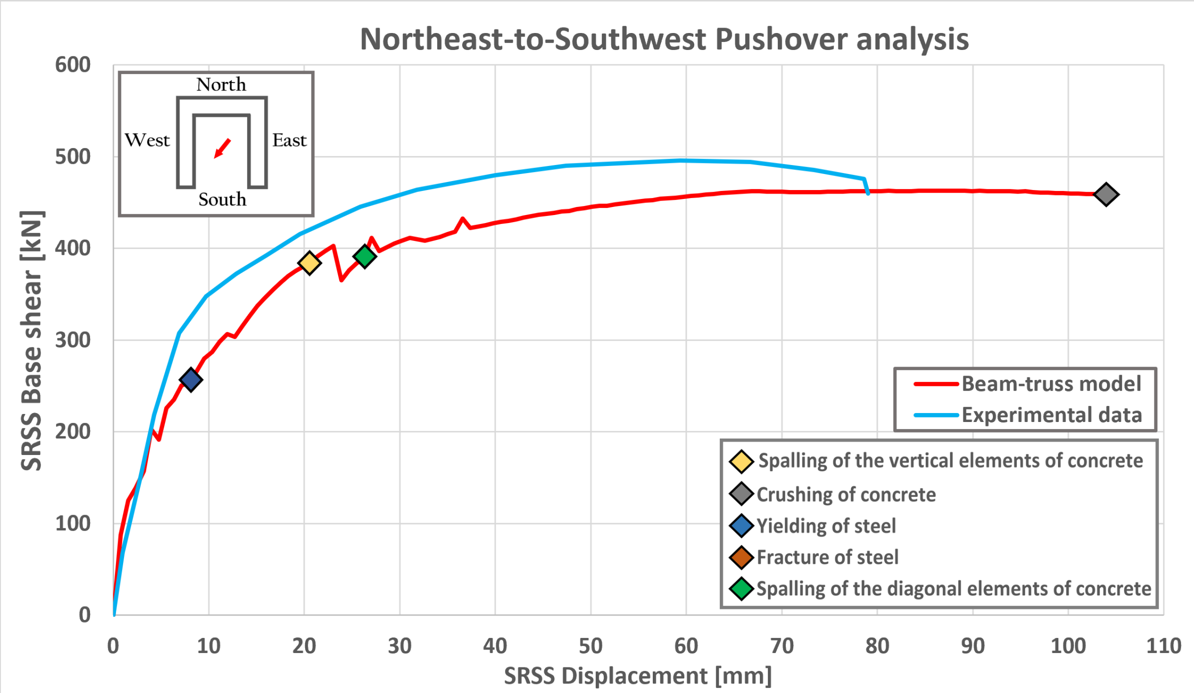

Figure 4.37: TUC: Force-displacement relationship when loaded from Northeast to Southwest.

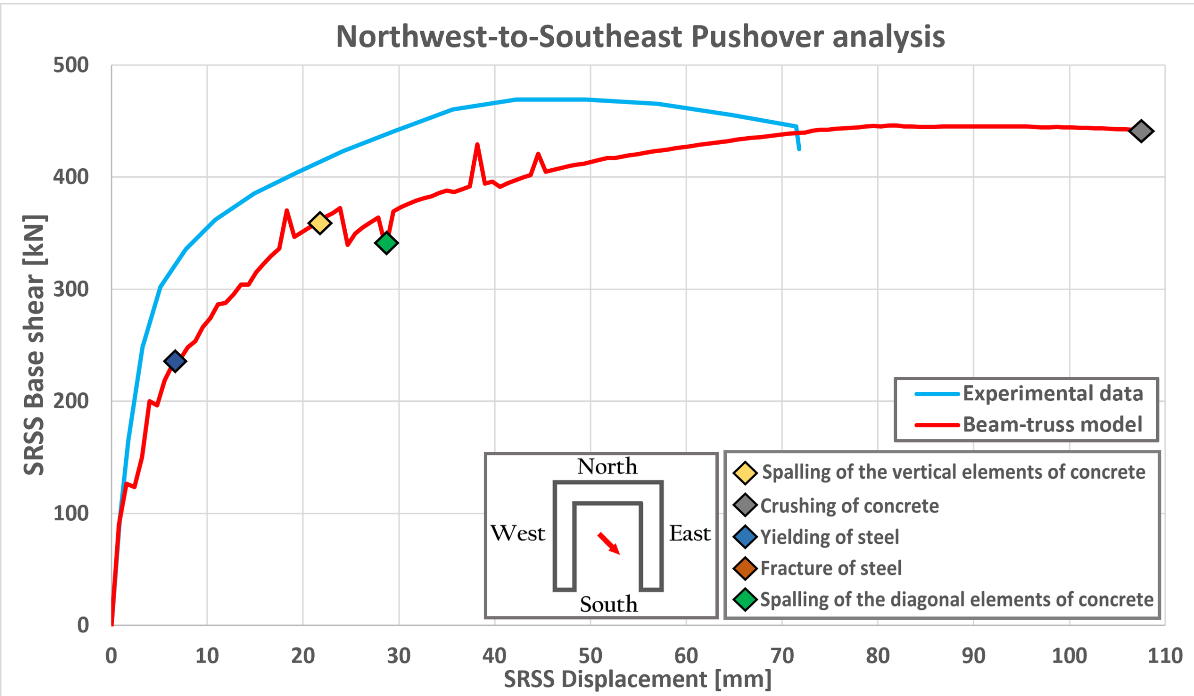

Figure 4.38: TUC: Force-displacement relationship when loaded from Northwest to Southeast.

4.4.3 TUD

4.4.3.1 Geometry

TUD is a U-section wall as shown in Figure 4.39. The properties and geometry of the wall have been taken from document [6] written by R. Constantin & al. (2016). The length of both flanges is equal to 1050 [mm] and the length of the web is equal to 1300 [mm]. The wall is 0.1 [m] thick in the web and flanges. The height of the wall is equal to 2950 [mm]. The axial load ratio of the wall is equal to 15 [%] which means that there is a total axial load of 1992 [kN] applied at the top of the wall.

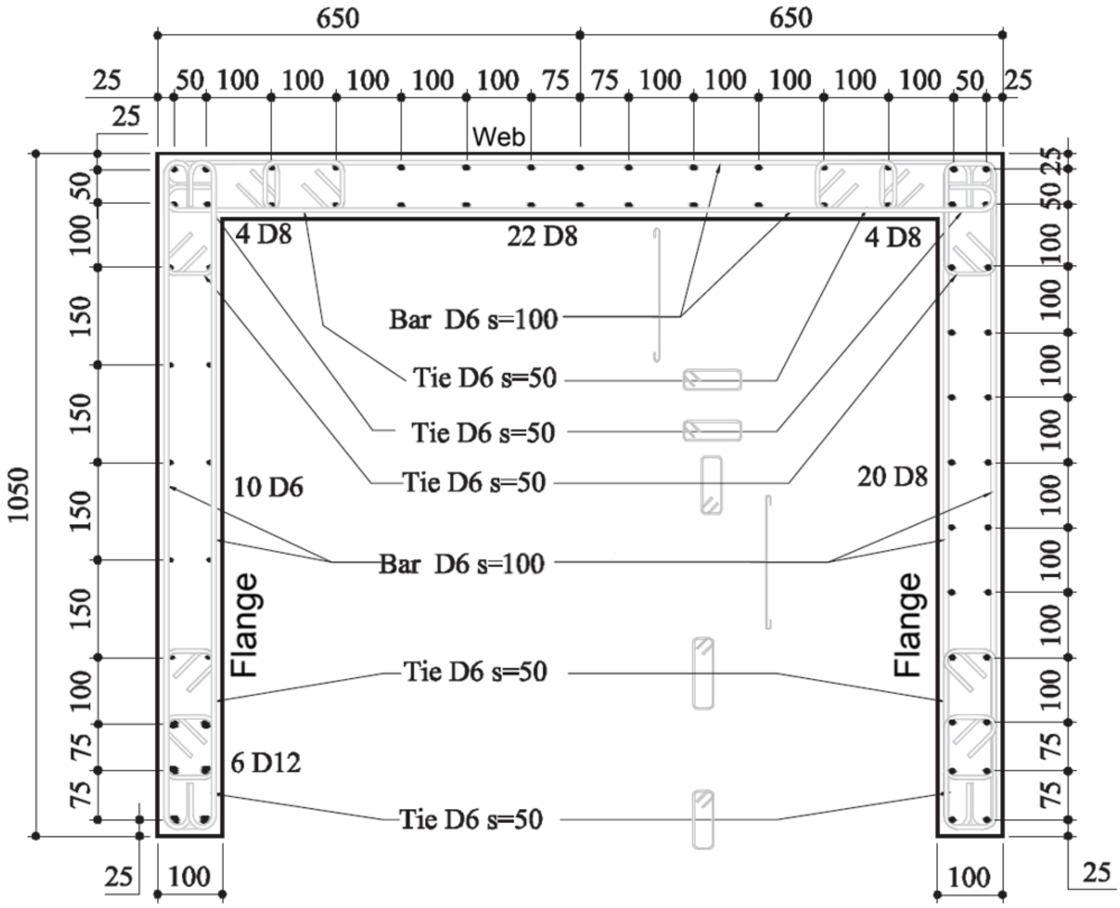

Figure 4.39: TUD: Cross section and reinforcement detailing from [6] [Unit: mm].

The reinforcement layout is the same as the one presented in Section 4.4.2 for TUC expected that the vertical spacing of the two sets of bars of 6 [mm] diameter that cross the full length of the web and flanges is equal to 100 [mm] instead of 125 [mm].

Figure 4.40 shows the plan and elevation views for the beam-truss model of the wall. The wall section is divided into 11 parts. The vertical elements located at both South extremities of the flanges and the ones in the corners are modeled with inelastic displacement-based frame elements whereas the other vertical elements are modeled with inelastic truss elements. The diagonal and horizontal elements are also modeled with inelastic truss elements.

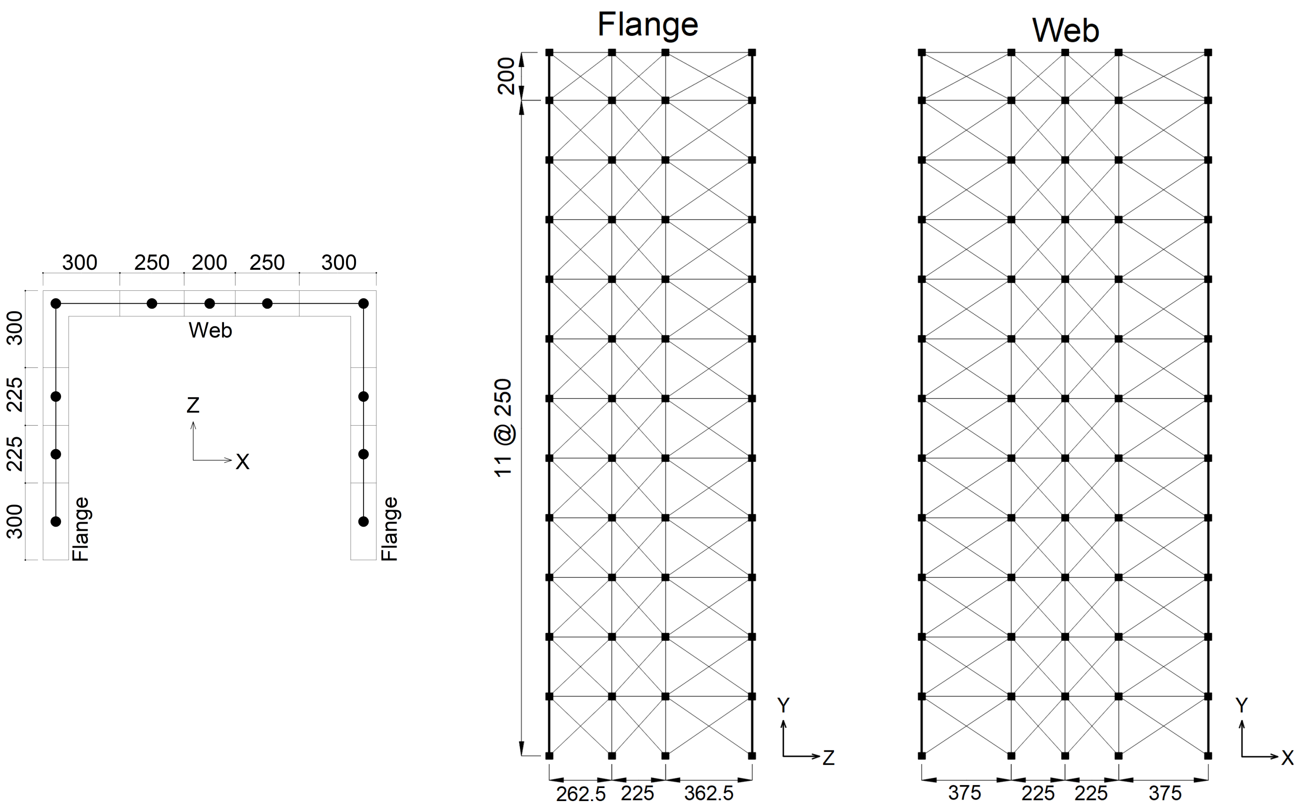

Figure 4.40: Plan and elevation views of the beam-truss model for TUD [Unit: mm].

4.4.3.2 Material properties

Tables 4.17 and 4.18 list respectively the properties for the steel reinforcement and the concrete that are used in the beam-truss model. Note that the tensile strength of concrete is considered as equal to zero for diagonal and horizontal elements.

Steel Mechanical Properties					
		Rebar $\phi 6$	Rebar $\phi 8$	Rebar $\phi 12$	
Diameter	d	6	8	12	mm
Modulus of elasticity	E_s	200	200	200	GPa
Yield tensile strength	f_y	492	563	529	MPa
Ultimate tensile strength	f_u	623	663	633	MPa
Yield strain	ϵ_y	0.246	0.2815	0.2645	%
Ultimate strain	ϵ_u	6.8	7.9	9.6	%
Strain hardening parameter	α	1	0.66	0.56	%
Specific weight	γ	78	78	78	kN/m^3

Table 4.17: Steel mechanical properties.

Concrete Mechanical Properties			
Compressive concrete strength	f_c	41.5	MPa
Tensile concrete strength	f_t	3	MPa
Modulus of elasticity	E_c	30.3	GPa
Strain at peak stress	ϵ_c	0.2	%
Specific weight	γ	24	kN/m^3

Table 4.18: Concrete mechanical properties.

4.4.3.3 Analysis output

Pushover analyses in the diagonal directions were performed on TUD. The results of those analyses in the Southeast-to-Northwest, Southwest-to-Northeast, Northeast-to-Southwest and in the Northwest-to-Southeast directions are respectively presented in Figures 4.41, 4.42, 4.43 and 4.44. In fact, the wall was loaded at the same time in both South-North and West-East directions in such a way that a resulting diagonal displacement was applied on top of the wall. In order to represent the data in a single graph, the base shear-displacement data were calculated thanks to the square root of the sum of the squares (SRSS) procedure. Therefore, at each pushover step, we calculate the square root of the sum of the squares of the base shear in the South-North direction and in the West-East direction. The same procedure is done for the displacements.

The results for the beam-truss model that has been presented, which correspond to the red curves in Figures 4.41, 4.42, 4.43 and 4.44, were obtained using the SeismoStruct software. We can see in Figures 4.41 and 4.42 that the beam-truss model curves have a really good match with the experimental data curves but are most of the time slightly below the experimental data curves. The beam-truss model curves in Figures 4.43 and 4.44 also have a good match with the experimental data curves but are most of time slightly below the experimental data curves.

Concerning the initial stiffness, we can see that all Figures 4.41, 4.42, 4.43 and 4.44 have an initial slope of their beam-truss model curves that match really well with the experimental data one, meaning that they have almost the same initial stiffness.

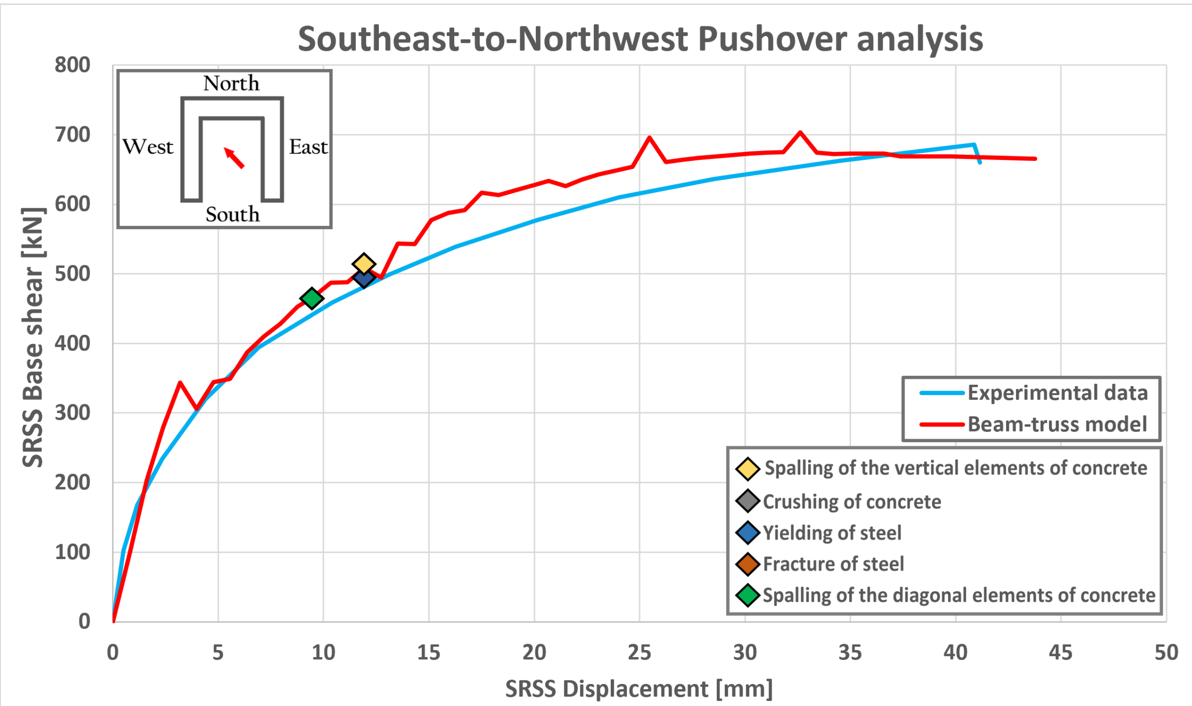

Figure 4.41: TUD: Force-displacement relationship when loaded from Southeast to Northwest.

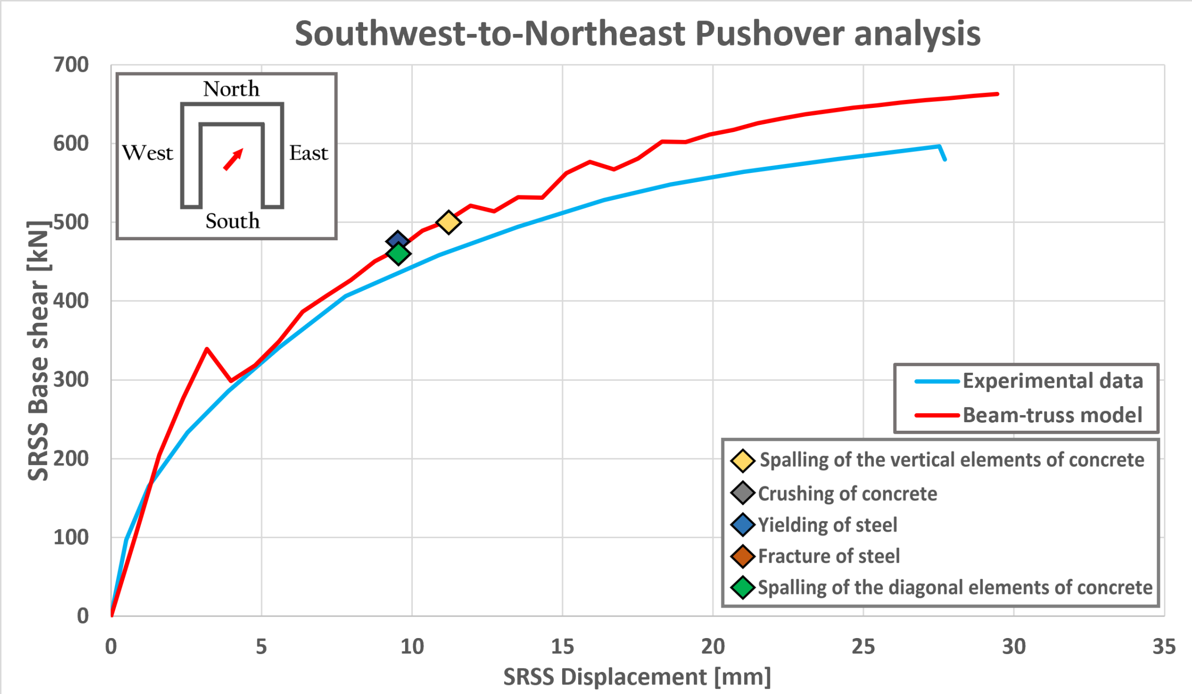

Figure 4.42: TUD: Force-displacement relationship when loaded from Southwest to Northeast.

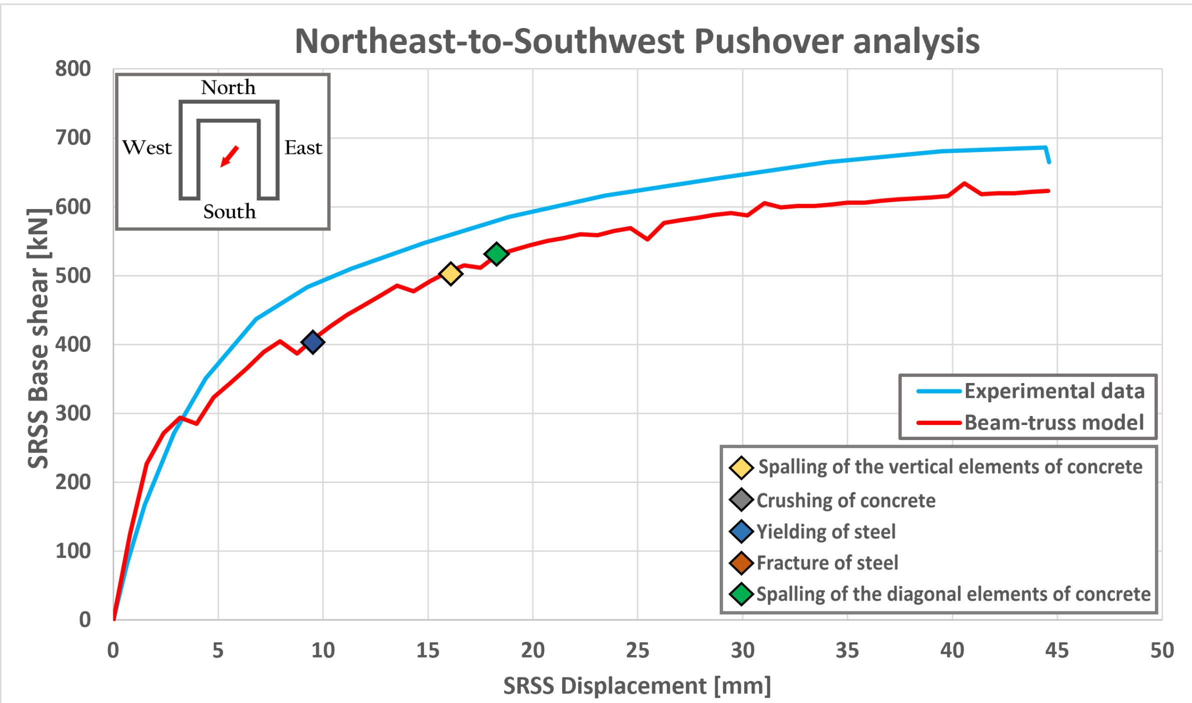

Figure 4.43: TUD: Force-displacement relationship when loaded from Northeast to Southwest.

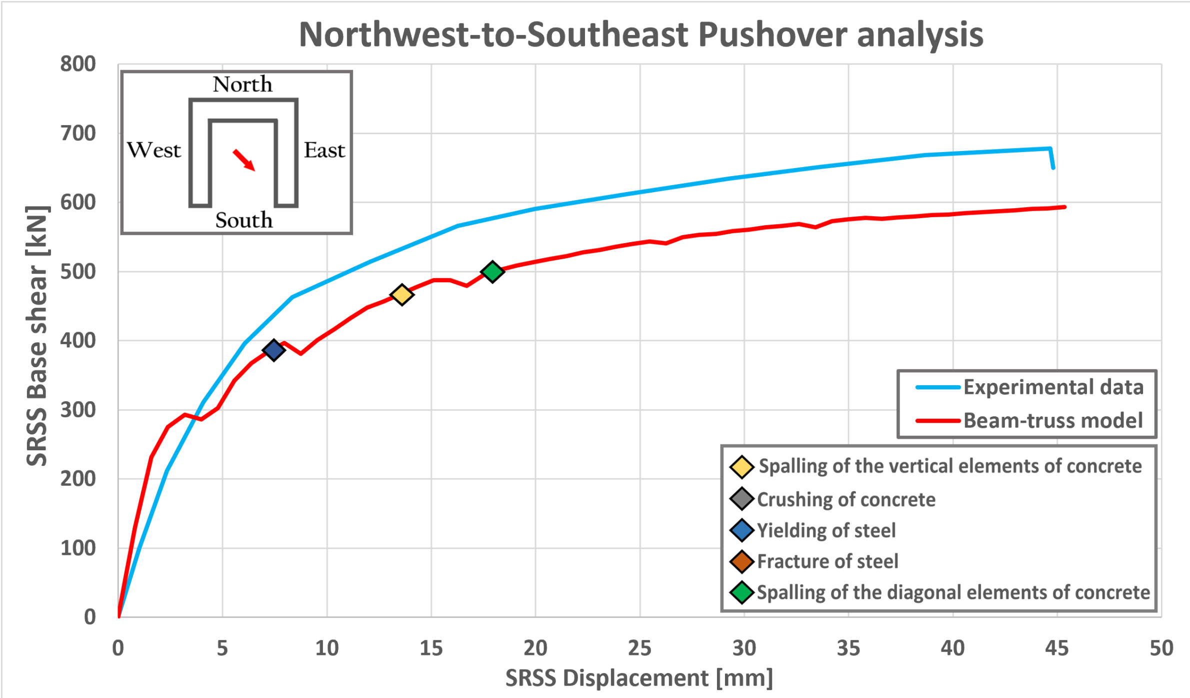

Figure 4.44: TUD: Force-displacement relationship when loaded from Northwest to Southeast.

4.4.4 TUE

4.4.4.1 Geometry

TUE is a U-section wall. Its cross-section is shown in Figure 4.45. The properties and geometry of the wall have been taken from document [13] written by R. Hoult & al. (2020). The length of both flanges is equal to 1050 $[mm]$ and the length of the web is equal to 1300 $[mm]$. The wall is 0.1 $[m]$ thick in the web and flanges.

When the wall is loaded in the North-South direction, its height is considered as equal to 4250 $[mm]$ since the North-South actuators, i.e, the system allowing to apply a horizontal displacement on the wall, are placed at this level. If the wall is loaded in the East-West direction, then the height of the wall is equal to 4650 $[mm]$. The shear span ratio when the wall is loaded in the North-South and in the East-West direction is respectively equal to 4.05 and 3.58. There is no axial load applied at the top of the wall.

In each flange of the wall, there are 7 longitudinal bars having a diameter of 6 $[mm]$. In the web, there are 10 longitudinal bars having also a diameter of 6 $[mm]$. In both corners of the wall, i.e., at the two intersections between the web and the flanges, and in the South extremities of the flanges, there are 3 longitudinal bars having a diameter of 16 $[mm]$. Regarding the transverse reinforcement, there are no hoops to confined the concrete in the extremities of the wall. However, there are one set of 6 $[mm]$ diameter bars spaced 100 $[mm]$ apart that cross the full length of the web and flanges.

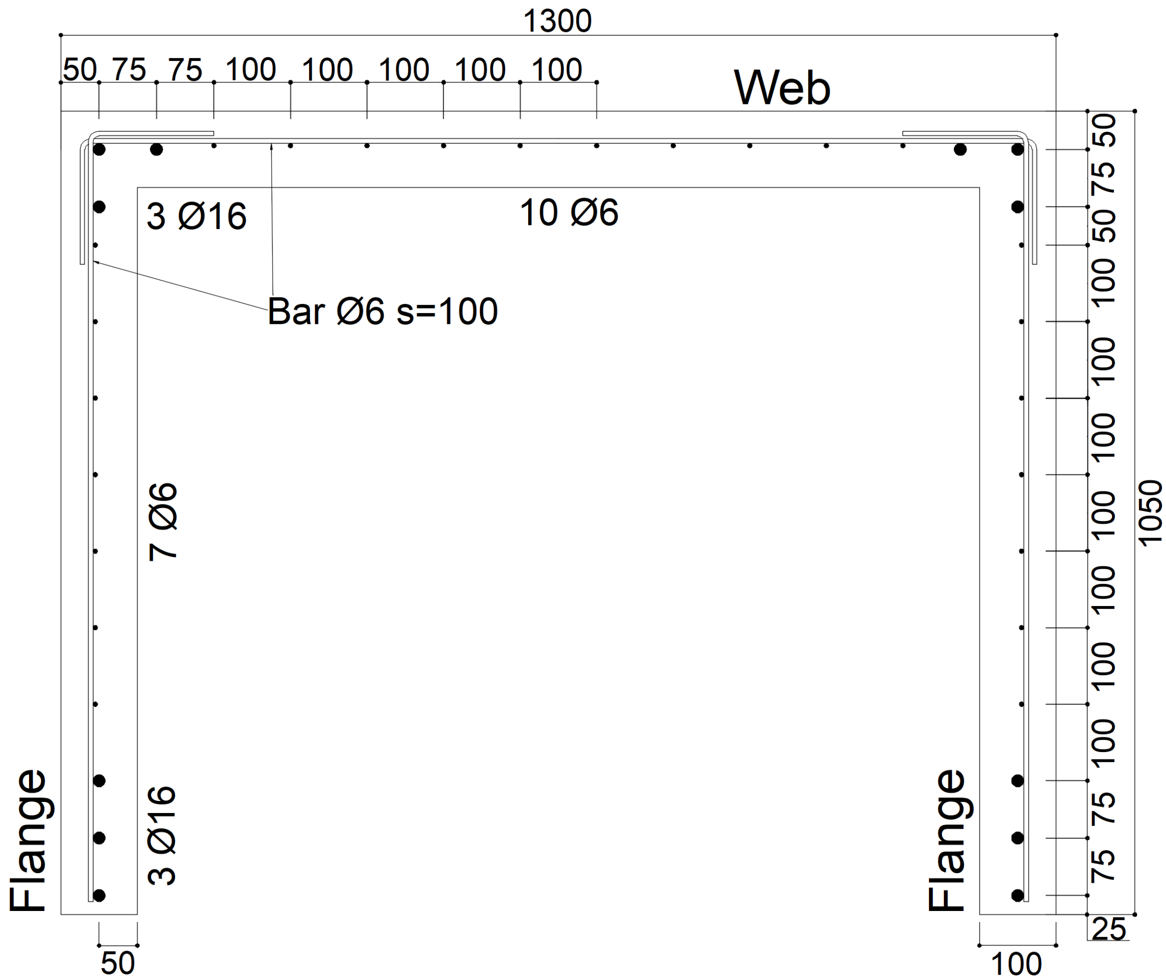

Figure 4.45: TUE: Cross section and reinforcement detailing [Unit: *mm*].

Figure 4.46 shows the plan and elevation views for the beam-truss model of the wall when it is loaded in the North-South direction. The wall section is divided into 15 parts. When loaded in the East-West direction, the plan view of the beam-truss model illustrated in Figure 4.46 remains the same but the elevation view changes. Instead of having 20 vertical elements with a height of 200 [*mm*] each, there are 22 of them. The last vertical elements at the top of the model having a height of 250 [*mm*] remains unchanged. The vertical elements located at both South extremities of the flanges and the ones in the corners are modeled with inelastic displacement-based frame elements whereas the other vertical elements are modeled with inelastic truss elements. The diagonal and horizontal elements are also modeled with inelastic truss elements.

4.4.4.2 Material properties

Tables 4.19 and 4.20 list respectively the properties for the steel reinforcement and the concrete that are used in the beam-truss model. Be aware that the tensile strength of concrete is considered as equal to zero for diagonal and horizontal elements.

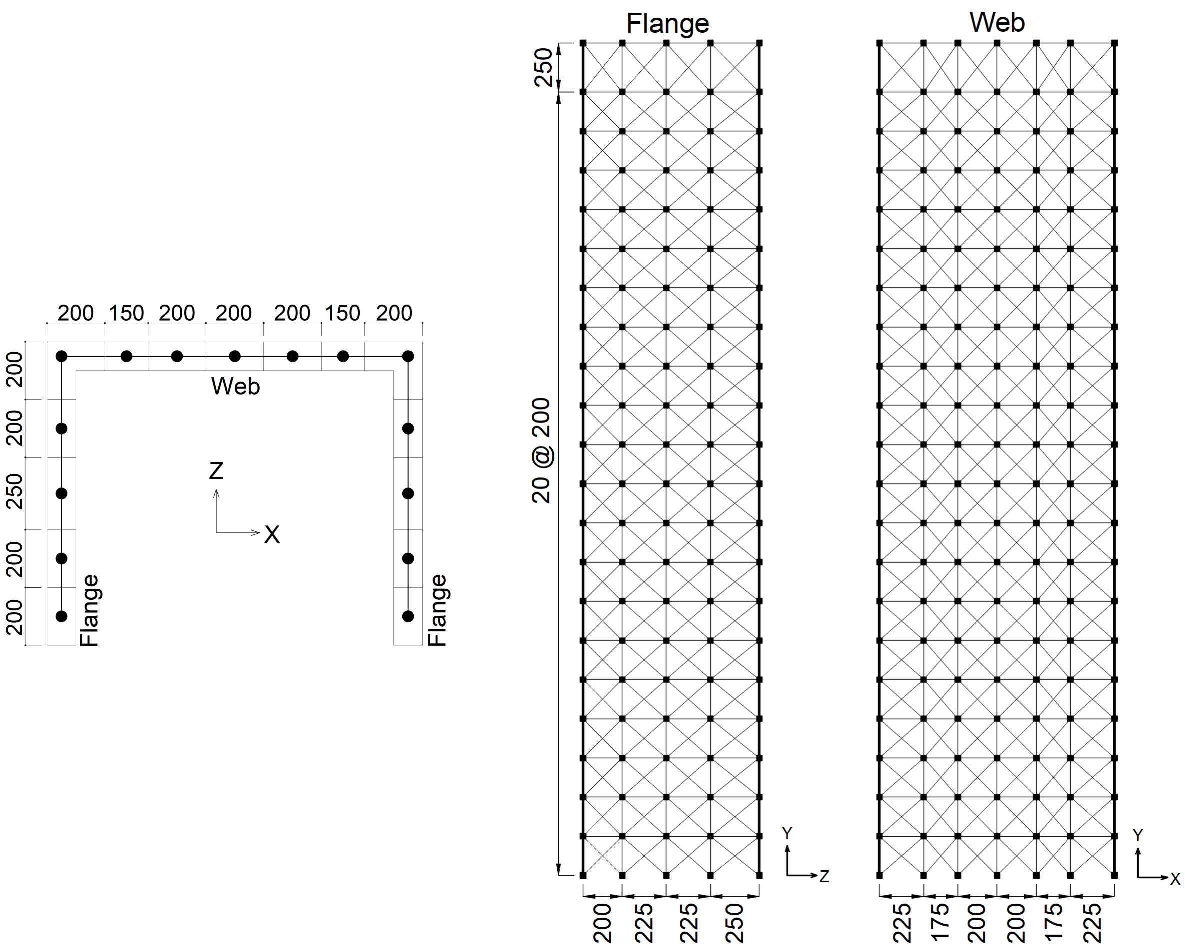

Figure 4.46: Plan and elevation views of the beam-truss model for TUE [Unit: mm].

Steel Mechanical Properties				
		Rebar $\phi 6$	Rebar $\phi 16$	
Diameter	d	6	16	mm
Modulus of elasticity	E_s	204	193	GPa
Yield tensile strength	f_y	475	521	MPa
Ultimate tensile strength	f_u	625	627	MPa
Yield strain	ϵ_y	0.233	0.27	%
Ultimate strain	ϵ_u	9.8	12.1	%
Strain hardening parameter	α	0.769	0.464	%
Specific weight	γ	78	78	kN/m^3

Table 4.19: Steel mechanical properties.

Concrete Mechanical Properties			
Compressive concrete strength	f_c	31.7	MPa
Tensile concrete strength	f_t	2.1	MPa
Modulus of elasticity	E_c	26.5	GPa
Strain at peak stress	ϵ_c	0.2	%
Specific weight	γ	24	kN/m^3

Table 4.20: Concrete mechanical properties.

4.4.4.3 Analysis output

Pushover analyses in the West-to-East, East-to-West and South-to-North directions were performed on TUE. The results of those tests can be seen in Figures 4.47, 4.48 and 4.49 in which the displacements correspond to the displacements at the top of the wall.

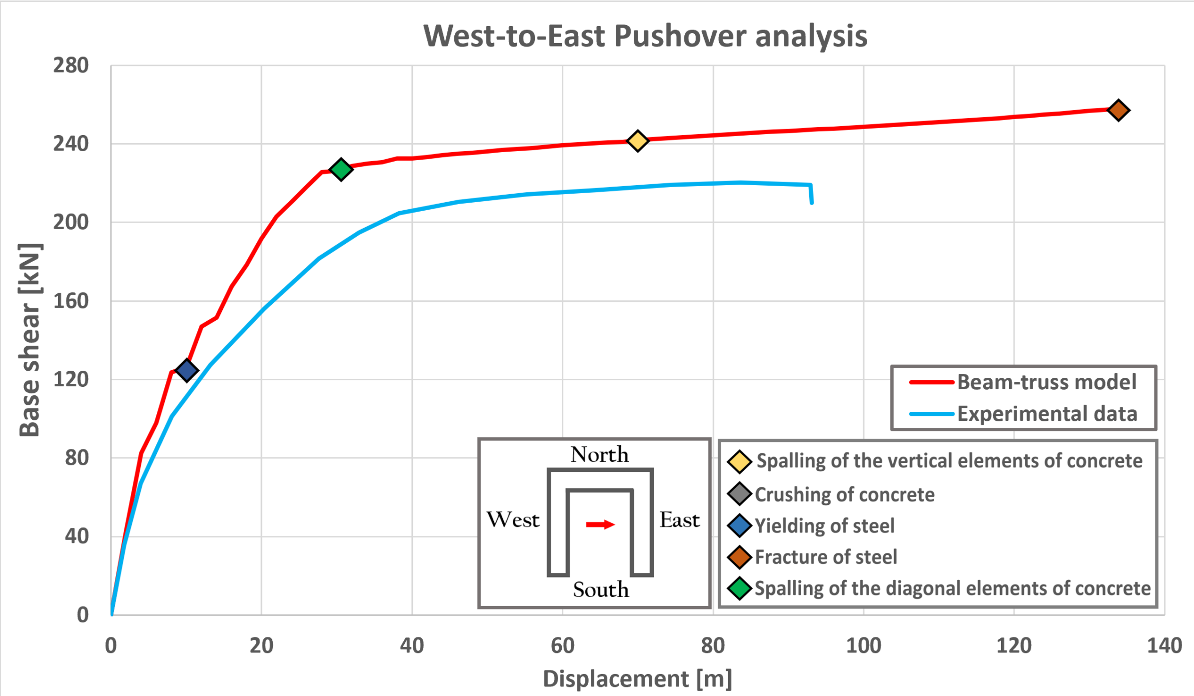

Figure 4.47: TUE: Force-displacement relationship when loaded from West to East.

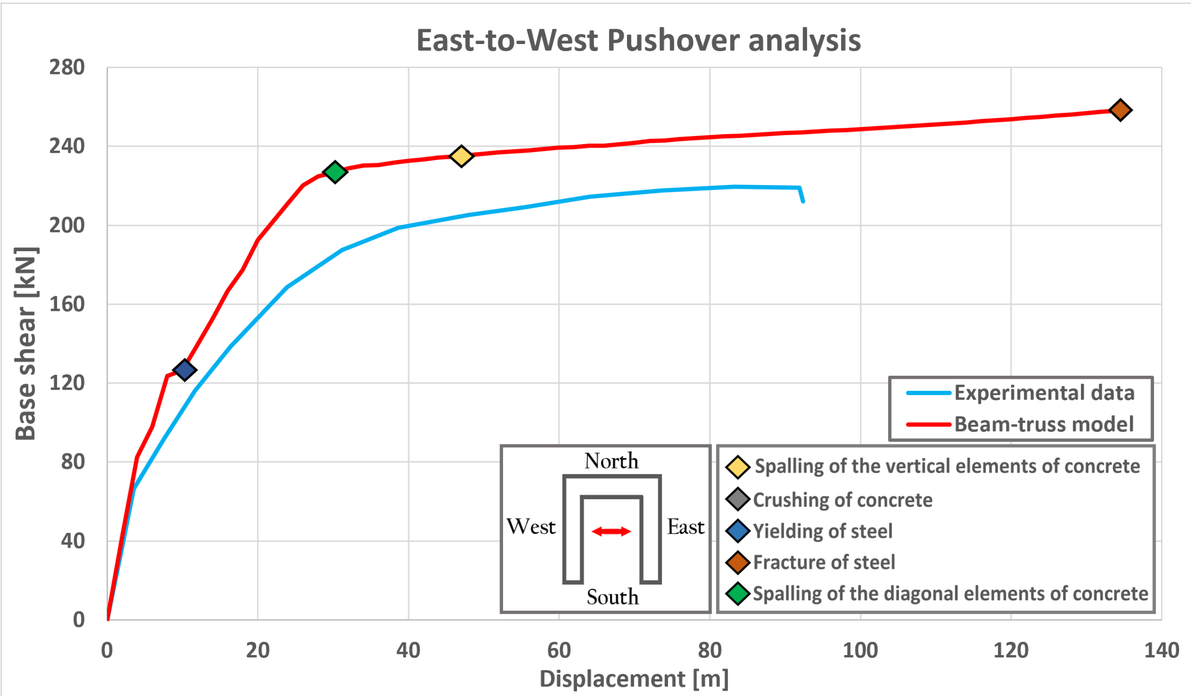

Figure 4.48: TUE: Force-displacement relationship when loaded from East to West.

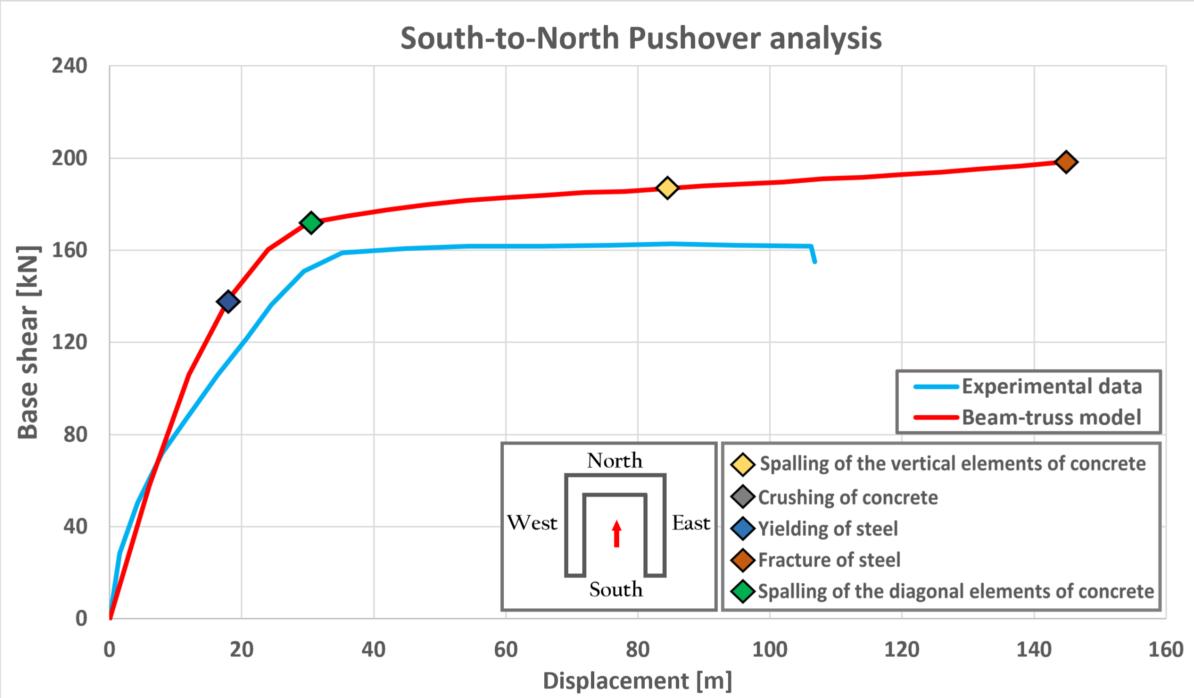

Figure 4.49: TUE: Force-displacement relationship when loaded from South to North.

The results for the beam-truss model that has been presented, which correspond to the red curves in Figures 4.47, 4.48 and 4.49, were obtained using the SeismoStruct software. We can see on those three graphs that the base shear is most of the time overestimated by the beam-truss model since the beam-truss model curves are most of the time above the experimental data curves.

However, concerning the initial stiffness, we can see in Figures 4.47, 4.48 and 4.49 that the initial slope of the beam-truss model curves match really well with the experimental data one, meaning that they have almost the same initial stiffness.

Finally, we can see in Figures 4.47, 4.48 and 4.49 that the beam-truss model curves stop due to fracture of the longitudinal steel bars in the vertical elements of the model.

4.4.5 TUF

Wall TUF is a U-shaped section wall as shown in Figure 4.50. The properties and geometry of the wall have been taken from document [13] written by R. Hoult & al. (2020). The length of both flanges is equal to 1050 [mm] and the length of the web is equal to 1300 [mm]. The wall is 0.1 [m] thick in the web and flanges. Its height is equal to 4250 [mm]. There is no axial load applied at the top of the wall.

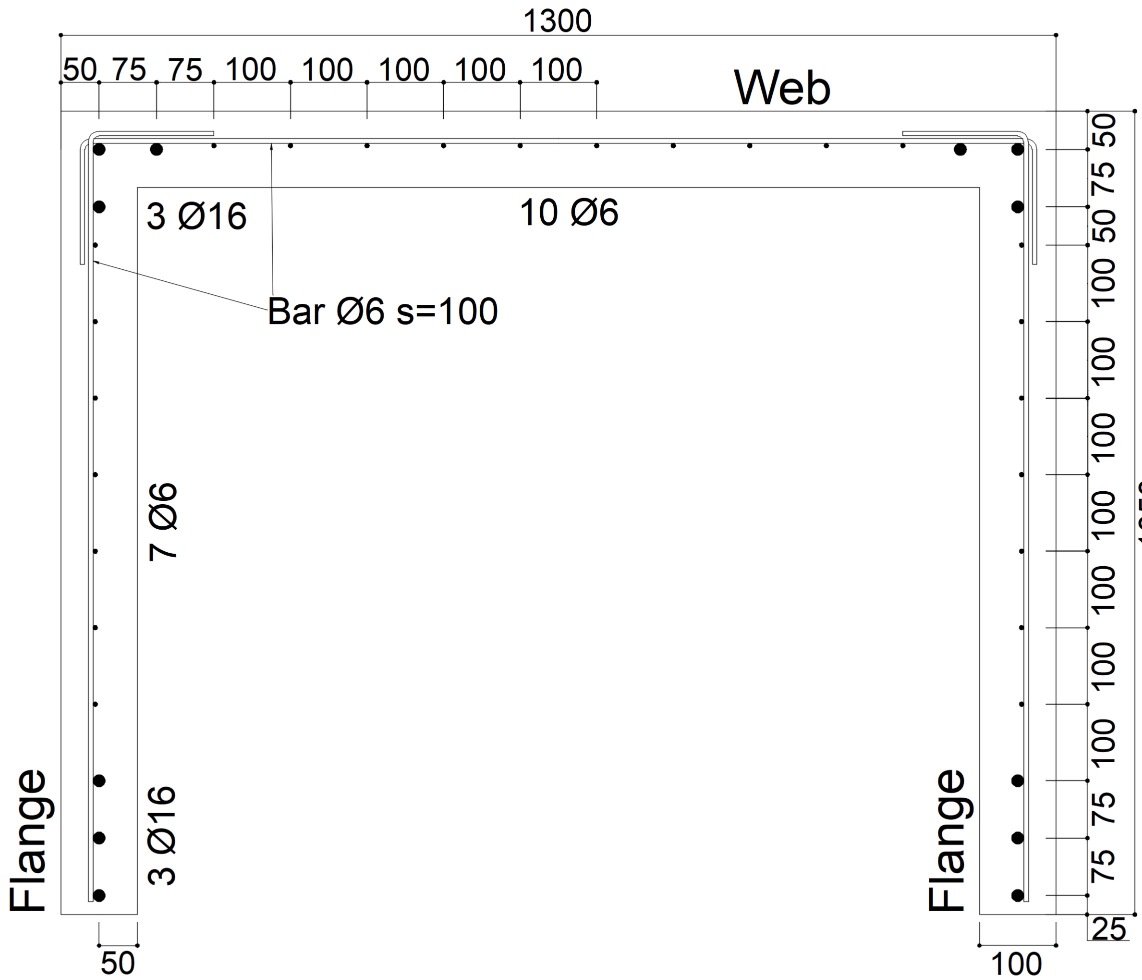

Figure 4.50: TUF: Cross section and reinforcement detailing [Unit: mm].

The reinforcement layout of the wall is exactly the same than the one of wall TUE that was presented in Section 4.4.4.

Figure 4.51 shows the plan and elevation views for the beam-truss model of the wall. The wall section is divided into 15 parts. The vertical elements located at both South extremities of the flanges and the ones in the corners are modeled with inelastic displacement-based frame elements whereas the other vertical elements are modeled with inelastic truss elements. The diagonal and horizontal elements are also modeled with inelastic truss elements.

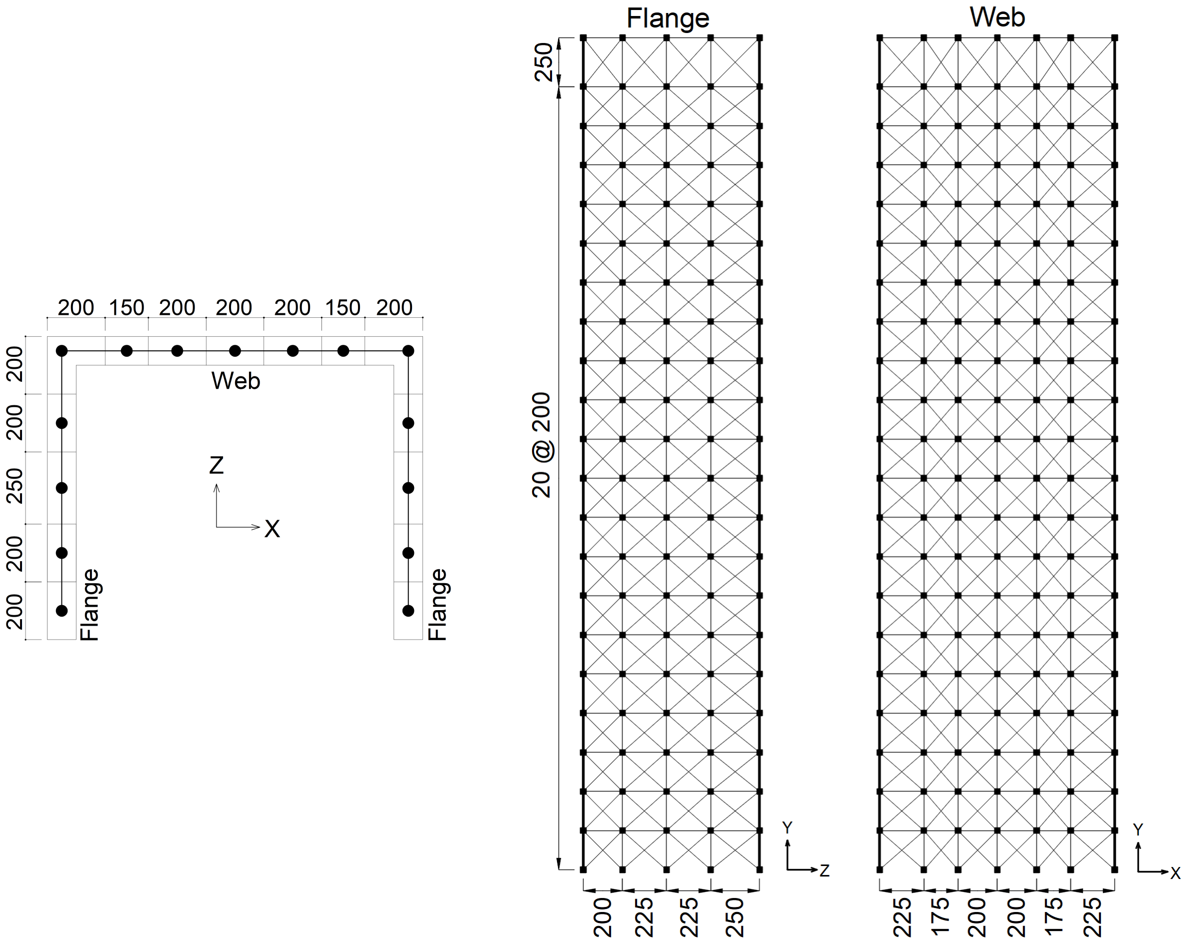

Figure 4.51: Plan and elevation views of the beam-truss model for TUF [Unit: mm].

4.4.5.1 Material properties

The main changes compared to TUE wall presented in Section 4.4.4 are in the mechanical properties of the concrete. Tables 4.21 and 4.22 list respectively the properties for the steel reinforcement and the concrete that are used in the beam-truss model. Note that the tensile strength of concrete is considered as equal to zero for diagonal and horizontal elements.

Steel Mechanical Properties				
		Rebar $\phi 6$	Rebar $\phi 16$	
Diameter	d	6	16	mm
Modulus of elasticity	E_s	204	183	GPa
Yield tensile strength	f_y	475	523	MPa
Ultimate tensile strength	f_u	625	637	MPa
Yield strain	ϵ_y	0.233	0.286	%
Ultimate strain	ϵ_u	9.8	8.3	%
Strain hardening parameter	α	0.769	0.777	%
Specific weight	γ	78	78	kN/m^3

Table 4.21: Steel mechanical properties.

Concrete Mechanical Properties			
Compressive concrete strength	f_c	28.7	MPa
Tensile concrete strength	f_t	2.7	MPa
Modulus of elasticity	E_c	25.2	GPa
Strain at peak stress	ϵ_c	0.2	$\%$
Specific weight	γ	24	kN/m^3

Table 4.22: Concrete mechanical properties.

4.4.5.2 Analysis output

Pushover analyses in the diagonal directions have been performed on TUF. The results of those analyses in the Southeast-to-Northwest and in the Southwest-to-Northeast directions are respectively presented in Figures 4.52 and 4.53. In fact, the wall was loaded at the same time in both South-North and West-East directions in such a way that a resulting diagonal displacement was applied on top of the wall. In order to represent the data in a single graph, the base shear-displacement data have been calculated thanks to the square root of the sum of the squares (SRSS) procedure. Therefore, at each pushover step, we calculate the square root of the sum of the squares of the base shear in the South-North direction and in the West-East direction. The same procedure is done for the displacements.

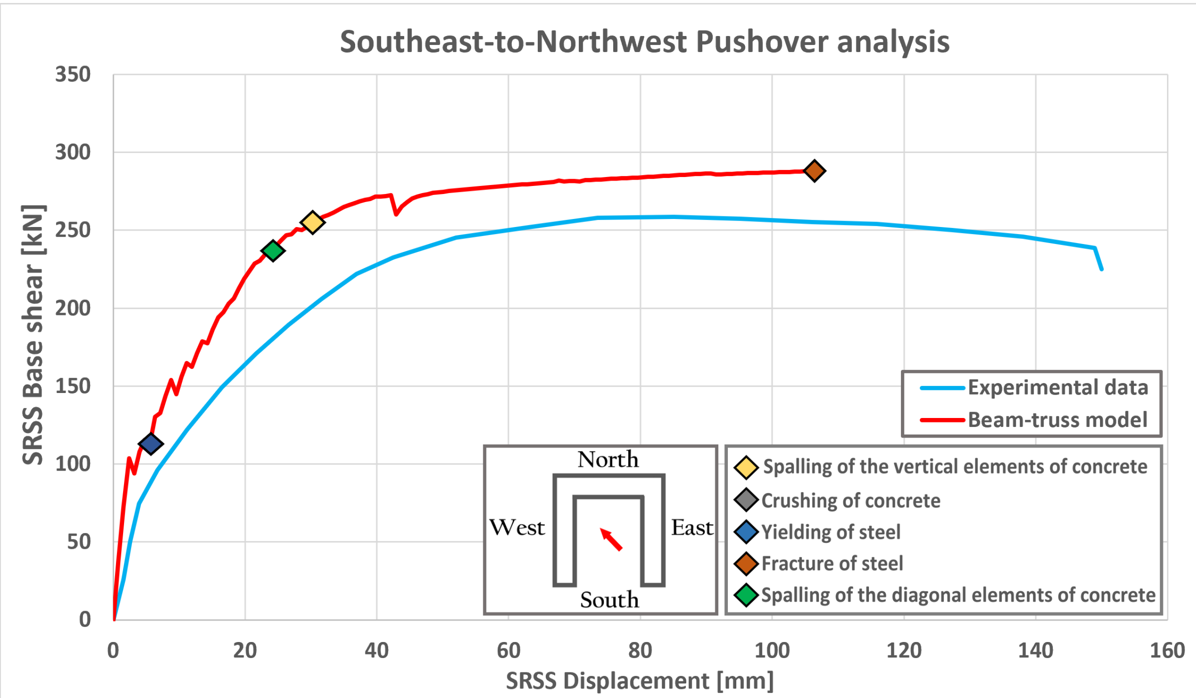

Figure 4.52: TUF: Force-displacement relationship when loaded from Southeast to Northwest.

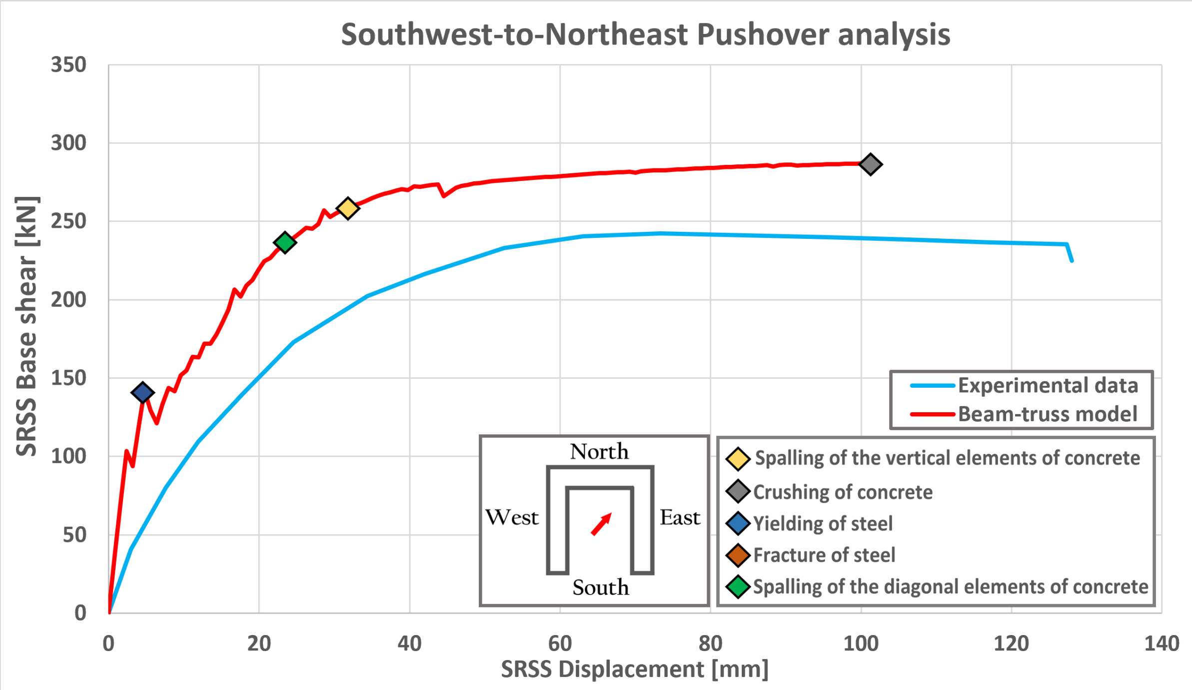

Figure 4.53: TUF: Force-displacement relationship when loaded from Southwest to Northeast.

The results for the beam-truss model that has been presented, which correspond to the red curves in Figures 4.52 and 4.53, were obtained using the SeismoStruct software. We can see in Figures 4.52 and 4.53 that the beam-truss model curves are all the time above the experimental data curves meaning that the beam-truss model overestimates the real base shear in the wall.

Concerning the initial stiffness, we can see in Figures 4.52 and 4.53 that the beginning of the beam-truss model curves have an initial slope that are steeper than the one of the experimental data curves, meaning that they have different initial stiffness.

4.4.6 UW1

4.4.6.1 Geometry

UW1 is a U-section wall that was tested in the Institute of Mechanics, Materials and Civil Engineering (iMMC) at the Université Catholique de Louvain (UCLouvain), Belgium. Its cross-section is shown in Figure 4.54. The properties and geometry of the wall have been taken from document [26]. The length of both flanges is equal to 1050 $[mm]$ and the length of the web is equal to 1300 $[mm]$. The wall is 0.1 $[m]$ thick in the web and flanges. The height of the wall is equal to 2250 $[mm]$. However, UW1 is subjected during the test to an overturning moment, shear force and axial force on the top of the wall because it has for objective to simulate the behavior of a 6720 $[mm]$ high wall. So, for ease of modelling, UW1 has been modeled as a 6720 $[mm]$ high wall to which only a total axial load of 611.2 $[kN]$ was applied at the top of it since the axial load ratio of the wall is equal to 5 $[\%]$.

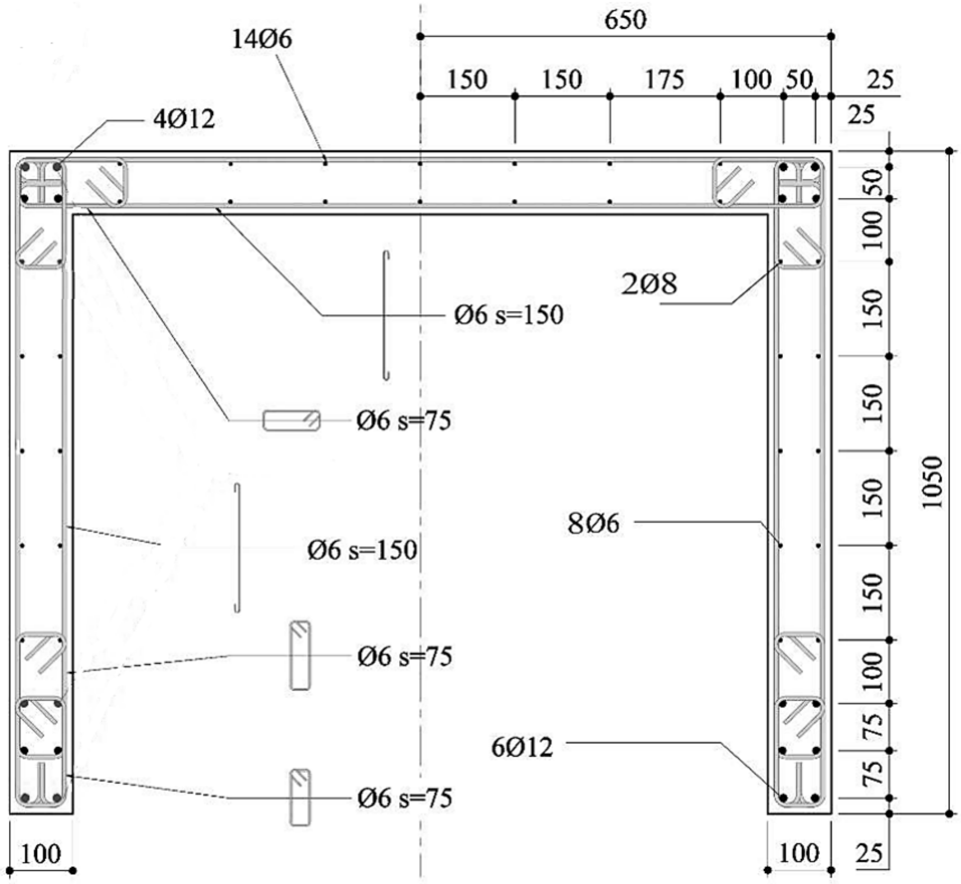

Figure 4.54: UW1: Cross section and reinforcement detailing from [26] [Unit: *mm*].

In each flange of the wall, there are 8 longitudinal bars having a diameter of 6 [*mm*] and 2 longitudinal bars having a diameter of 8 [*mm*]. In the web, there are 10 longitudinal bars having also a diameter of 6 [*mm*] and 4 longitudinal bars having a diameter of 8 [*mm*]. In both corners of the wall, i.e., at the two intersections between the web and the flanges, there are 4 longitudinal bars having a diameter of 12 [*mm*]. In both South extremities of the flanges, there are 6 longitudinal bars having a diameter of 12 [*mm*]. Regarding the transverse reinforcement, there are 2 sets of hoops of 6 [*mm*] diameter spaced 75 [*mm*] apart in each corner of the wall and in both South extremities of the flanges. There are also two sets of 6 [*mm*] diameter bars spaced 150 [*mm*] apart that cross the full length of the web and flanges.

Figure 4.55 shows the plan and elevation views for the beam-truss model of the wall. The wall section is divided into 11 parts. The vertical elements located at both South extremities of the flanges and the ones in the corners are modeled with inelastic displacement-based frame elements whereas the other vertical elements are modeled with inelastic truss elements. The diagonal and horizontal elements are also modeled with inelastic truss elements.

4.4.6.2 Material properties

Tables 4.23 and 4.24 list respectively the properties for the steel reinforcement and the concrete that are used in the beam-truss model. Note that the tensile strength of concrete is considered as equal to zero for diagonal and horizontal elements.

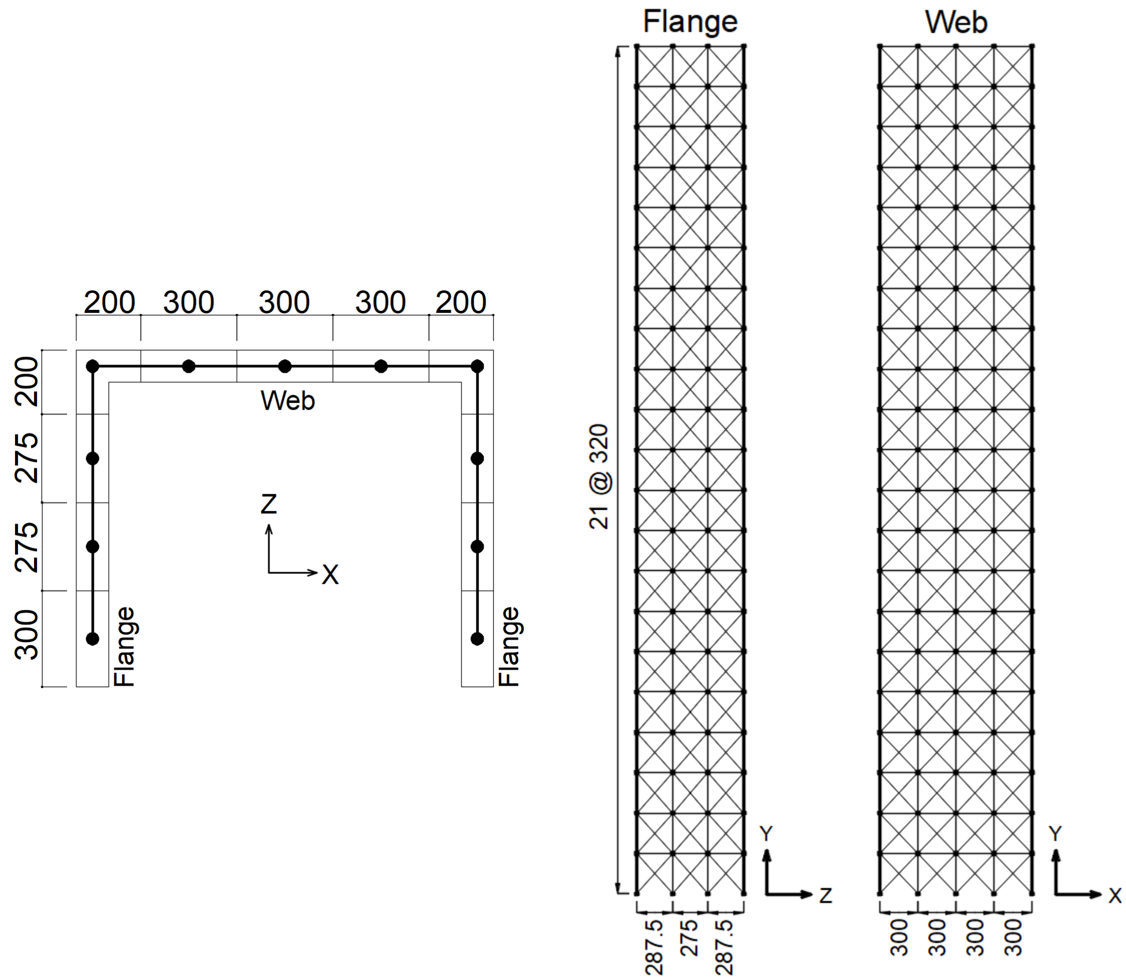

Figure 4.55: Plan and elevation views of the beam-truss model for UW1 [Unit: mm].

Steel Mechanical Properties					
		Rebar $\phi 6$	Rebar $\phi 8$	Rebar $\phi 12$	
Diameter	d	6	8	12	mm
Modulus of elasticity	E_s	207	196	199	GPa
Yield tensile strength	f_y	550	538	580	MPa
Ultimate tensile strength	f_u	676	664	690	MPa
Yield strain	ϵ_y	0.27	0.27	0.29	%
Ultimate strain	ϵ_u	9.5	12	10.1	%
Strain hardening parameter	α	0.66	0.55	0.56	%
Specific weight	γ	78	78	78	kN/m^3

Table 4.23: Steel mechanical properties.

Concrete Mechanical Properties			
Compressive concrete strength	f_c	38.2	MPa
Tensile concrete strength	f_t	3.07	MPa
Modulus of elasticity	E_c	29	GPa
Strain at peak stress	ϵ_c	0.2	%
Specific weight	γ	24	kN/m^3

Table 4.24: Concrete mechanical properties.

4.4.6.3 Analysis output

Pushover analyses in the North-to-South and South-to-North directions were performed on UW1. The results of those tests can be seen in Figures 4.56 and 4.57 in which the displacements correspond to the displacements at a height of 2.25 $[m]$.

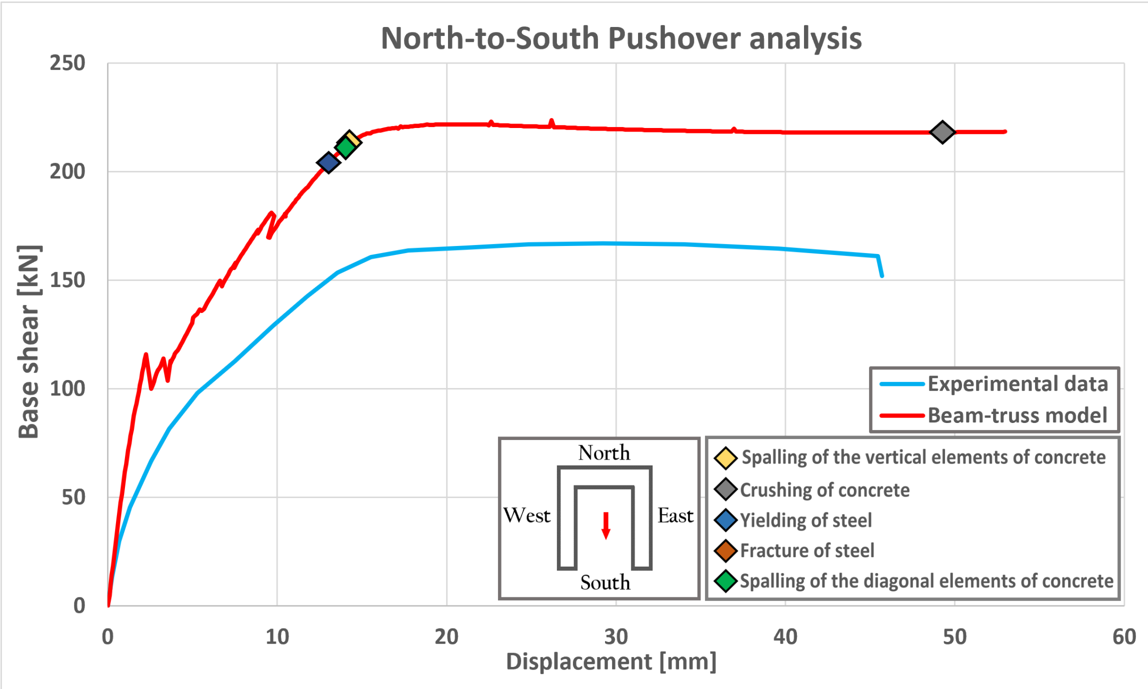

Figure 4.56: UW1: Force-displacement relationship when loaded from North to South.

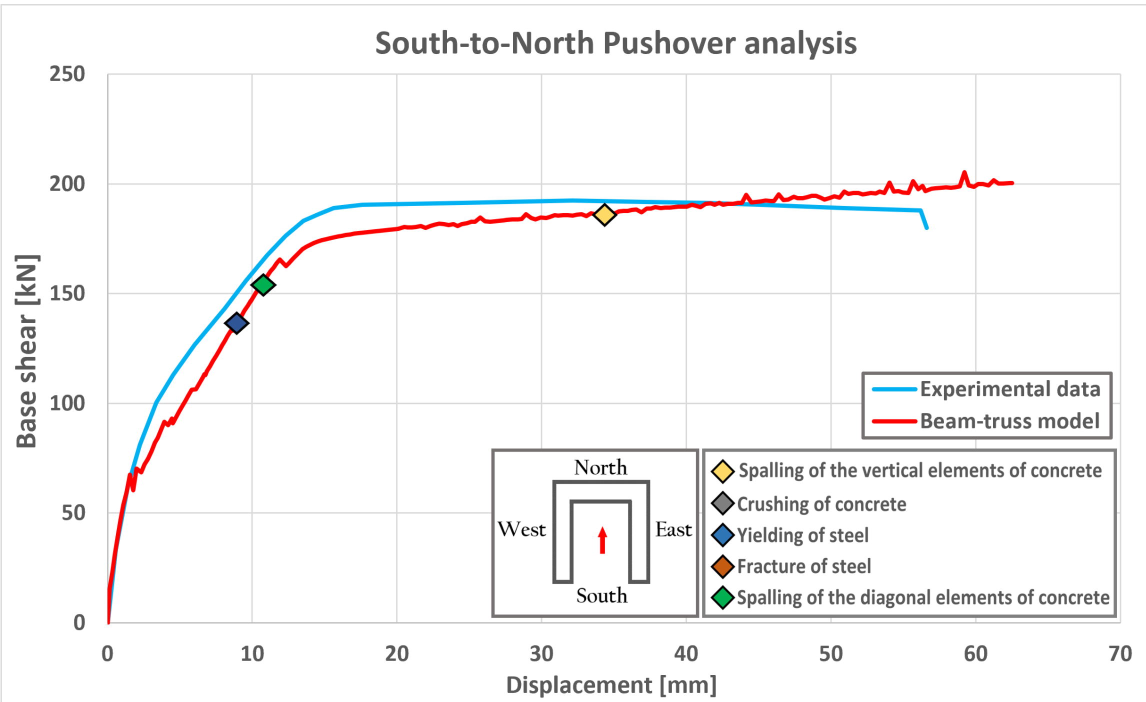

Figure 4.57: UW1: Force-displacement relationship when loaded from South to North.

The results for the beam-truss model that has been presented, which correspond to the red curves in Figures 4.56 and 4.57, were obtained using the SeismoStruct software. We can see in Figure 4.56, when the wall is loaded from North to South, that the beam-truss model curve is all the time above the experimental data one meaning that the base shear is overestimates by the model. However, the beam-truss model curve when the wall is loaded from South to North in Figure 4.57 has a really good match with the experimental data one.

Regarding the initial stiffness, we can see in both Figures 4.56 and 4.57 that the initial slope of the beam-truss model curves match really well with the experimental data one, meaning that they have almost the same initial stiffness.

Finally, we can see in Figure 4.56 that the beam-truss model curve stops due to the crushing of concrete in the South extremities of the flanges of the wall.

Chapter 5

Effective stiffness

This chapter will present different procedures that have been chosen to compute the effective stiffness ratio for all the walls that have been previously analyzed. A comparison of the results obtained with these different procedures will also be presented.

5.1 Calculation procedures

This section describes the different methods enabling to obtain the effective stiffness ratio of walls from either their force-displacement relationship or from an empirical formula.

5.1.1 First procedure

The first procedure that has been chosen is based on the first definition of the effective stiffness which was discussed in Section 2.1.2. As a reminder, this method consists in taking the slope of the secant of the lateral force versus lateral displacement relationship passing through the point at which the applied force reaches 75 % of the maximum lateral force that the structure can withstand [15]. The slope of the line passing though point A in Figure 2.3 shows an illustration of this definition.

The value of the obtained slope is indeed equal to the effective stiffness K_{eff}. In order to have the effective stiffness ratio $\frac{I_{eff}}{I_g}$, we should calculate the initial stiffness K_i of the wall. This latter value is obtained by the following expression in which I_g is the gross moment of inertia of the corresponding wall cross-section, E_c is the Young's modulus of concrete and H is the height of the wall [28]:

$$K_i = \frac{3E_cI_g}{H^3}$$

Therefore, it can be deduced the effective stiffness ratio thanks to the following equality:

$$\frac{I_{eff}}{I_g} = \frac{K_{eff}}{K_i}$$

5.1.2 Second procedure

The second procedure that has been chosen is based on the second definition of the effective stiffness which was also discussed in Section 2.1.2. As a reminder, this method consists in taking the slope of the secant of the lateral force versus lateral displacement relationship passing through the first yield point of the wall. This first yield point is defined as the point when either the first longitudinal reinforcing bar yields or when the maximum concrete compressive strain of the wall reaches 0.002. The slope of the line passing though point B in Figure 2.3 shows an illustration of this definition. The obtained slope is indeed equal to the effective stiffness K_{eff}. Therefore, for obtaining the effective stiffness ratio $\frac{I_{eff}}{I_g}$, the exact same process as the one explained in the First procedure (5.1.1) will be used.

5.1.3 Third procedure

The third procedure is taken from the European code EN 1998-2 [24] and was discussed in details in Section 2.2.1. As a reminder, this method consists in computing the effective moment of inertia I_{eff} with the following formula:

$$I_{eff} = \nu \frac{M_{Rd}}{E_c \phi_y}$$

5.1.4 Fourth procedure

The last method that can be used to assess the effective stiffness ratio is the one proposed by M. N. Fardis & al. (2015) [11] and was already discussed in details in Section 2.2.2. As a reminder, this method consists to use the following expression to compute the effective stiffness ratio:

$$\frac{I_{eff}}{I_g} = a\left(0.8 + ln\left(max\left(\frac{L_s}{H}; 0.6\right)\right)\right)\left(1 + 0.048\ min\left(50\ [MPa]; \frac{P}{A_g}\right)\right)$$

The choice of the procedures hereabove was not made at random. The First and Second procedures are analytical methods based on both definitions of the effective stiffness that have been presented in Section 2.1.2. The Third one is a hybrid analytical-empirical method as we need to insert the design ultimate moment M_{Rd}, which can be calculated from the numerical force-displacement results, into an empirical expression. Finally, the Fourth procedure uses an empirical expression to assess the effective stiffness ratio without the need of numerical results.

5.2 Comparison of experimental vs numerical

Figures 5.1, 5.2, 5.3 and 5.4 show the values of the effective stiffness ratio $\frac{I_{eff}}{I_g}$ that were calculated with one of the four procedures described in Section 5.1 for all walls that have been previously analyzed.

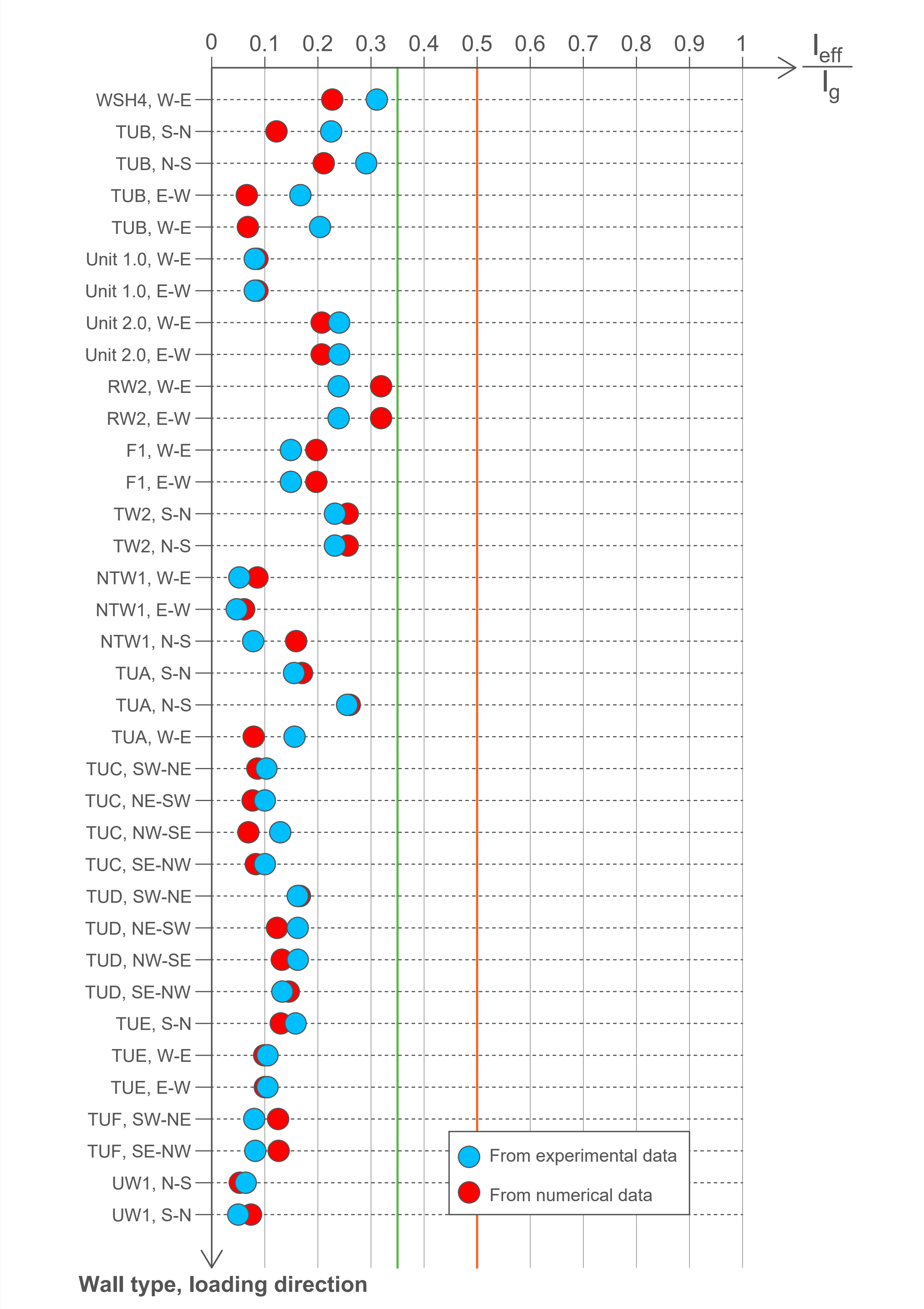

Figure 5.1: Effective stiffness ratio values when the First procedure is applied on the numerical data.

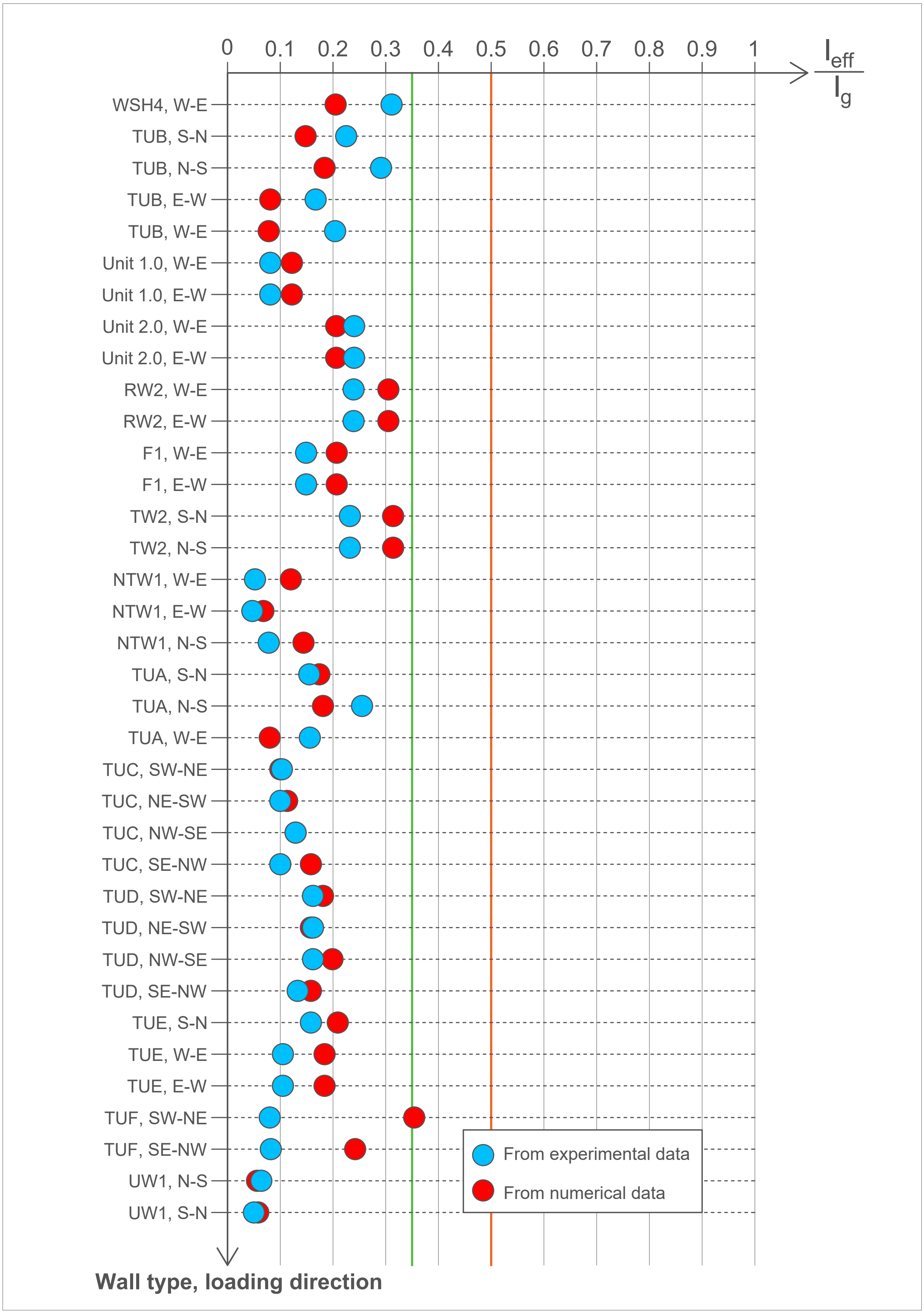

Figure 5.2: Effective stiffness ratio values when the Second procedure is applied on the numerical data.

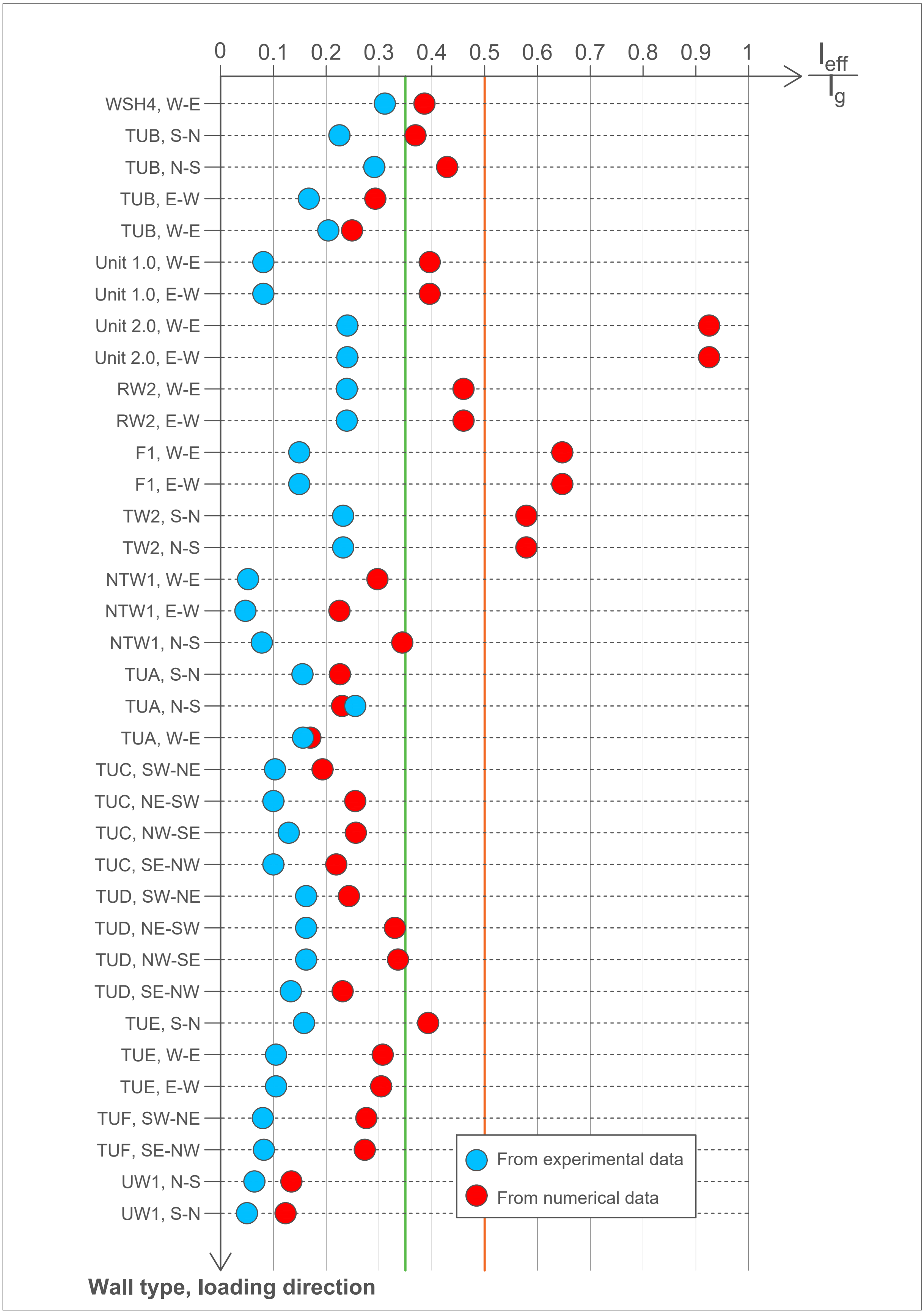

Figure 5.3: Effective stiffness ratio values when the Third procedure is applied on the numerical data.

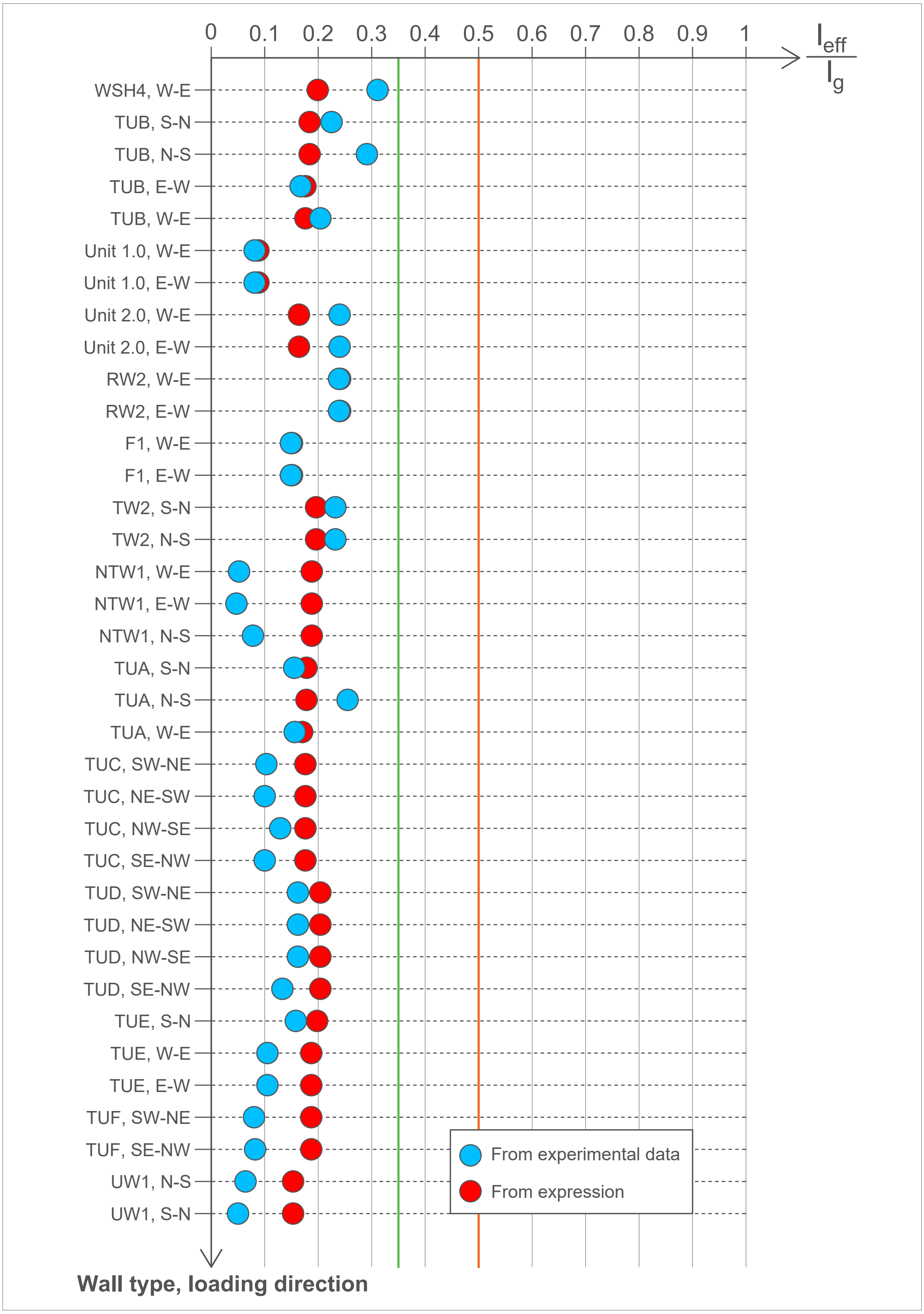

Figure 5.4: Effective stiffness ratio values when the Fourth procedure is applied on the numerical data.

In Figure 5.1, the blue points correspond to the values of the effective stiffness ratio obtained by applying the First procedure 5.1.1 on the experimental data force-displacement curves of each wall. Besides that, the red points correspond to the values of the effective stiffness ratio obtained by applying the First procedure 5.1.1 on the numerical data force-displacement curves of each wall.

The blue points in Figure 5.2 correspond to the values of the effective stiffness ratio obtained by applying the First procedure 5.1.1 on the experimental data force-displacement curves of each wall. Whereas the red points correspond to the values of the effective stiffness ratio obtained by applying the Second procedure 5.1.2 on the numerical data force-displacement curves of each wall.

In Figure 5.3, the blue points correspond again to the values of the effective stiffness ratio obtained by applying the First procedure 5.1.1 on the experimental data force-displacement curves of each wall. Whereas the red points correspond to the values of the effective stiffness ratio obtained by applying the Third procedure 5.1.3 on the numerical data force-displacement curves of each wall.

Finally, the blue points in Figure 5.4 correspond to the values of the effective stiffness ratio obtained by applying the First procedure 5.1.1 on the experimental data force-displacement curves of each wall whereas the red points correspond to the values of the effective stiffness ratio obtained by applying the Fourth procedure 5.1.4 on the characteristics each wall.

Moreover, Figures 5.1, 5.2, 5.3 and 5.4 show two colored vertical lines. The purpose of these lines are to show the values of the effective stiffness ratio that codes require us to take. The green vertical line corresponds to an effective stiffness ratio equal to 0.35 as proposed in the ACI 318-11 and CSA A23.3-14 codes while the orange vertical line corresponds to an effective stiffness ratio equal to 0.5 as proposed in EN 1998-1 code.
A discussion about these comparisons can be found in the next Section 5.3.

5.3 Discussion

In Figure 5.1, when using the First procedure 5.1.1 to calculate the effective stiffness ratio for both experimental and numerical data, we can see that blue and red points are really close to each other for most of the wall types. Only wall WSH4, TUB and RW2 have a difference of about 10 % between experimental and numerical effective stiffness ratio. It can also be noted that the values of the effective stiffness ratio of each wall are lower than the ones proposed in the codes since all the points in Figure 5.1 are on the left side of the green vertical line represented an effective stiffness ratio of 0.35. This means that codes overestimate the real effective stiffness.

When using the Second procedure 5.1.2 to calculate the effective stiffness ratio from the numerical data force-displacement curves in Figure 5.2, it can be seen again that most of the red points are close to the blue one. However, there is a gap of over 10% for the effective stiffness ratio for the following walls: WSH4, TUB when it is loaded from North-to-South and from West-to-East and for TUF. Regarding the values of effective stiffness ratio required by codes, we can see that almost every points are at the left side of the vertical green line except for wall TUF when it is loaded from the Southwest-to-Northeast direction.

In Figure 5.3, when using the Third procedure 5.1.3 to calculate the effective stiffness ratio from the numerical data force-displacement curve, we can see that most of the time the red points are really far away from the blue ones. This means that the Third procedure 5.1.3 fails at evaluating the real effective stiffness ratio. Concerning the values of effective stiffness ratio required by codes, we can see that about half of the red points are on the right side of the vertical green line while all blue points are on its left side. It should also be noted that walls Unit 2.0, F1 and TW2 have numerical effective stiffness ratio on the right side of the vertical orange line.

When using the Fourth procedure 5.1.4 to calculate the effective stiffness ratio from the characteristics of each walls in Figure 5.4, we can see that most of the red points are really close to the blue ones, except for walls WSH4, NTW1, TUF and UW1 that have a gap of over 10% for their effective stiffness ratio. It can also be noticed that almost every red points have approximately the same value of 0.2. Finally, we can see that all the red and blue points are on the left side of the vertical green line meaning that the effective stiffness ratio of each wall is below the value proposed by codes.

Chapter 6

Conclusions and Outlook

This chapter sums up all the work that has been presented in this master's thesis and gives conclusions concerning values of effective stiffness ratio for non-rectangular RC walls.

Chapter 3 has shown a comparison between different ways of modeling RC structural walls which do not require the use of finite elements as shell, membrane or solid elements. It has been shown that beam-truss models give more accurate results than stick and wide-column models. Moreover, compared to the wide-column model, beam-truss model is less confusing to build as it does not require to make a lot of assumptions. It was for these reasons that all the analyzed walls in the report have been modeled as beam-truss models in order to have the corresponding force-displacement curves.

As explained in Chapter 2, the ACI 318-11 and the CSA A23.3-14 design codes proposed using a constant value of 0.35 for the effective stiffness ratio whereas the European code EN 1998-1 proposed to take a value equal to 0.5. These proposed values were based on investigations on rectangular cross-section RC walls. Therefore, the main goal of this master's thesis was to compare these ratios with the ones obtained by applying one of the four procedures that have been presented in Chapter 5 on the numerically obtained force-displacement curves for rectangular and non-rectangular cross-section walls.

Taking only into account the results for the effective stiffness ratio obtained using the First, Second and Fourth procedures presented in Chapter 5 enables to make some interesting conclusions:

- Firstly, the values of the effective stiffness ratio for the analyzed rectangular cross-section RC walls are greater than the one from non-rectangular cross-section walls. Therefore, the value of 0.35 proposed by the ACI 318-11 and the CSA A23.3-14 design codes seems to be a good approximation when dealing with rectangular cross-section walls.

- Secondly, when looking to the values of the effective stiffness ratio of non-rectangular U-shaped walls, the value of 0.35 proposed by design codes overestimates the numerically obtained effective stiffness ratio. Thanks to the work produced in this report, a new value specifically made for U-shaped walls can be proposed. Indeed, **instead of using a value of 0.35 as suggested in design codes, a value of 0.25 for the effective stiffness ratio seems to be more accurate when dealing with U-shaped walls**.

- Thirdly, the value for the effective stiffness ratio of 0.5 proposed by the European code EN 1998-1 is overestimated for both rectangular and non-rectangular cross-section walls. As explained in Chapter 2, using an overestimated effective stiffness ratio will yield to an overestimation of the internal forces and an underestimation of the displacement at the top of the corresponding wall.

Finally, some further possible developments of this master's thesis can be interesting to be done for a future work:

- All the beam-truss models that have been built for this report were done with some assumptions regarding the division of the wall cross-section into different parts. Therefore, a parametric study consisting in changing the number of vertical and horizontal elements in those models could be interesting to be done to see if it has an influence on the force-displacement curve results.
- Moreover, another possible development of this document could be to look at the influence of the axial load ratio (ALR), i.e., the vertical load applied on top of the wall, on the effective stiffness ratio.
- A last improvement of this master's thesis could be to calculate the effective stiffness ratio for T-shaped and U-shaped walls using the empirical expressions proposed by Zhang & al. (2018) [28]. The obtained ratios could be then compared with the other procedures presented in Chapter 5.

Appendix A

Beam-truss models perspective views

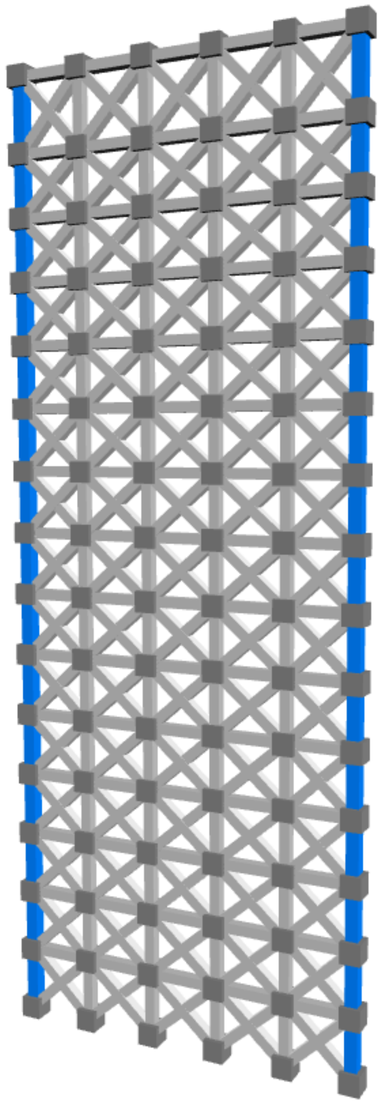

Figure A.1: Perspective view of the beam-truss model for WSH4.

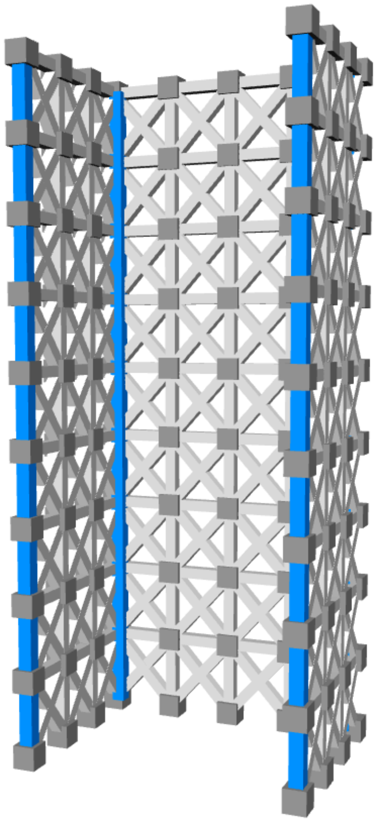

Figure A.2: Perspective view of the beam-truss model for TUB when loaded in the South-North direction.

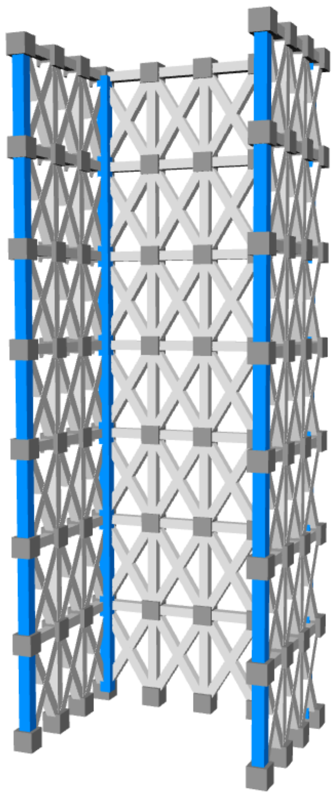

Figure A.3: Perspective view of the beam-truss model for TUB when loaded in the West-East direction.

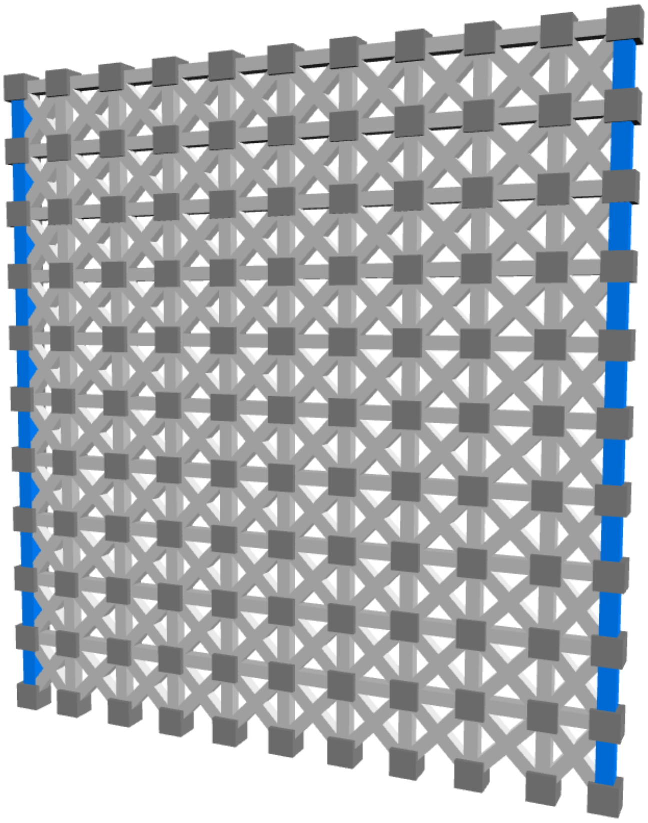

Figure A.4: Perspective view of the beam-truss model for Unit 1.0.

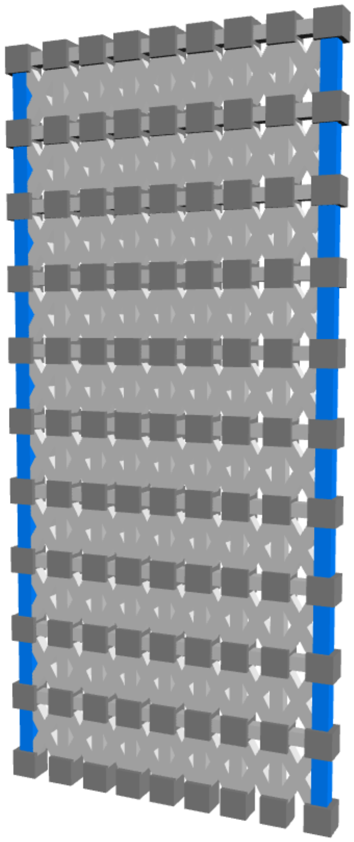

Figure A.5: Perspective view of the beam-truss model for Unit 2.0.

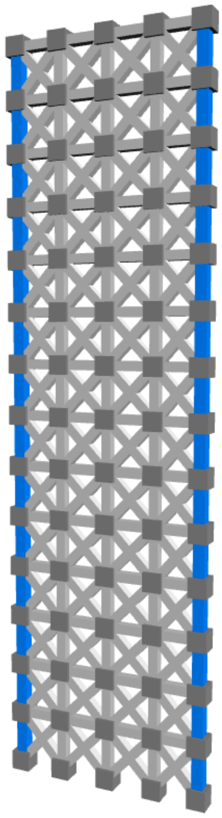

Figure A.6: Perspective view of the beam-truss model for RW2.

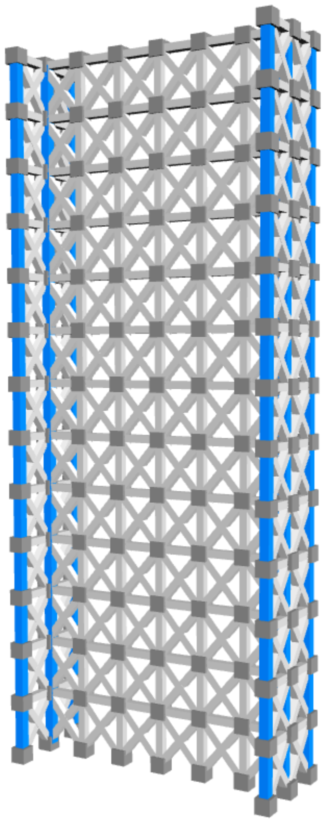

Figure A.7: Perspective view of the beam-truss model for F1.

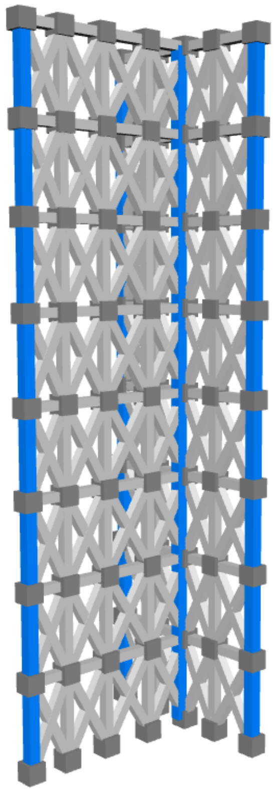

Figure A.8: Perspective view of the beam-truss model for TW2.

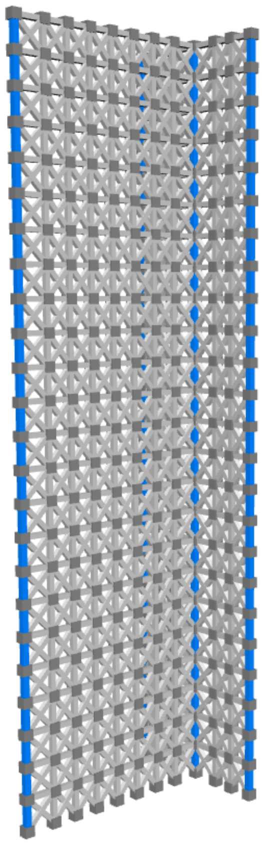

Figure A.9: Perspective view of the beam-truss model for NTW1.

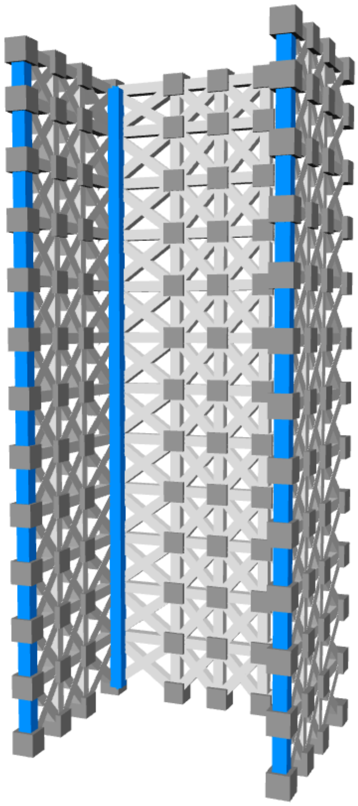

Figure A.10: Perspective view of the beam-truss model for TUA when loaded in the South-North direction.

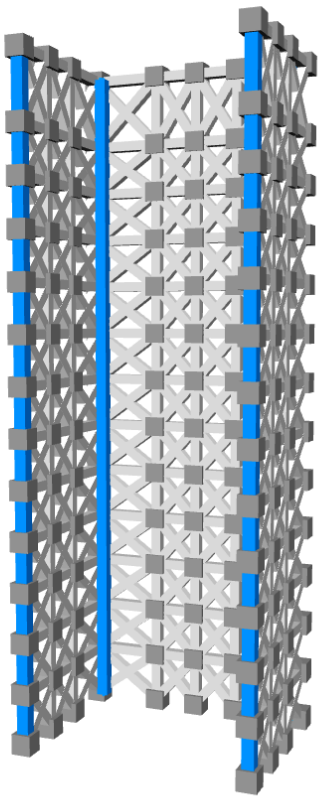

Figure A.11: Perspective view of the beam-truss model for TUA when loaded in the West-East direction.

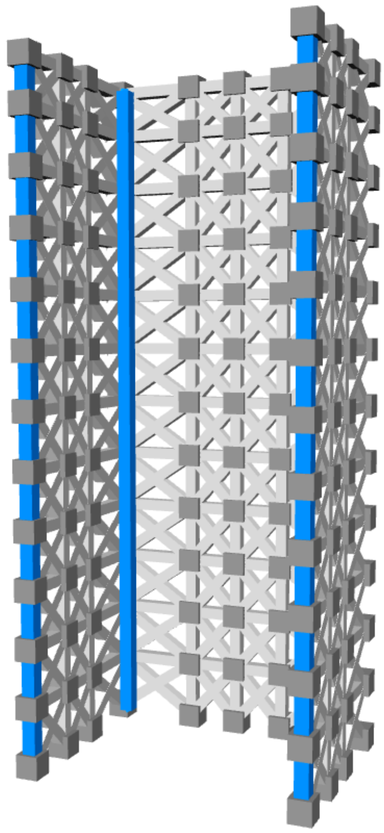

Figure A.12: Perspective view of the beam-truss model for TUC.

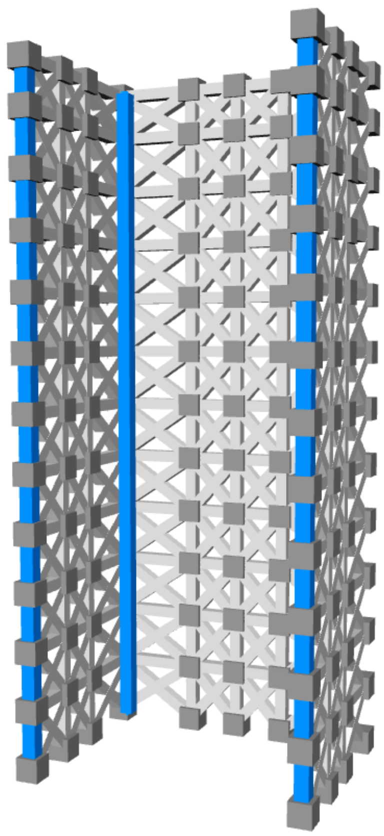

Figure A.13: Perspective view of the beam-truss model for TUD.

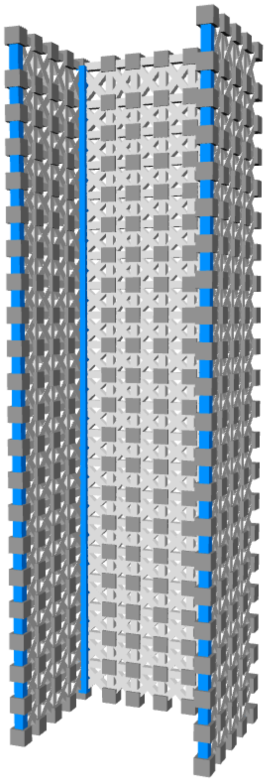

Figure A.14: Perspective view of the beam-truss model for TUE when loaded in the South-North direction.

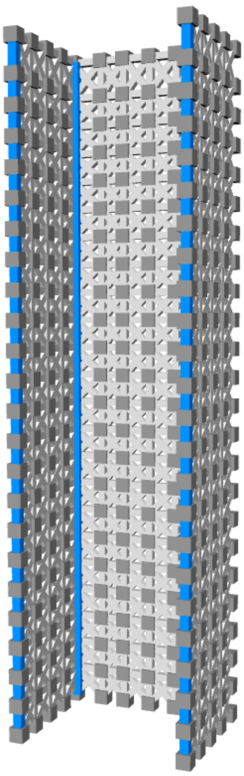

Figure A.15: Perspective view of the beam-truss model for TUE when loaded in the West-East direction.

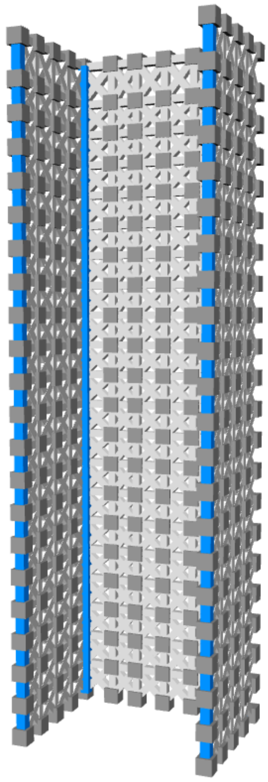

Figure A.16: Perspective view of the beam-truss model for TUF when loaded in the South-North direction.

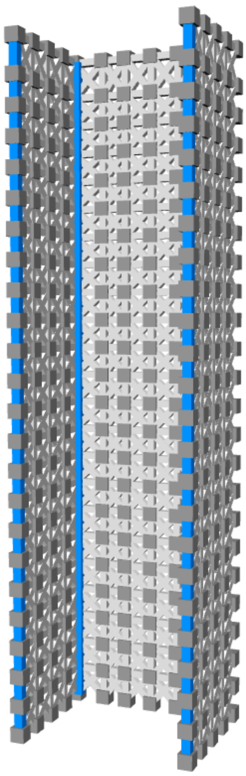

Figure A.17: Perspective view of the beam-truss model for TUF when loaded in the West-East direction.

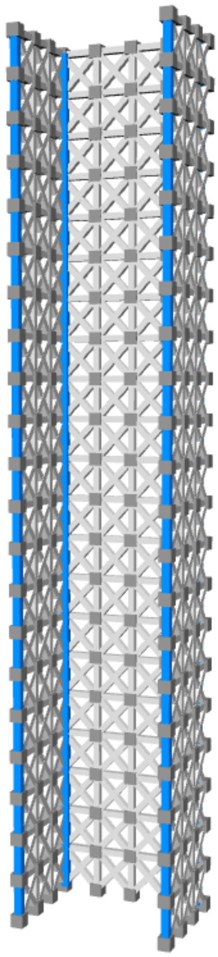

Figure A.18: Perspective view of the beam-truss model for UW1.

Bibliography

[1] Arteta, Carlos A et al. “Hybrid approach for simulating shear–flexure interaction in RC walls with nonlinear truss and fiber models”. In: *Bulletin of Earthquake Engineering* 17.12 (2019), pp. 6437–6462.

[2] Beyer, K, Dazio, A, and Priestley, MJN. “Inelastic wide-column models for U-shaped reinforced concrete walls”. In: *Journal of Earthquake Engineering* 12.S1 (2008), pp. 1–33.

[3] Beyer, Katrin, Dazio, Alessandro, and Priestley, MJN. “Quasi-static cyclic tests of two U-shaped reinforced concrete walls”. In: *Journal of earthquake engineering* 12.7 (2008), pp. 1023–1053.

[4] Brueggen, Beth L, French, Catherine E, and Sritharan, Sri. “T-shaped RC structural walls subjected to multidirectional loading: test results and design recommendations”. In: *Journal of Structural Engineering* 143.7 (2017), p. 04017040.

[5] Committee, ACI. “Building code requirements for structural concrete (ACI 318-11) and commentary”. In: American Concrete Institute. 2011.

[6] Constantin, Raluca and Beyer, Katrin. “Behaviour of U-shaped RC walls under quasi-static cyclic diagonal loading”. In: *Engineering structures* 106 (2016), pp. 36–52.

[7] CSA. “Canadian Standards Association Design of Concrete Structures”. In: CSA Standard Update Service. 2014.

[8] Das, Sourav and Choudhury, Satyabrata. “Influence of effective stiffness on the performance of RC frame buildings designed using displacement-based method and evaluation of column effective stiffness using ANN”. In: *Engineering Structures* 197 (2019), p. 109354.

[9] Dazio, Alessandro, Beyer, Katrin, and Bachmann, Hugo. “Quasi-static cyclic tests and plastic hinge analysis of RC structural walls”. In: *Engineering Structures* 31.7 (2009), pp. 1556–1571.

[10] De Visscher, Sammy, Saraiva Esteves Pacheco De Almeida, João, and Correia, Antonio. “Harmonisation des approches force et déplacement selon la seconde génération de l’Eurocode 8: application aux ossatures en béton armé”. In: ().

[11] Fardis, Michael et al. *Seismic design of concrete buildings to Eurocode 8*. Crc Press, 2015.

[12] Fenwick, R and Bull, D. “What is the stiffness of reinforced concrete walls”. In: *SESOC journal* 13.2 (2000), pp. 23–32.

[13] Hoult, Ryan et al. “Seismic performance of slender RC U-shaped walls with a single-layer of reinforcement”. In: *Engineering Structures* 225 (2020), p. 111257.

[14] Hoult, Ryan D and Almeida, João Pacheco de. "Residual displacements of reinforced concrete walls detailed with conventional steel and shape memory alloy rebars". In: *Engineering Structures* 256 (2022), p. 114002.

[15] Li, Bing and Xiang, Weizheng. "Effective stiffness of squat structural walls". In: *Journal of Structural Engineering-Reston* 137.12 (2011), p. 1470.

[16] Lu, Yuan, Panagiotou, Marios, and Koutromanos, Ioannis. *Three-dimensional beam-truss model for reinforced-concrete walls and slabs subjected to cyclic static or dynamic loading*. Tech. rep. 2014.

[17] Mestyanek, James Michael. "The earthquake resistance of reinforced concrete structural walls of limited ductility". In: (1986).

[18] Oesterle, RG et al. "Earthquake resistant structural walls-tests of isolated walls". In: *Research and Development Construction Technology Laboratories, Portland Cement Association* (1976).

[19] Palermo, Dan and Vecchio, Frank J. "Simulation of cyclically loaded concrete structures based on the finite-element method". In: *Journal of Structural Engineering* 133.5 (2007), pp. 728–738.

[20] Paulay, Thomas and Priestley, MJ Nigel. *Seismic design of reinforced concrete and masonry buildings*. Vol. 768. Wiley New York, 1992.

[21] Seismosoft. "SeismoStruct 2021- A computer program for static and dynamic nonlinear analysis of framed structures". In: *https://seismosoft.com/* (2021).

[22] Stafford-Smith, B and Girgis, Amal M. "Deficiencies in the wide column analogy for shearwall core analysis". In: *Concrete International* 8.4 (1986), pp. 58–61.

[23] Standard, British. "Eurocode 8: Design of structures for earthquake resistance". In: *Part* 1 (2005), pp. 1998–1.

[24] Standardization, European Committee for. "Eurocode 8: Design of structures for earthquake resistance – Part 2: Bridges." In: *Part* 2 (2005), pp. 1998–2.

[25] Thomsen IV, John H and Wallace, John W. "Displacement-based design of slender reinforced concrete structural walls—experimental verification". In: *Journal of structural engineering* 130.4 (2004), pp. 618–630.

[26] "UCLouvain 2022 Blind Prediction Competition - Test description". In: *Institute of Mechanics, Materials and Civil Engineering (iMMC)* (2022).

[27] Wong, JM et al. "Effective stiffness for modeling reinforced concrete structures: a literature review". In: *Structure magazine* (2017), pp. 18–21.

[28] Zhang, Zhongwen and Li, Bing. "Effective stiffness of non-rectangular reinforced concrete structural walls". In: *Journal of Earthquake Engineering* 22.3 (2018), pp. 382–403.

UNIVERSITÉ CATHOLIQUE DE LOUVAIN
École polytechnique de Louvain
Rue Archimède, 1 bte L6.11.01, 1348 Louvain-la-Neuve, Belgique | **www.uclouvain.be/epl**